I. Efficient Discovery of Fluorescent Chemosensors Based on a Biarylpyridine Scaffold

II. Visual Detection of the Explosive TATP The Origins of Sulfoxides "non-emission"

Dissertation

zur

Erlangung der naturwissenschaftlichen Doktorwürde (Dr. sc. nat.)

vorgelegt der

Mathematisch-naturwissenschaftlichen Fakultät

der

Universität Zürich

von

Sergey Malashikhin

aus Russland

Promotionskomitee:

Prof. Dr. Jay S. Siegel (Vorsitz)

Prof. Dr. Roland K. O. Sigel

PD Dr. Nathaniel S. Finney (Leitung der Dissertation)

Zürich, 2010

Die vorliegende arbeit wurde von

der Mathematisch-naturwissenschaftlichen Fakultät

der Universität Zürich im Januar 2008

als Dissertation angenommen

Promotionskomitee:

Prof. Dr. Jay S. Siegel

Vorsitz

Prof. Dr. Roland K. O. Sigel

PD Dr. Nathaniel S. Finney

Universität Zürich 2010

Abstract.

Fluorescent chemosensors for ions and neutral molecules have been a subject of numerous research publications and review articles over the last decades.[1] Relatively recently a new fluorescent signaling mechanism, binding induced conformational restriction, was discovered.

In the first part of this dissertation a library of 10 potential fluorescent chemosensors with chelating groups known to have high affinity for cations and anions is presented. All are based on the biarylpyridine scaffold appended with two identical receptor arms. The previous synthesis of the biaylpyridine core fluorophore was improved with significant reduction of the number of steps and increase in the overall yield. This made the core fluorophore more accessible.

Three fluoroionophores capable of sensing Hg(II) and Ag(I) ions in aqueous solution were identified. As binding domains phenylthiourea (with (*Gly-Thio*) and without (*Thio*) glycine as a linker between the binding site and a signaling subunit) and dithioazacrown (*Crown*) were used. Despite high affinity for Hg(II) and Ag(I) in case of *Thio* and *Crown* chemosensors, both fail to distinguish between the two ions when they are contained in one sample. *Gly-Thio* chemosensor suggests the possibility of discriminating Hg(II) and Ag(I) due to significant (80 nm) blue shift upon addition of Hg(II) accompanied by an increase in emission intensity. Ratiometric detection of this type (with single-fluorophore) is comparatively rare and provides more accurate and quantitative measurements of metal ion concentration.

Computational study of simple analogues of the Hg-complexes of the fluorescent chemosensors identified from the library showed high steric congestion of complexes, which may prevent cooperative ion binding in some cases.

This result explains why the majority of library members are not effective chemosensors and makes it possible to predict structural changes of the binding site necessary to design next-generation chemosensors with improved properties.

The second part of the dissertation reports a fluorescence assay for the visual detection of the common terrorist explosive triacetone triperoxide (TATP). Our fluorescent probe for TATP relies on the sulfoxide/sulfone redox couple attached to a

[1] Literature references are listed on p. 28 (Chapter 1).

fluorophore (pyrene). In this couple the sulfone is much more fluorescent than the corresponding sulfoxide. In the presence of a catalyst (methyltrioxorhenium) sulfoxides react rapidly with H_2O_2 generated by UV irradiation of TATP. Oxidation of the sulfoxide to sulfone leads to ca. 50-fold fluorescence increase, which can be seen with naked eye. This fluorescence assay is capable of detecting as little as 100 nmol of TATP.

Further development of sulfur based fluorescent chemosensors and use of longer wavelength fluorophore makes it essential to understand the photophysical origin of low sulfoxide emission relative to sulfones. A combined experimental and computational approach has been taken. Several sulfide/sulfoxide/sulfone series differing in the number of carbon atoms between sulfur and the fluorophore (pyrene) as well as substituents (alkyl or aryl) attached to the sulfur atom were prepared.

Our initial assumption, photoinduced electron transfer as a fluorescence quenching mechanism, was rejected on the basis of distance (the number of carbon atoms) independency between the fluorophore and the sulfur atom. Results from photolysis experiments have established that the excited state of aryl sulfoxides is quenched by reversible radical formation/recombination (so-called α-cleavage). For an efficient quenching of fluorescence the presence of an S-Ar fragment is required. Computational study has identified a low lying excited state (S_2) of the sulfoxide in which the S-Ar fragment is electronically coupled to the excited pyrene chromophore and the excited state energy is transferred to the S-Ar, leading to C-S bond cleavage. The subsequent radical recombination in the solvent cage leads to sulfoxide re-formation. Excitation energy is consumed and fluorescence quenching is observed.

These studies provide the basis for designing TATP-responsive fluorescent probes with longer emission wavelength.

Zusammenfassung.

Fluoreszierende Chemosensoren für Ionen und neutrale Moleküle waren Thema zahlreicher Forschungspublikationen und Übersichtsartikel in den letzten Jahrzehnten. Vor kurzem wurde ein neuer Mechanismus zur Anregung der Fluoreszenz entdeckt, der auf Konformationsrestriktion beruht, die durch die Bindung eines Substrates an den Sensor verursacht wird.

Im ersten Teil dieser Dissertation wird eine Bibliothek aus zehn potentiell fluoreszierenden Chemosensoren vorgelegt. Die Zielverbindungen sind mit chelierenden Rezeptorgruppenruppen ausgestattet, die für ihre hohe Affinität zu Kationen und Anionen bekannt sind. Alle Verbindungen beruhen auf einem Biarylpyridin-Gerüst mit zwei identischen Rezeptorgruppen. Der bisherige Syntheseweg zum Biarylpyridin Kern-Fluorophor wurde erheblich verbessert, indem die Zahl der Syntheseschritte verringert wurde. Die Verbesserung der Gesamtausbeute machte den Kern-Fluorophor somit zugänglicher.

Drei Fluoroionophore wurden gefunden, die in der Lage sind Hg(II)- und Ag(I)-Ionen in wässriger Lösung nachzuweisen. Phenylthioharnstoff (mit Glycin (*Gly-Thio*) und ohne Glycin (*Thio*) als Linker Zwischen der Bindungsstelle und dem fluoreszierenden Teil des Sensors) und Dithioaza-Kronenether (*Crown*) wurden als Bindungseinheiten verwendet. Trotz der hohen Affinität von *Thio* und *Crown* zu Hg(II) und Ag(I), konnte in einer Probe nicht zwischen diesen Ionen unterschieden werden. *Gly-Thio* bietet jedoch die Möglichkeit zwischen Hg(II) und Ag(I) zu unterscheiden, da die Bindung von Hg(II) zu einer erheblichen Blauverschiebung (80nm) und einem Anstieg der Emissionsintensität führt. Dadurch können durch Ratiometrische Fluoreszenz-Messungen, vergleichsweise selten mit einzelnen Fluorophoren, Konzentrationen von Metall-Ionen genau bestimmt werden.

Rechnergestützte Strukturanalysen einfacher Analogverbindungen der fluoreszierenden Chemosensoren aus der Bibliothek zeigten hohe sterische Überlastung im Falle der Hg-Komplexe. In manchen Fällen kann dadurch kooperative Ionen-Bindung verhindert werden. Dieses Ergebnis erklärt, weshalb die Mehrheit der synthetisierten Moleküle keine effektiven Chemosensoren darstellen. Weiterhin können strukturelle Veränderungen vorhergesagt werden, die nötig sind, um die

nächste Generation von Chemosensoren mit verbesserten Eigenschaften zu entwickeln.

Im zweiten Teil der Arbeit wird eine Methode zur Detektion des Sprengstoffs Triacetontriperoxid (TATP) vorgestellt, der häufig von Teroristen verwendet wird. Unsere Fluorophore beruhen auf Sulfoxid/Sulfon Redox-Paaren, welche an Pyren gebunden sind, wobei das jeweilige Sulfon generell intensiver fluoresziert als das Sulfoxid. In Anwesenheit des Katalysators Methyltrioxorhenium reagieren Sulfoxide schnell mit dem durch UV-Bestrahlung von TATP erzeugten Wasserstoffperoxid. Dabei wird eine 50-fache Erhöhung der Fluoreszenz bobachtet, die mit blossem Auge zu sehen ist. Mit der vorgestellten Fluoreszenzanalyse ist der Nachweis von weniger als 100 nmol TATP möglich.

Für weitere Entwicklungen Schwefel basierter Fluoreszenz-Sensoren ist es entscheidend, die photophysikalischen Grundlagen der geringeren Emission von Sulfoxiden relativ zu Sulfonen zu verstehen. Ein experimenteller und rechnergestützter Ansatz wurde zu diesem Zweck gewählt. Homologe Reihen von Sulfiden/Sulfoxiden/Sulfonen mit unterschiedlicher Anzahl von Kohlenstoffatomen zwischen dem Schwefelatom und dem Fluorophor (Pyren) sowie mit verschiedenen Substituenten (Alkyl or Aryl) wurden hergestellt.

Die ursprüngliche Annahme, Fluoreszenzlöschung beruhe auf photoinduziertem Elektronentransfer, wurde aufgrund der fehlenden Korrelation zwischen Fluoreszenzlöschung und Abstand Schwefelatom–Fluorophor abgelehnt. Photolytische Experimente mit Sulfoxiden ergaben, dass der angeregte Zustand von Sulfoxiden durch reversible Radikalbildung und Rekombination (a-Spaltung) gelöscht wird. Für eine effiziente Löschung der Fluoreszenz ist die Anwesenheit eines S-Ar-Fragmentes unabdingbar.

Berechnungen ergaben einen tief liegenden angeregten Zustand (S_2) der Sulfoxide. In diesem Zustand ist das S-Ar Fragment mit dem angeregten Pyren elektronisch gekoppelt, was die Übertragung der Anregungsenergie vom Pyren auf den S-Ar Teil ermöglicht. Dies führt zur Spaltung der C–S Bindung und anschließender Rekombination der Radikale zum ursprünglichen Sulfoxid. Dadurch wird die Anregungsenergie verbraucht und Fluoreszenzlöschung wird beobachtet.

Diese Untersuchungen bilden die Grundlage zur Synthese fluoreszierender Chemosensoren für TATP die bei größeren Wellenlängen absorbieren und emittieren.

Table of Contents

Part 2.

Chapter 3

Visual Detection of the Explosive TATP

Chapter 4

The Origins of Sulfoxides “non-emission”

Chapter 1.

Introduction to Fluorescent Chemosensors.

1.1. Luminescence. A historical overview.

Luminescence is the emission of light that occurs at low temperatures from a photochemically generated electronically excited state of any substance.

In 1845 Sir John Frederick William Herschel reported the first observation of the fluorescence of a quinine solution in sunlight and presented his finding to the Royal Society of London. It is evident that Herschel recognized an unusual phenomenon, which could not be explained by the scientific knowledge of that time.

One of the important generalizations of luminescence study during the nineteenth century was made by G. G. Stokes (1852). During his study Stokes noticed that in producing fluorescence, light is always "degraded", i.e. shorter wavelengths excite the fluorescence emission of longer wavelength.

The term "*Lumineszenz"* was coined in 1888 by German physicist and historian of science Eilhardt Wiedemann for "all those phenomena of light which are not solely conditioned by the rise in temperature"[1].

There exist several types of luminescence e.g. photoluminescence, radioluminescence, chemoluminescence, bioluminescence.

In general luminescence of organic molecules can be divided into two phenomena: fluorescence and phosphorescence. The processes, which occur in the molecule upon irradiation, are illustrated by means of Jablonsky diagram (***Scheme 1.1***).

The singlet ground, first and second electronic states are depicted by S_0, S_1 and S_2 respectively. At each of these electronic energy levels the fluorophores can exist in a number of vibrational energy levels, denoted by 0, 1, 2 etc. [2]. Absorption of a photon of appropriate energy results in the promotion of an electron to an orbital of higher energy S_n (n=1,2,…). This process is known as *excitation* and has an instantaneous nature (10^{-15}s, depicted as vertical lines on the diagram)[1]. The lowest energy and the most important electronic transitions from an organic perspective take

[1] Throughout the text approximate rate constants are provided.

place between the highest occupied molecular orbital (HOMO) and the lowest unoccupied molecular orbital (LUMO) of the ground state configuration. $n \rightarrow \pi^*$ and $\pi \rightarrow \pi^*$ transitions are of particular importance (other transitions include $\sigma \rightarrow \sigma^*$, $n \rightarrow \sigma^*$, $\pi \rightarrow \sigma^*$).

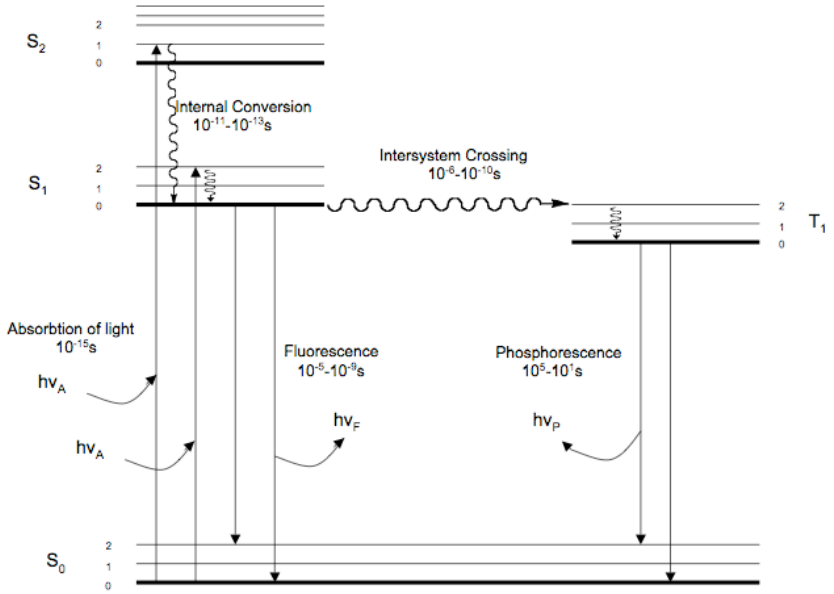

Scheme 1.1. Jablonski diagram.

Following light absorption, several processes usually occur: a fluorophore is excited to some higher vibrational level of S_1 (or S_2 followed by internal conversion (IC) to S_1) then relaxes to the lowest vibrational level of S_1. This process occurs in 10^{-12}s or less. Intersystem crossing (ISC) takes place if the singlet excited state undergoes a change in spin multiplicity and converts to the triplet manifold followed by IC to the lowest vibrational level of T_1.

Emission from the singlet state is defined as *fluorescence*. It typically occurs in 10^{-9}s. The emitted light is always of longer wavelength than the incident light, a characteristic of fluorescence emission known as *Stokes shift*.

Emission from triple state is called *phosphorescence*. The spin-forbidden process of ISC and formation of the triplet excited state is facilitated by the presence of $n\pi^*$ states or heavy-atoms. The large separation between the T_1 and S_0 states ensures that phosphorescence is a slow process (10^{-5}-10^{1}s), favoring nonradiative, collisional

deactivation of T_1. Only at low temperature and/or in a rigid medium, can luminescence from the triplet state be detected.

1.2. Luminescence and Chemical Sensors.

1.2.1. Definition of Terms.

A *sensor* is a device that interacts with matter or energy and yields a measurable signal in response. A sensor can be a microscopic devise such as pH electrode or even individual molecules capable of performing useful work on other molecules. A very good example of such a sensor is phenolphthalein. Following are some related definitions.

Chemical sensor: a micro- or macroscopic devise that interacts reversibly with a chemical analyte with signal transduction. *Chemosensor:* a molecule of abiotic origin that signals the presence of matter or energy. Thus, phenolphthalein is a chemosensor. In the presence of a sufficient concentration of OH^-, phenolphthalein is deprotonated and provides a visible signal (color change). *Signal transduction:* is the mechanism by which an interaction of sensor with analyte yields a measurable signal, which may be characterized by various spectroscopies. A *fluorescent chemosensor* operates with fluorescence to signal the particular binding event the sensor is engaged in.

1.2.2. Fluorescent Chemosensors.

There are several reasons for which fluorescence may be identified as the optimal signaling in potential sensing application. Fluorescence is an enormously sensitive technique. Fluorescence signaling permits the monitoring of both excitation and emission wavelengths. The emission signal may be observed by intensity, intensity ratio or life time measurement. Fluorescence is usually nondestructive [3].

The requisite research issues essential to the creation of fluorescent chemosensors are:

- *how can one bind a molecular entity with selectivity (preferably from water)*
- *what molecular changes result in fluorescence change*
- *what mechanism accounts for signal transduction upon binding*

The most common type of fluorescent chemosensors is ion (cation or anion) selective chemosensors that is molecules that are capable of reporting the ion coordination process. In the concept for ion recognition binding sites can be coupled to certain

groups that are capable of "reporting" the ion coordination process. In this case the binding process is transduced into a signaling event. One basic principle in this multicomponent system is that the sensing event has to be related with an easy-to-measure signal.

A general approach to the development of ion chemosensors is the coupling of at least two units, each one playing a particular role: the binding site and the signaling subunit [4].

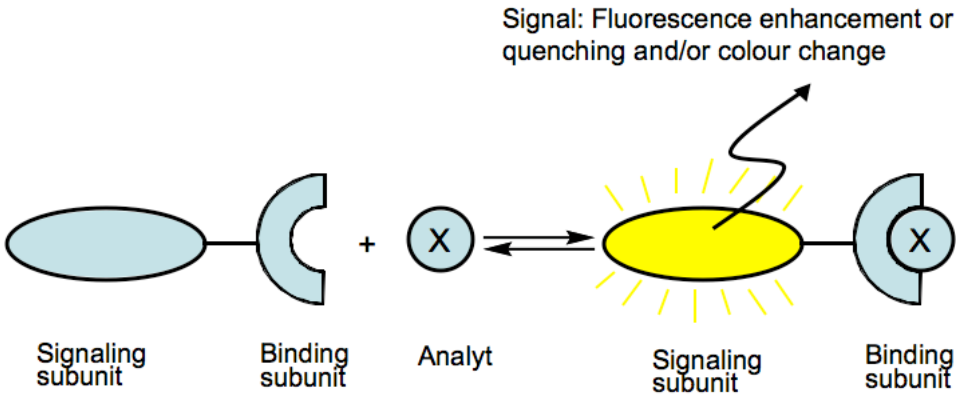

Scheme 1.2. Principle of fluorescent chemosensors.

If the binding site coordinates to a certain ion, the signaling site changes its spectroscopic characteristic (fluorescence) upon coordination (***Scheme 1.2***).

Coordination is always a reversible process.

There are a number of signaling mechanisms that are used in fluorescent chemosensor design. The next section provides a survey of most common mechanisms.

1.3. Fluorescent Signaling Mechanisms.

1.3.1. Photoinduces Electron Transfer (PET).

Photoinduces Electron Transfer (PET) is the one of the most important mechanisms for fluorescent chemosensors that has been intensively studied and widely used for sensing purposes of cations and anions. The thermodynamic basis for PET has been described for intermolecular systems by the pioneering work of Weller [5].

It is well known, that fluorescence in a molecule occurs when an excited electron in the lowest unoccupied molecular orbital (LUMO of the ground state S_0) goes to the highest occupied molecular orbital (HOMO of the ground state S_0), releasing the

excess of energy as light. If an orbital from another part of the molecule or from another molecular entity has energy between that of the HOMO and that of the LUMO and if this orbital if occupied (e.g. if we have a donor group "D" (Step 1)), a PET from this full orbital to the HOMO of the fluorophore can take place (Step 2). A further electron transfer from the LUMO of the fluorophore to the external orbital retrieves the stable ground state (Step 3). The fluorescence quenching occurs because the transition from the excited to the ground state follows a nonradiative pathway [4]. What is observed is a decrease of emission intensity (***Scheme 1.3***).

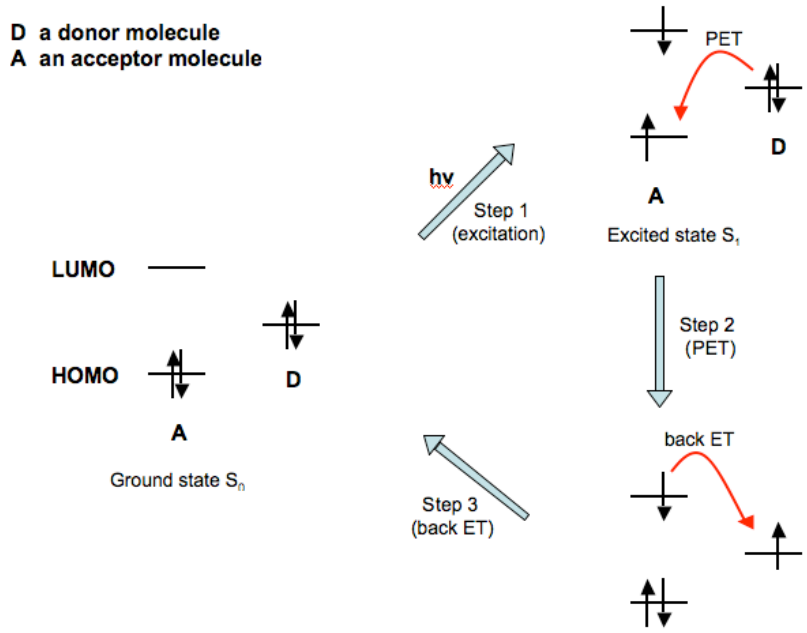

Scheme 1.3. Frontier energy diagram illustrating PET and reverse back ET.

If the donor and acceptor are to be fixed within the same molecular framework, then they must be separated by a spacer that is short enough for efficient electron transfer, but long enough to minimize the extent of electronic delocalization between the partners [5].

The design of fluorescent chemosensors tries to take advantage of PET effects in such a way that the presence of an ion should induce or suppress PET leading to quenching or enhancement of fluorescence intensity.

For example, a simple proton signaling system **1** may be designed by combining an amine with the common fluorophore antracene *via* a methylene spacer [6]. Low emission intensity of **1** is caused by lone electron pair of nitrogen atom (donor) *via* the PET mechanism. Upon protonation the lone pair forms the new N-H bond and cannot

act as an electron acceptor in PET quenching. As a result fluorescence intensity increases (***Figure 1.1***).

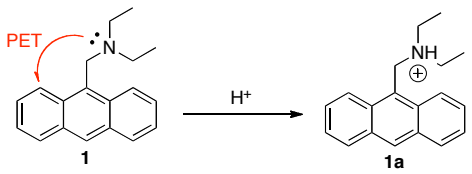

Figure 1.1. PET quenching and its suppression upon protonation.

One of the first specially designed chemosensors for cation detection was molecule **2** (***Figure 1.2***). Chelation-enchanced fluorescence (CHEF) on $ZnCl_2$ addition is a result of metal ion complexation of the amine lone pair, which decreases amine oxidizability such that it can not reduce the antracene S_1 excited state [7].

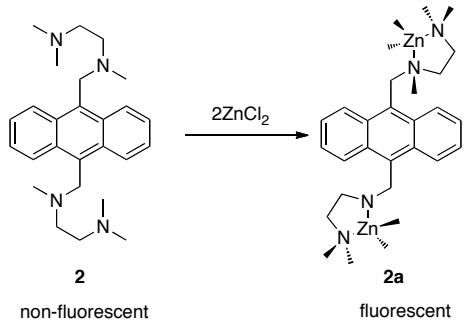

Figure 1.2. PET-based chemosensor for Zn.

Since Zn is an essential nutrient required for normal growth and development. The understanding of the beneficial and deleterious role of zinc in neurobiology should help in treatment of a number of pathologies.

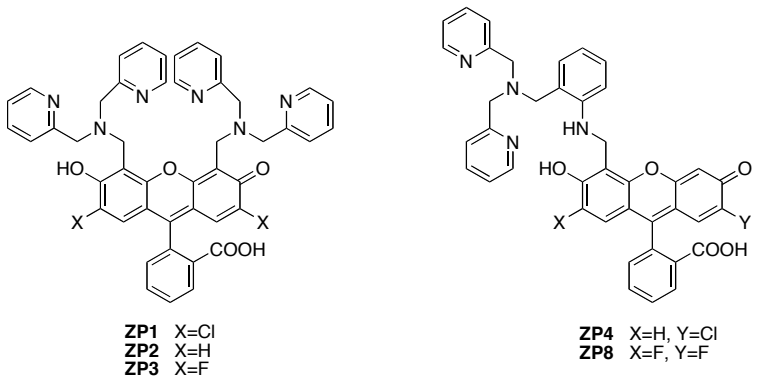

Figure 1.3. "Zinspy" fluorescent chemosensors.

Therefore the creation of new tools and approaches for optical imagining in biology is an important goal. The so-called "Zinspy" sensors (***Figure* 1.3**) have been synthesized for Zn detection under aqueous simulated physiological conditions. All compounds of Zinspy family except for ZS3 display 1.4 to 4.5 fold fluorescence enhancement upon Zn(II) complexation.

A very interesting example of utilizing of PET mechanism is a receptors containing boronic group that can be used for the chiral discrimination of D- and L-monosacharides (***Figure 1.4)*** [8].

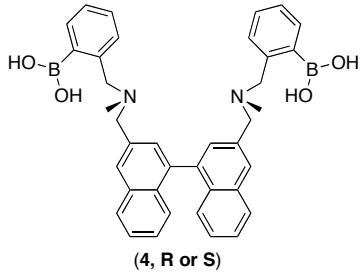

Figure 1.4. Structure of PET molecular sensor for distinguishing between enantiomers.

When sacharides form cyclic boronate ester with boronic acid, the acidity of the boronic acid is enhanced and therefore the Lewis acid-base interaction with the tertiary amine is strengthened. The strength of this interaction modulates the photoinduced electron transfer from the amine to naphthalene.

1.3.2. Photoinduced Charge Transfer.

When a fluorophore contains an electron-donating group (often an amino group) conjugated to an electron-withdrawing group, it undergoes intramolecular charge transfer (ICT) from the donor to the acceptor upon excitation by light. The consequent change in dipole moment results in a Stokes shift that depends on the microenviroment of the fluorophore [9]. Usually the donor and acceptor groups are conjugated in the ground state and undergo significant charge transfer in the excited state. If the two groups are able to adopt an orthogonal geometry, then full charge separation occurs, producing a twisted intramolecular charge transfer (TICT) state. The archetypal example of a molecule exhibiting both ICT and TICT emission is *p*-N, N-dimethylaminobenzonitrile **5a**. It was discovered to emit a dual fluorescence [10].

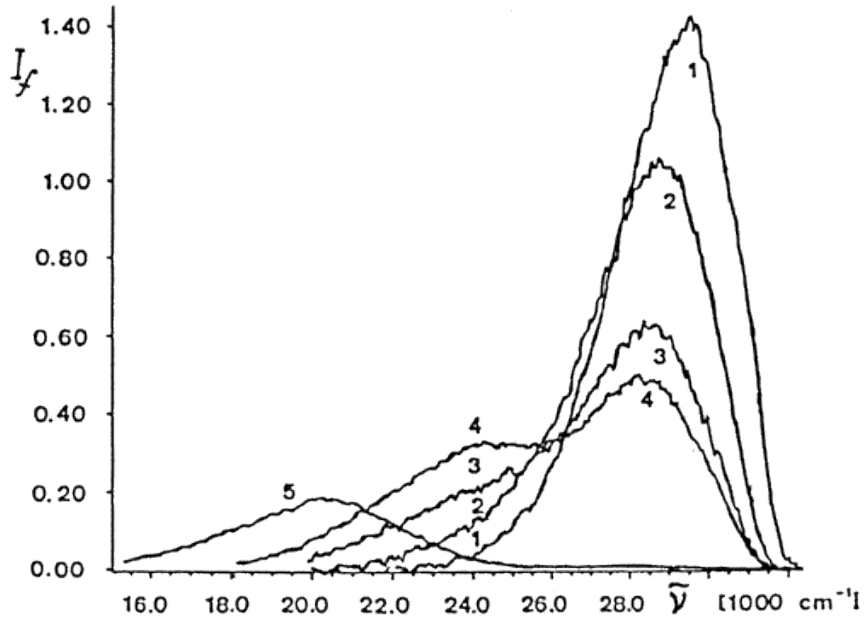

Figure 1.5. Dual Fluorescence of DMABN in several solvents: (1) n-hexane, (2) dibuthyl ether, (3) diethyl ether, (4) butyl chloride, (5) acetonitrile. Reproduced from ref. [11].

The properties of the two bands depend on solvent polarity and temperature. In nonpolar solvents, only one fluorescent band appears, originally from the *locally excited state (fluorescence)* LE or *Franck-Condon state* (that is an excited state formed at the ground state geometry), which is produced most often upon excitation [12]. Increasing the solvent polarity facilitates formation of ICT (or TICT) state; a further long-wavelength fluorescent band grows in relative intensity, while the intensity of the first band decreases (***Figure 1.5***).

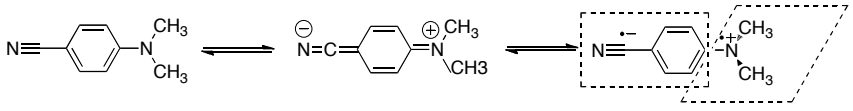

Figure 1.6. Exciting state conformations of DMABN.

Hence, the role of solvent polarity is not only to alter the energy of the excited state owing to general solvent effect, but also to govern which state has the lowest energy. Rotation of dimethylamino group until it is twisted at right angle leads to the loss of conjugation. In the resulting *twisted intramolecular charge transfer (TICT),* stabilized by the polar solvent molecules, there is a total charge separation between the dimethylamino group and the cyanophenyl moiety.

Shorter-wavelength band is assigned to a ICT structure and longer wavelength band to a CT excited-state conformation (***Figures 1.6, 1.7***) [13-15].

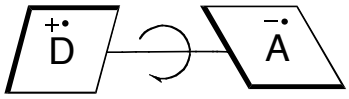

Figure 1.7. Model of a TICT excited state for a D-A molecule.

Twisting can be demonstrated by comparing the fluorescence characteristics of the bridged model compounds (**6-8**) shown on ***Figure 1.8*** with those of DMABN (**6**) in polar solvents: no twist is possible in bridged compounds and LE fluorescence is solely observed; the twisted compound (**8**) exhibits only the TICT fluorescence band. In contrast DMABN shows both LE and TICT fluorescence ***(Figure 1.8)*** [16].

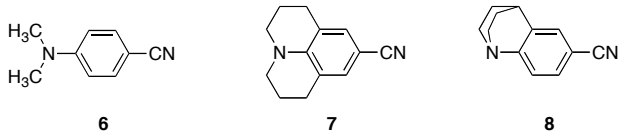

6 **7** **8**

Figure 1.8. Model compounds.

It can be expected that cations in close interaction with the donor or the acceptor moiety will change the photophysical properties of the fluorophore because the complexed cation affects the efficiency of intramolecular charge transfer.

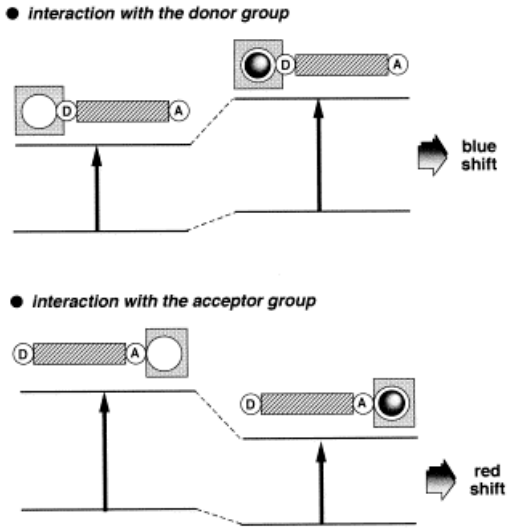

Scheme 1.4. Spectral displacement of PCT sensor resulting from interaction of a bound cation with an electron-donating or electron-withdrawing group [9].

When an electron donating group (like amino group) within the fluorophore interacts with a cation, its electon-donating character is reduced. What can be expected is the

blue shift in the absorption spectra. Conversely, a cation interacting with the acceptor group enhances its electron-withdrawing character. This leads to the red shift in absorption spectra and the molar absorption coefficient is increased. The fluorescence spectra are in principle shifted in the same direction. These shifts are usually accompanied by changes in quantum yields and lifetime. All these photophysical effects depend on the charge and the size of the cation as well as on the nature of the receptor (***Scheme 1.4)*** [9].

In practice, PCT sensors incorporating the cation at the donor most often result in only modest increases in quantum yields ($I/I_0 \approx$ 2-5) and emission shift upon ion recognition.

The idea of internal charge transfer can be applied to the design of fluorescent chemosensors. Most chemosensors of this type contain an azacrown as the cation receptor, which is conjugated to an electron-withdrawing group. For instance (4-dicyanomethylene-2-methyl-[6-p-(dimethylamino)styryl]-4H-pyran), the so-called DCM-crown **9** ***(Figure 1.9)***.

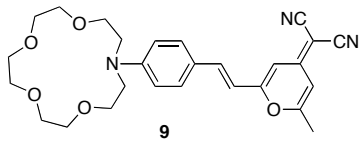

9

Figure 1.9. PCT based sensor.

Upon complexation with alkaline-earth metal cations, it undergoes dramatic changes in absorbtion spectra (hypsochromic shift and hypochromic effect) and fluorescence quantum yield (quenching), whereas the emission spectra is only slightly blue-shifted and fluorescence lifetime is almost unchanged. In this DCM derivative the nitrogen atom belongs to the crown, and therefore, complexation by cation reduces its donor character and thus hinders the charge transfer depending on the nature of the cation [17].

While most examples of fluorescent sensing in ICT systems rely on coordination of the analyte near the donor, a few examples exist where the electron-accepting region participates in the binding event. In coumarin derivatives linked to crown the cation interacts direct with the electron-withdrawing group, i.e. the carbonyl group. Both absorbtion and emission spectra are red shifted upon binding (***Figure 1.10***) [18].

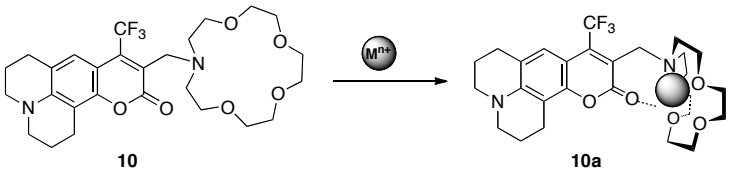

Figure 1.10. Example of PCT sensor incorporating cation near electron-acceptor.

However the strongest reason for the population of this class is due to success of low molecular weight sensors in physiological monitoring of H^+, Ca^{2+}, Mg^{2+}, Na^{2+} largely due to R. Tsien and his collaborators.

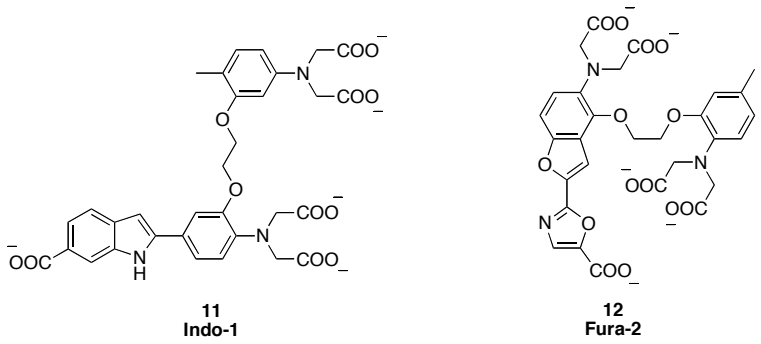

Figure 1.11. Tsien's Indo-1 and Fura-2 systems.

Probably two most important examples of such fluorescent dyes which bind to intracellular calcium are Indo-1 and Fura-2 systems [19]. Fura-2 was the first widely used dye for calcium imaging. Indo-1 is similar to Fura-2 but has a dual emission peak ***(Figure 1.11)***.

1.3.3. Monomer-Eximer Formation.

The formation of excited state collision complexes (excited dimers) can take place between two identical fluorophores (excimer) or two distinct fluorophores (exciplex). Both excimer and exciplex involve the association of an excited state species with a ground state entity if one comes into close approach to another during the lifetime of the excited state (***Scheme 1.5***).

The net stabilization that results from this type of interaction lengthens the lifetime of the excited state dimer. The absence of an absorbtion band arising from the dimer indicates that any ground state association is considerably weak.

$$M^* + N \rightarrow M^* - N \text{ (exciplex)}$$

$$M^* + M \rightarrow M^* - M \text{ (excimer)}$$

$$N^* + N \rightarrow N^* - N \text{ (excimer)}$$

Scheme 1.5. Schematic representation of the excited state complex formation. (Organic molecules capable of such type of complexation are designated as M and N).

Excimer formation is most often observed for planar, aromatic hydrocarbons that are capable of π-stacking interaction. The aggregation process is controlled by diffusion, monomer concentration and solvent viscosity. Pyrene is a classic example that illustrates this π-stacking interaction (***Figure 1.12***).

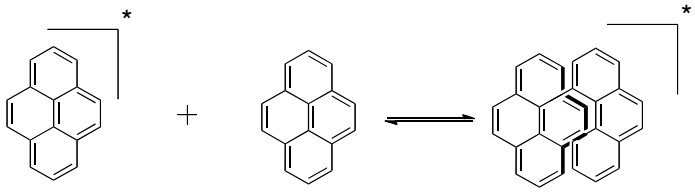

Figure 1.12. *Excimer formation by pyrene.*

At concentration below approximately 5×10^{-5}M, the fluorescence emission from pyrene in *n*-heptane is virtually concentration-independent and is composed of pure monomer fluorescence. As the concentration of pyrene increases, two effects are observed. Firstly, a new fluorescence emission band appears at longer wavelength relative to the monomer emission, and secondly, the intensity of the monomer emission decreases as this new band increases.

The enhanced stabilization of a M^*A collision pair can be explained by means of simple theory of MO interactions. The major interaction for M and N collision will be between their HOMO and LUMO. Combination of the HOMO of the M with the HOMO of the N will yield two new HOMO's of the complex. The same can be applied for the LUMO's. Due to splitting of orbitals one orbital in the collision complex and exciplex (and respectively excimer) will be higher in energy and the second orbital will be lower in energy relative to the original HOMO's. Similarly, the LUMO's of the collision complex split in energy above and below the original LUMO's.

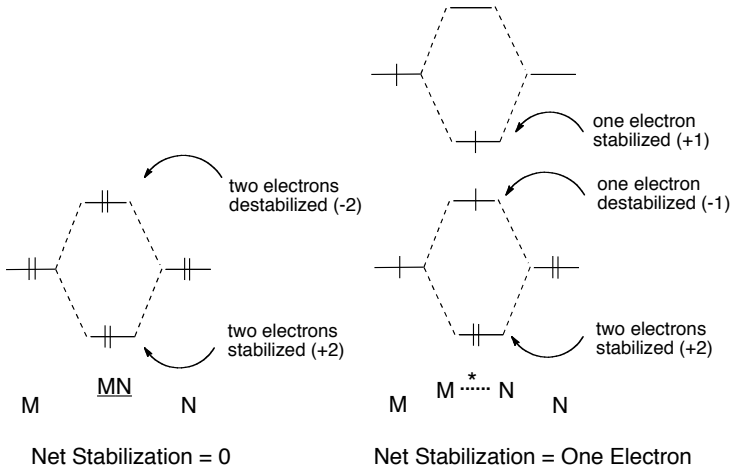

Scheme 1.6. Orbital Interaction of MN collision pairs and MN^* exciplex [20].

In the collision complex of M and N, the four electrons will occupy the new set of HOMO's. No gain in energy can be achieved (***Scheme 1.6, left***). In the exciplex (or excimer), however, since one of the partners is electronically excited, three electrons are stabilized and only one electron is destabilized. Such electron distribution leads to the gain in energy upon formation of exciplex (***Scheme 1.6, right)*** [20].

Tha same scheme is applicable to the intramolecular exciplex formation

Bifluorophoric molecules consisting of two identical fluorophores linked by a short flexible chain may form an excimer. In such case fluorescence signaling takes place *via* a decrease in the ratio of monomer to excimer (or exciplex) emission. Binding of an appropriate analyte results in a conformational rearrangement and in a decrease in the effective distance between the respective π-systems of the bichromophoric pair (***Scheme 1.7)***. In practice, one observes the appearance of longer wavelength emission that increases in intensity as a function of guest concentration.

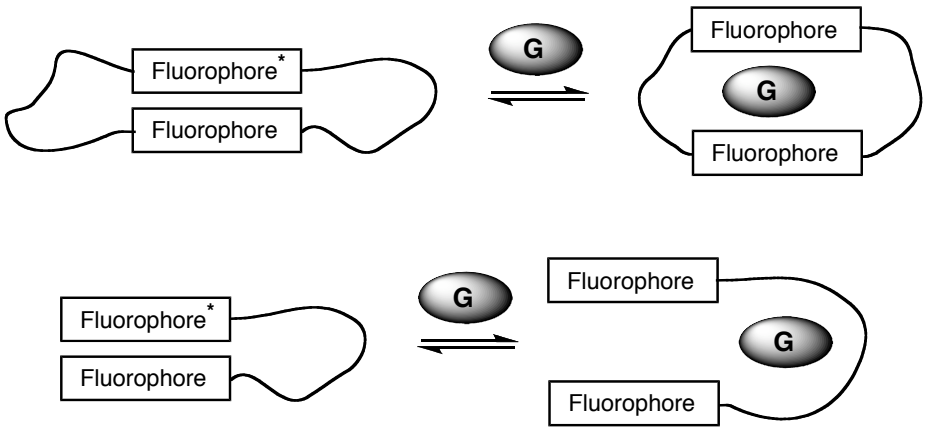

Scheme 1.7. Monomer formation upon complexation.

There exist fluorescent systems, in which guest incorporation increases the ratio of monomer to excimer (or exciplex) emission. Schematically this can be depicted as follows (***Scheme 1.7***).

This basic signaling principle has been utilized in various coronands, podands, calixarenes, and cyclodextrins containing π-framework of pyrene, anthracene, or naphthalene.

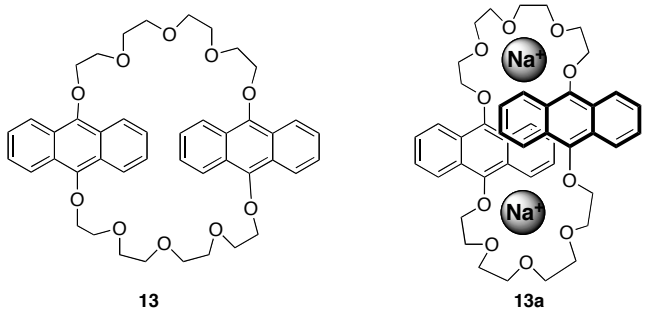

Figure 1.13. Excimer-forming bisantraceno-crown sensor [9].

The bisanthraceno-crown ether (**13**) exhibits a fluorescence spectrum composed of the characteristic monomer and excimer bands. Gradual addition of sodium perchlorate to a solution in methanol induces a decrease in the monomer band and an increase in the excimer band. Complexation is expected to bring closer together the two anthracene units which favors excimer formation. A 1:2 complex is formed (***Figure 1.13***) [21].

Host molecules with more than one pyrenyl group can form excimer by two different mechanisms. One demonstrates described above π-π stacking of the pyrene rings in the free state, which leads to the characteristic decrease of the excimer emission intensity and the concomitant increase of monomer emission. The second mechanism is owing to interaction of an excited pyrene unit with ground-state pyrene molecule.

The noncyclic ethers (**14a-d**) with two pyrenes at the both terminals of polyoxyethylene compounds show strong intramolecular excimer formation at around 480 nm. On the complexation with alkaline earth metal cations, the increase of monomer emission at around 400 nm accompanied by the disappearance of intramolecular excimer emission was observed. Compound (**14b**) showed the response specific for Li^+ and Mg^{2+}. Compound (**14c-d**) responded strongly to alkaline earth cations Ca^{2+}, Sr^{2+} and Ba^{2+} (***Figure 1.14***) [22].

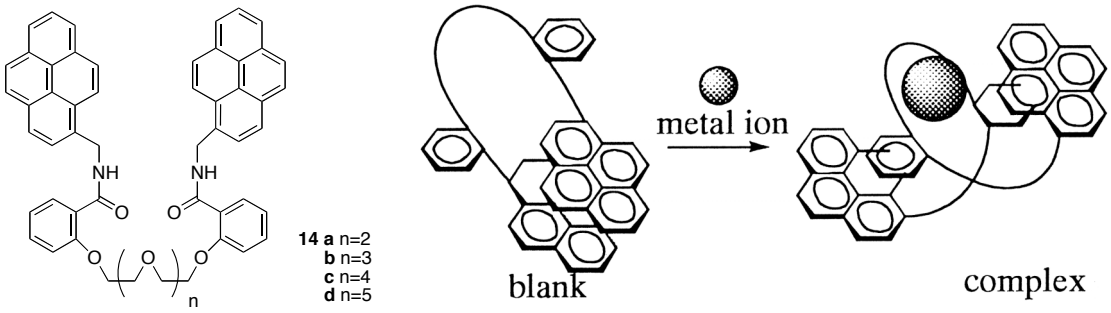

Figure 1.14. Proposed conformational change before and after complex formation on the ground state [22].

A very interesting example is compound (**15**), which combines photoinduced-charge transfer (PCT) and excimer formation and contains two cation recognition sites, a crown ether ring and two facing pyrenamide groups. Compound (**15**) displays both monomer (λ_{em}=384 nm) and excimer (λ_{em}=484 nm) fluorescence emission. Titration of (**15**) with Pb^{2+} and Cu^{2+} gives a decrease in fluorescence intensity for both bands. Pb^{2+} is reported to coordinate by the oxygen atom of an amide ligand, while the nitrogen atom coordinates Cu^{2+}.

Formation of a *dynamic* (a dimer formed in the excited state) or *static* (a dimer formed in the ground state) excimer [23] is depended on the distance between two pyrene moieties. Based on λ_{em}^{max} and its shift upon complexation the copper complex has been assigned to the *static* excimer. When Cu^{2+} is added to the solution of **15**, the distance between the two pyrenes becomes shorter due to the formation of $NH^{\cdots}Cu^{2+\cdots}NH$ binding. In the case of Pb^{2+}, the distance between two pyren units is lengthened because of $C{=}O^{\cdots}Pb^{2+\cdots}O{=}C$ binding.

Interestingly, the addition of K^+ causes the change in fluorescence different from that observed upon addition of Pb^{2+} and Cu^{2+}. An increase in excimer emission could be seen. It can be speculated, that K^+ makes a HOMO-LUMO interaction of two pyrene units more favorable in the excited state than those in the ground state. Addition of K^+ to the **15**·Pb^{2+} complex causes ion exchange process and both the excimer and monomer bands are gradually reforming (***Figure 1.15***) [24].

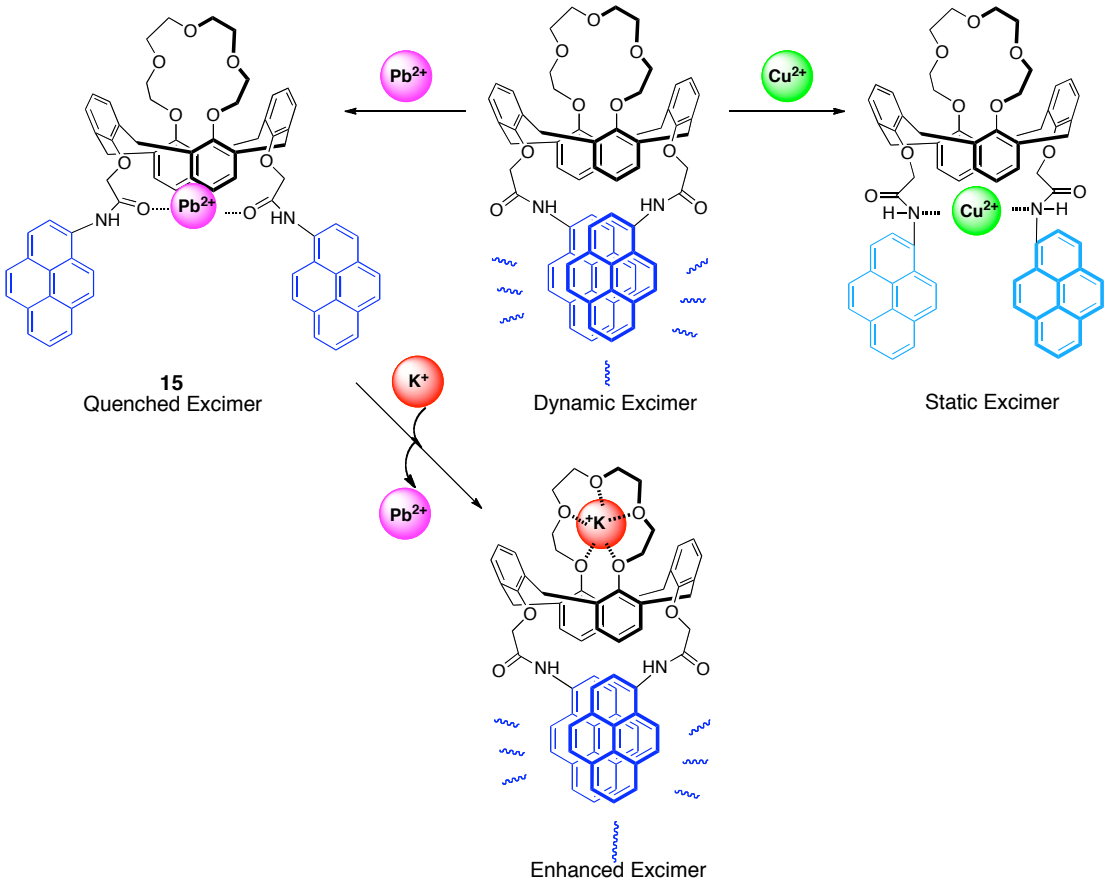

Figure 1.15. Double-Site Calix[4]crown Fluoroionophore [24].

The concept of unstacking of the fluorophore to achieve enhanced monomer emission was realized in cryptand (**16**) capable of encapsulating α,ω-heptamethylendiammoniumcation $NH_3^+(CH_2)_7NH_3^+$. This was the first example of optical detection of a linear molecular cation (***Figure 1.16)*** [25].

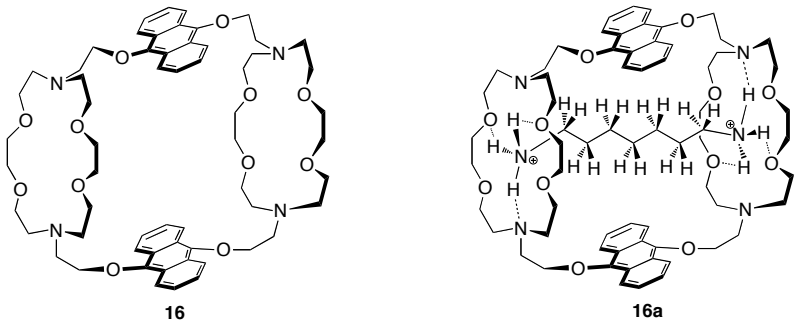

Figure 1.16. Cryptand exhibiting enhanced monomer emission upon binding and the hypothetical structure of the inclusion complex [26].

1.3.4. Electronic Energy Transfer (EET).

This is another signaling mechanism, which fluorescent chemosensors can be relied on. Energy transfer occurs according to ***Scheme 1.8*** from an excited part of the molecule (donor) to another that is chemically different (acceptor; can be linked by a spacer with the donor).

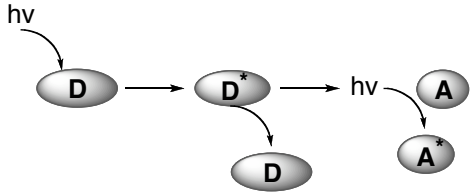

$$D^* + A \rightarrow D + A^*$$

Scheme 1.8. Mechanism of "trivial" radiative energy transfer.

A simple emission of a quantum of light by one molecule followed by absorption of the emitted light by a second molecule is sometimes referred to as the "trivial" mechanism. The difference from PET is that the net result of EET is transfer of the excitation energy from a donor to an acceptor, whereas PET initially excites the acceptor, however donor is never converted to an excited state (photoinduced electron transfer takes place from the ground state of the donor).

One should distinguish between radiative and non-radiative transfer. As described above during radiative transfer a molecule A absorbs a photon emitted by a molecule D. The average distance between A and D should be larger than the wavelength. This kind of transfer does not require any interaction between A and D, but is dependent on the spectral overlap and on the concentration. Non-radiative transfer takes place without emission of photons at distances less than the excitation wavelength and is a result of an interaction between molecules [16]. There are four major factors, on which the rate of energy absorption by A is dependent: i. fluorescent quantum yield of D, ii. the concentration of A, iii. the overlap of the emission spectra of D and the absorption spectra of A, iv. distance between D and A. Spectral overlap integral *J* is defined as

$$J \equiv \int_0^\infty I_D \varepsilon_A \mathrm{d}v$$

Equation 1.1.

where I_D is a graph of the experimental emission of D, ε_A is a graph of experimental absorbtion spectrum of A, both plotted on an energy scale and normalized so that complete overlap would correspond to J=1 [20].

Non-radiative energy transfer occurs over short distances (≤ 100 Å), requires some interaction between a donor and an acceptor molecule and is very sensitive to variations in donor-acceptor separations. The term *resonance energy transfer* (RET) was introduced because if the emission spectra of the donor overlaps the absorbtion spectra of acceptor, several vibronic transitions in the donor have practically the same energy as the corresponding transitions in the acceptor, so they are coupled in resonance.

Two different mechanisms exist for energy transfer because the total interaction energy can be expressed as a sum of two terms: a *Coulombic term* U_c and an *exchange term* U_{ex}. The interaction therefore may be Coulombic (also called Förster-type or induced-dipole energy transfer) and/or due to intermolecular orbital overlap (often called Dexter-type or collision EET). These two ideas can be visualized as it is illustrated on ***Scheme 1.9***.

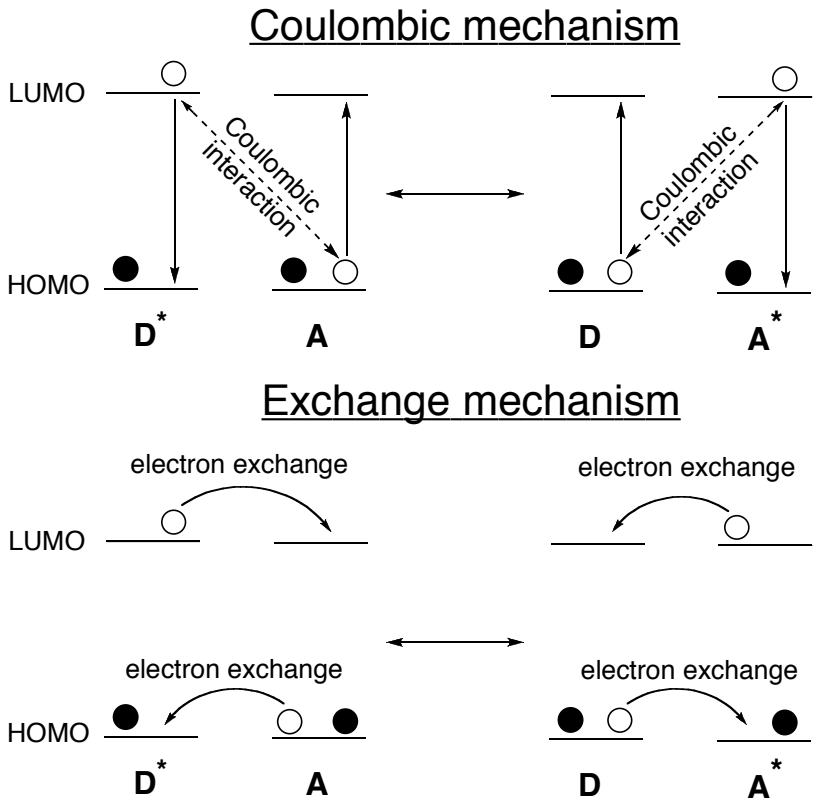

Scheme 1.9. Simplified schematic orbital representation of the Coulombic and Exchange mechanisms of EET.

The solid circles on the picture are so-called "passive" electrons whose interactions with other electrons are assumed to be almost constant during the energy transfer. The open circles indicate electrons that actively participate in the EET process either of two mechanisms. The Coulombic interaction is shown by the dotted line, which represents electrostatic interaction between an electron in the LUMO of the excited D and an electron in the HOMO of the ground state A. The orbital motions or oscillations of the excited electron in D^* cause perturbation of the orbital motions of electron in the ground state of A. If resonance occur, then the electron on A may be set into oscillatory motion as the electron on D^* relaxes. Such energy transfer does not require physical contact of the interacting partners.

Exchange mechanism of EET is characterized by the overlap of the electron cloud in the LUMO of D^* with the LUMO of the ground state of A and the overlap of an electron cloud in the HOMO of A with HOMO of the excited D^*. In the extreme case, charge transfer occur and the electron in the LUMO of D^* jumps to the LUMO of A whereas the electron in the HOMO of A jumps to the HOMO of D^*. Such interaction leads to the collisionally-induced energy transfer from the donor to the acceptor and requires physical contact between D and A.

The ***Equation 1.2*** derived by Förster shows factors on which the Coulombic induced-dipole interaction is dependent and how the magnitude of this interaction relates to k_{ET} (the rate constant for transfer between a donor and an acceptor).

$$k_{ET} = \frac{\mathrm{k}^2 \, k_D^{\circ}}{r_{DA}^6} J(\varepsilon_A)$$

Equation 1.2.

The constant will be determined by the experimental conditions such as solvent refraction index and concentration (k). k^2 shows that the interaction between two oscillating dipoles depends on the orientation of the dipoles in space. For a random distribution of interacting dipoles, k^2 is a constant and equal to 2/3. The term $J(\varepsilon_A)$ is the spectral overlap integral whereas the extinction coefficient of the acceptor is included in the integration, k_D is the pure radiative rate of the donor, r is the distance between D and A [20].

The ***Equation 1.2*** can be rewritten taking into account Förster critical transfer radius R_0 (a distance at which transfer and spontaneous decay of the excited donor are

equally probable, i.e. $k_T = 1/\tau_D^0$) and the excited-state lifetime of the donor in the absence of transfer:

$$k_T = \frac{1}{\tau_D^0}\left[\frac{R_0}{r}\right]^6$$

Equation 1.3.

The efficiency of energy transfer is given by

$$\phi_{ET} = \frac{k_{ET}}{\tau_D^{-1} + k_{ET}} = \frac{1}{1 + (r/R^6)}$$

Equation 1.4.

The sixth power dependence accounts for the sensitivity of energy transfer to the donor-acceptor distance when it is comparable to the Förster critical radius [16].

RET has been widely used to determine distances in biomolecules and supramolecular units. The distance between D and A should be >10 Å in order to avoid short-range interactions.

For molecular sensing purposes of particular interest are bichromophoric molecules consisting of a donor and an acceptor linked by a spacer. Since EET is distance and orientation dependent it is possible to modify the rate of transfer by inducing changes in these two parameters by means of an external perturbation. One basic opportunity is to make the chain (linker) form a complex with metal cations causing the external perturbation. Molecule (**17**) called DXA is an example (***Figure 1.17***).

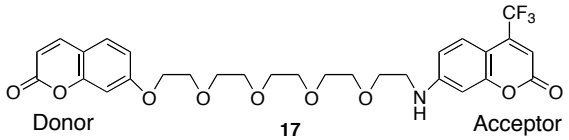

17

Figure 1.17.

This sensor consists of two coumarins (one donor and one acceptor) and a linker of the crown-type capable of complexation with cations. The addition of Pb^{2+} brings the donor and acceptor coumarins into closer proximity leading to change in EET efficiency. Change in excitation and emission spectra allows detection of lead ions [27].

Molecule **18** (***Figure 1.18***) demonstrates a combination of hydroxyphenyltriazole derivative (in blue) showing a very high ability to detect Al^{3+} ions and Coumarin 343 connected by an ethylene spacer [28].

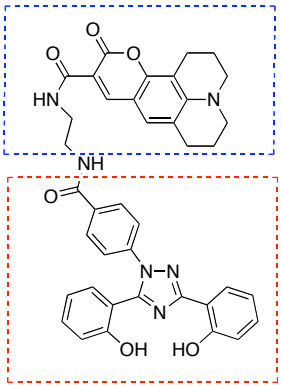

18

Figure 1.18.

The absorbance of coumarin overlaps well with the weak emission of the Al^{3+}-complex, which can act as a donor in EET.

Electronic energy transfer concept was employed to design fluorescent chemosensors for neutral organic molecules. Still's laboratory produced the first small FRET-based molecule sensors for peptides **19** [29]. Small peptides are highly flexible, what makes their detection difficult. Compound **19** is based on synthetic, amide-linked oligomer of isophtalic acid and a cyclic *trans*-1,2-diamine derivative. This sensor bindes only one tripeptide sequence for every ≈1600 sequences in the library used (***Figure 1.19***).

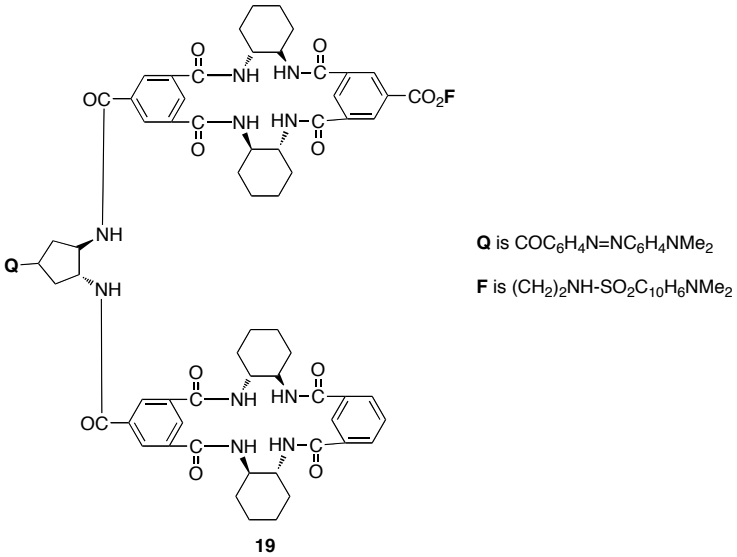

19

Figure 1.19.

1.3.5. Conformational Restriction.

1.3.5.1. A New Luminescence Signaling Mechanism.

Thus far, photoinduced electorn transfer (PET) and intramolecular charge transfer (ICT) based fluorescent chemosensors categorize the majority of luminescent molecular sensors.

In the last decade a new approach to the development of fluorescent chemosensors based on a signal transduction pathway in which metal binding induces conformational restriction of the fluorophore, resulting in enhanced fluorescence has been described [30, 31].

The interaction between reporter and receptor that is responsible for signaling event necessitates that the two entities be in close proximity and communicate electronically. Therefore the design of fluorescent chemosensors relying on common mechanisms is determined by several factors:

- the presence of atoms that can interact with the desired analyt (an ion or a neutral molecule)
- the arrangement of atoms must allow electron transfer or charge transfer
- the distance between reporter and receptor must be minimal (this however may preclude positive signaling of most redox active metals and heavy metals that are known to quench fluorescence)

However, every signaling mechanism places limitations on potential receptor structure, and no single mechanism will be universally suitable. There is thus continued need for the development of new ways to turn recognition events into changes in fluorescence.

It is well established that more rigid fluorophores are more fluorescent.

The idea of the rigidification of the diboronic acid skeleton upon formation of macrocycles with saccharides was used in the design of the first fluorescent chemosensor for disaccharides (***Figure 1.20)*** presented by Shinkai and coworkers in 1994 [32]. The main path of nonradiative deactivation of the lowest excited singlet state of stilbene is known to be *via* rotation of the ethylenic double bond. In the described system fluorescence of stilbene-3,3'-boronic acid increases upon binding to disaccharides in basic aqueous media.

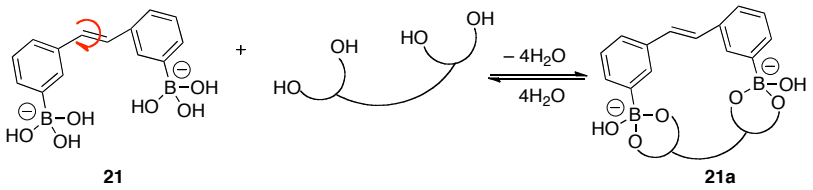

Figure 1.20.

This fluorescence increase was attributed to the formation of a cyclic complex of diboronic acid with the disaccharides and subsequent freezing of ethylenic bond rotation in the excited state.

This example shows that modulation of two π systems comprising a single fluorophore is an attractive alternative to the common mechanisms used in the fluorescent chemosensor design.

The observation that the quantum yield (ϕ) of dihydrophenantrene is approximately 50-fold greater than that of 2,2'-dimethylbiphenyl (***Figure 1.21***) stimulated the investigation of biphenyl derivatives [30].

ϕ=0.01 ϕ=0.55

Figure 1.21. Quantum yield of reference biaryls.

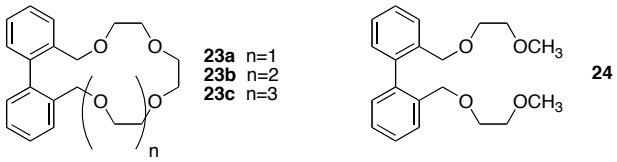

Figure 1.22. Biarylfluorescen chemosensors [30].

It was found, that **23b** (***Figure 1.22***) respondes selectively to Ca^{2+} in acetonitrile solution. A hypsochromic shift (~15 nm) was observed accompanied by a 4-fold fluorescence enhancement. The origin of fluorescent enhancement upon complexation was refered to the reduction of the efficiency of ISC [30]. These results were complemented by studying the properties of other simplest fluorescent compounds with appreciable conformational flexibility, namely diphenylacetylene (DPA) derivatives (***Figure 1.23***).

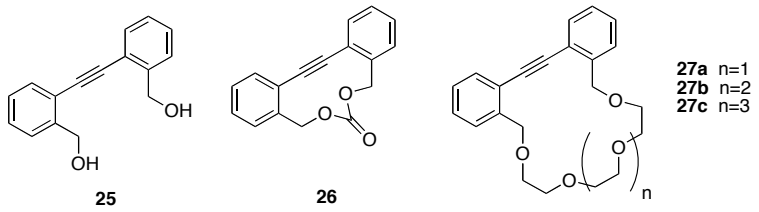

25 26

Figure 1.23. Tolan based fluorescent chemosensors [31].

The addition of alkali (Li^+, Na^+, K^+) and alkaline earth metal cations (Mg^{2+}, Ca^{2+}) led to the fluorescence intensity increase. Of the three crowns, **27a** is the most discriminating, with a strong preference for Li^+ and Ca^{2+}, while **27b** and **c** exhibited less selective binding. Through the determination of photophysical properties in these fluorophores it was postulated that conformational restriction leads to a reduction in the rate of internal conversion (k_{IC}).

These results demonstrated that conformational restriction could be used as a signaling mechanism to perturb the two fundamental non-radiative deactivation pathways for most common organic fluorophores; intersystem crossing (k_{ISC}) and internal conversion (k_{IC}). As an extension of this work with the aim to find a fluorophore with a longer emission wavelength than that of biaryls, an investigation into the biarylpyridine fluorophore scaffold was conducted.

1.3.5.2. 2,6-Biarylpyridines: Dual-Signaling Fluorescent Chemosensors.

In 2001 a series of interesting fluoroionophores consisting of a rotable biaryl fluorophore and an oligoethyleneglycol chain was designed and synthesized [33]. Biarylpyridines were chosen because of their synthetic accessibility and modest fluorescence emission from the locally excited state (LE) (***Figure 1.24)***.

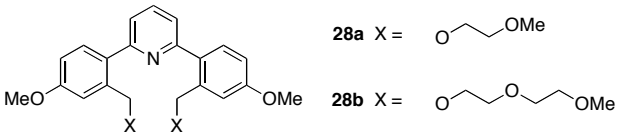

Figure 1.24. Biarylpyridine fluoroionophores [33].

Biarylpyridine **28a** is capable of uniquely identifying Li^+, Mg^{2+} and Ca^{2+} ions through selective increase or diminution of the corresponding LE or CT emission, while **28b** can readily distinguish Mg^{2+} and Ca^{2+} ions.

A further comprehensive structural study lead to the identification of promising long wavelength biarylpyridine system, which possesses optimal photophysical properties [34] such as low initial quantum yield and emission in the visible region (***Figure 1.25***).

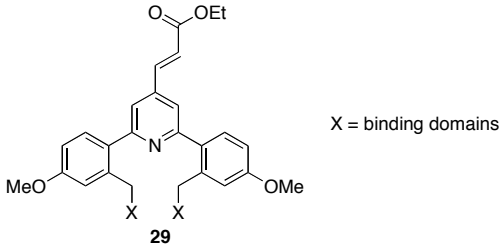

Figure 1.25.

The underlying principle of this particular system and its main advantage is that each binding event leads to conformational restriction and fluorescence enhancement as a result (***Scheme 1.10***). This allows for wide structural variations and binding domains of any nature can be attached to the core fluorophore **29**.

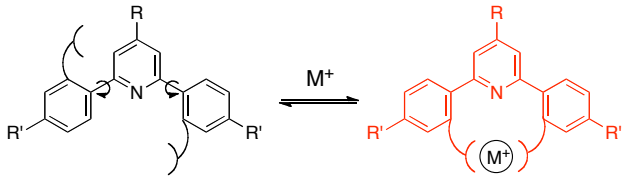

Scheme 1.10.

To broaden the use of the novel biarylpyridine system and to search for new binding events a combinatorial discovery of fluorescent chemosensors was established. It is stated that with this approach it is no longer necessary to synthesize and test prospective molecular sensors one-at-a-time for binding affinity and selectivity. Instead, it is possible to construct libraries that can be screened simultaneously for activity. The library of 198 potential fluorescent chemosensors was prepared. The fluorophore precursor 2,6-biarylpyridine-4-vinylcarboxylate was attached to PEG-derivatized aminomethyl polystyrene.

This approach was approved by the ease with which a new class of Hg^{2+}-responsive chemosensors was found. The response of library element **30a** was confirmed by the synthesis of a solution-phase analogue **30b** (***Figure 1.26)*** [35].

Titration of **30b** in CH_3CN revealed $K_a=1.8 \times 10^{-6}$ M^{-1} for the formation of Hg^{2+} complex.

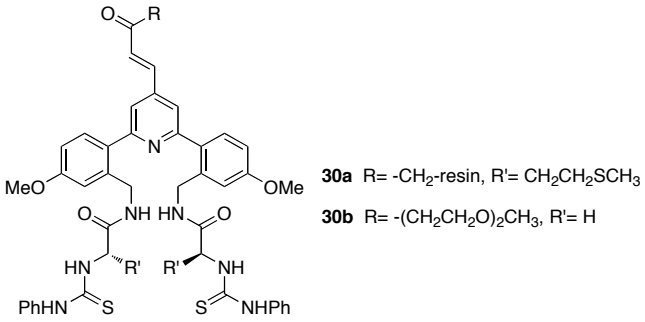

Figure 1.26. Solid- and solution-phase chemosensors for Hg^{2+}.

Beside biarylpyridine core fluorophores other dyes were used in the conformational restriction approach. An interesting implication of the conformational restriction was shown on boron-dipyromethene derivatives **31**, which were used in preparation of higly sodium-selective fluoroionophore (***Figure 1.27)*** [36]. Boron-dipyromethene derivatives have the advantage that the absorbtion and emission wavelengths are adjustable by replacing appropriate substituents. To convert the metal binding event into a change in a dihedral angle, the oligoethyleneglycol bridge is introduced between each of the m-position on the 3- and 5-phenyl rings.

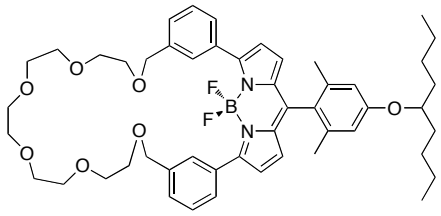

31

Figure 1.27. Boron-dipyrromethene fluoroionophore.

A representative example of anion detection by the conformational restriction of 2,2'-binaphthalene derivatives was published by S. Kondo and M. Sato (***Figure 1.28***) [37].

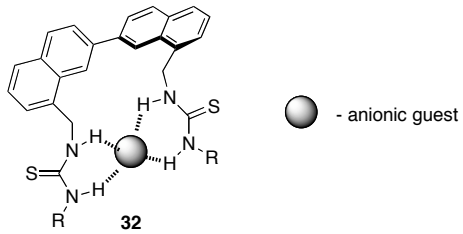

32

Figure 1.28. Suggested structure of anionic complex.

Here a 2,2'-binaphthalene bearing two thiourea moieties exhibited high selectivity for AcO^-, and F^-, however addition of F^- induces a different change in fluorescent spectrum. The stoichiometry of complex formation was shown to be 1:1.

1.4. Conclusion.

Fluorescent chemosensors are powerful tools for the detection of cationic, anionic and neutral species as well as for the measurements of the concentration of certain analytes in biological and environmental samples. The most common signaling mechanisms for the development of fluorescent chemosensors remain photoinduced electron transfer (PET), internal charge transfer (ICT), monomer-excimer formation, electronic energy transfer (EET), whereas PET is the most widely used mechanism.
Relatively recently a new approach to the development of fluorescent chemosensors based on binding induced conformational restriction was described. Biaryl chromophores such as biphenyl and biphenylacetylene were used at first. Later on biarylpyridines were chosen for the further development of the above-mentioned approach. On the basis of this core fluorophore fluorescent chemosensors with polyether ligands were discovered. Further extension to the construction of a solid-state combinatorial library of potential chemosensors lead to the discovery of new fluoroionophores for Hg (II). The key advantage of the new approach minimization of structural limitations on potential binding domains because the signaling mechanism is independent of the structure of the binding domain.
It is evident, that understanding of minimal structural requirements to the binding domains will lead to further validation of the binding-induced conformational restriction as a general signaling mechanism and facilitate an intelligent experimental design of novel fluorescent chemosensors.

References.

[1] Harvey, N., *A History of Luminescence*, **1957**.

[2] Lakowicz, J.R. *Principles of Fluorescent Spectroscopy*, **1999**.

[3] Czarnik, A. *Fluorescent Chemosensors for Ion and Molecule Recognition*. ACS Symposium Series, **1992**, Washington: American Chemical Society.

[4] Martinez-Manez, R., Sancenon, F. *Chem. Rev.* **2003**, 103, 4419.

[5] Weller, A. *Pure Appl. Chem.* **1968**, 16, 115.

[6] de Silva, A.P., Rupasinghe, A. D. D. *J. Chem. Soc., Chem. Commun.* **1985**, 1969.

[7] Czarnik, A. *Acc. Chem. Res.* **1994**, 27, 302.

[8] James, T., Sandanayake K. R. A. S., Shinkai S. *Nature*, **1995**, **374**, 345.

[9] Valeur, B., Leray, I. *Coordination Chemistry Reviews* **2000**, 205, 3.

[10] Lippert E., Boos H. *Advances in Molecular Spectroscopy* **1962**, Pergamon Press, London, 443.

[11] Köhler, G., Wolschann, P., Rotkiewicz, K. *Indian Acad. Sci. (Chem. Sci.)*, **1992**, 104, 197.

[12] Grabowski, Z.R., Rotkiewicz K. *Chem. Rev.* **2003**, 103, 3899.

[13] Siemiarczuk, A., Grabowski, Z. R., Krowczynski, A., Asher, M., Ottolenghi, M. *Chem. Phys. Lett*. **1977**, 51, 315.

[14] Grabowski, Z.R., Rotkiewicz K., Siemiarczuk, A., *J. Lumin.* **1979**, 18/19, 420.

[15] Rotkiewicz, K., Grellmann, K., H., Grabowski, Z. R. *Chem. Phys. Lett.* **1973**, 315.

[16] Valeur, B., *Molecular Fluorescence*, **2002**, WILEY-VCH.

[17] Bourson, J., Valeur B., *J. Phys. Chem.* **1989**, 93, 3871.

[18] Bourson, J., Pouget, J., Valeur B. *J. Phys. Chem.* **1993**, 97, 4552.

[19] Grynkiewicz, G., Tsien, R. *J. Biol. Chem.* **1985**, 260, 3440.

[20] Turro, N.J. *Modern Molecular Photochemistry* **1991**, University Science Books.

[21] Bouas-Laurent, H., Castellan, A., Daney, M., Desvergne, J.-P., Guinand, G., Marsau, P., Riffaud, M.-H. *J. Am. Chem. Soc.* **1986**, 108, 315.

[22] Suzuki, Y., Morozumi, T., Nakamura, H. *J. Phys. Chem. B* **1998**, 102, 7910.

[23] Winnik, F.M. *Chem. Rev.* **1993**, 93, 587.

[24. Choi, J.K., Kim, S. H., Yoon, J., Lee, K.-H., Bartsch, R., Kim, J. S. *J. Org. Chem.* **2006**, 71, 8011.

[25] Fages, F., Desvergne, J.-P., Bouas-Laurent, H., Lehn, J.-M., Konopelski, J. P., Marsau, P., Barrans, Y. *J. Chem. Soc. Chem. Commun.* **1990**, 655.

[26] Fages, F., Desvergne, J.-P., Kampke, K., Bouas-Laurent, H., Lehn, J.-M. *J. Am. Chem. Soc.* **1993**, 115, 3658.

[27] Valeur, B., Pouget, J., Bourson, J., Kaschke, M., Ernsting, N. P. *J. Phys. Chem.* **1992**, 96, 6545.

[28] Arduini, M., Felluga, F., Mancin, F., Rossi, P., Tecilla, P., Tonellato, U., Velentinuzzi, N. *Chem. Comm.* **2003**, 1606.

[29] Chen, C.-T., Wagner, H., Still, W. C. *Science* **1998**, 279, 851.

[30] McFarland, S.A., Finney, N. S. *J. Am. Chem. Soc.* **2001**, 123, 1260.

[31] McFarland, S.A., Finney, N. S. *J. Am. Chem. Soc.* **2002**, 124, 1178.

[32] Samankumara, K.R., Nakashima, K., Shinkai, S. *J. Chem. Soc. Chem. Commun.* **1994**, 1621.

[33] Mello, J.V., Finney, N. S. *Angew. Chem. Int. Ed.* **2001**, 40, 1536.

[34] Fang, A.G., Mello, J. V., Finney, N. S. *Tetrahedron* **2004**, 60, 11075.

[35] Mello, J.V., Finney, N. S. *J. Am. Chem. Soc.* **2005**, 127, 10124.

[36] Yamada, K., Nomura, Y., Citterio, D., Iwasawa, N., Suzuki, K. *J. Am. Chem. Soc.* **2005**, 127, 6956.

[37] Kondo, S.-i., Sato, M. *Tetrahedron* **2006**, 62, 4844.

Chapter 2.

Efficient Discovery of Fluorescent Chemosensors Based on a Biarylpyridine Scaffold.

2.1. Synthesis.

Previously, on the basis of a biarylpyridine scaffold, fluoroionophores with simple polyether ligands have been prepared [1-4]. This approach was further extended to the construction of a ca. 200-member solid-phase combinatorial library of potential chemosensors with amino acid/acyl end-cap binding domains, leading to the discovery of new fluorescent chemosensor for aqueous Hg^{2+} [5] (*see also* the introductory chapter).

Missing between these two extremes is an evaluation of smaller sets of conjugates of the biarylpyridine core. Given the task of pursuing the lead structures identified in the library, we expanded our efforts to include the concurrent synthesis of other simple biarylpyridines with chelating groups known to have high affinity for cations and anions, such as catechols and guanidines. In the course of these efforts, we took the opportunity to improve the previous synthesis of our core fluorophore in order to make it more accessible.

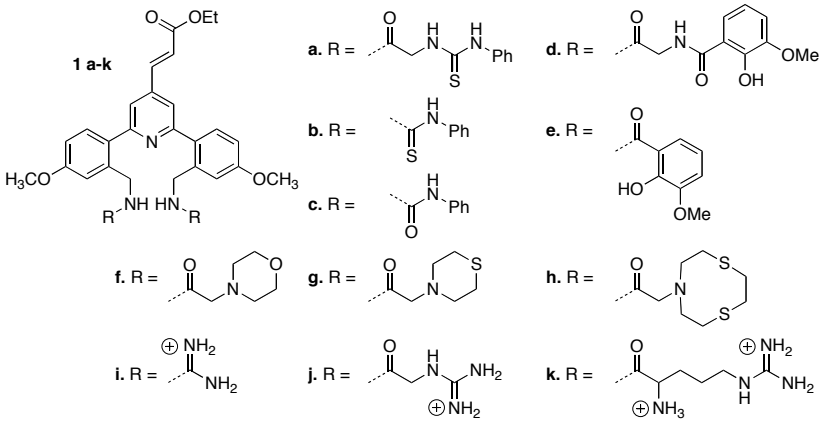

Figure 2.1. Collection of potential fluorescent chemosensors.

We present here a collection of ten compounds, readily prepared from our priveleged scaffold, which we expected might be ion-responsive chemosensors. All are based on fluorophore **1** (***Figure 2.1***, R=H; cations as Cl^- salts), appended in two or three steps with two identical receptor arms. Compounds **1a-h** were anticipated to

display affinity for metal cations, while it was envisioned that **1a**, **1b** and **1i-k** would interact with mono- or dianionic analytes.

The first class of compounds (**1a-c**) consist of a phenylthiourea moiety with or without glycine as a linker, and a urea analog. (**1a** is closely related to the chemosensors discovered from the solid-phase combinatorial library [5]) The second set of fluorophores contains 2-hydroxy-3-methoxy-benzoic acid as a binding domain (**1d**,**e**). The third group comprises simple azacrown ethers (**1f-h**), and in the last guanidine derivatives are appended to the fluorophore (**1i-k**).

The preparation of **1a-k** began with the synthesis of an advanced intermediate that could then be converted to the desired potential chemosensors. The previous synthetic approach to **1** (depicted with dotted lines on all schemes [5]) has been significantly improved, reducing the number of total steps and enhancing the overall yield. (We can now routinely prepare 1-2 gram quantities of the Boc-protected precursor to **1.**)

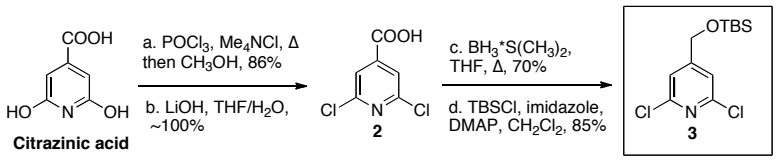

Figure 2.2. Synthesis of the dichloropyridine precursor.

The synthesis of the first key intermediate, **3**, begins with the inexpensive pyridine derivative citrazinic acid (***Figure 2.2***). Treatment with $POCl_3$, quenching with methanol and subsequent saponification provided **2** in good yield. Reduction with BH_3•SMe_2 and protection of the alcohol efficiently provided **3** in an overall yield of 51%.

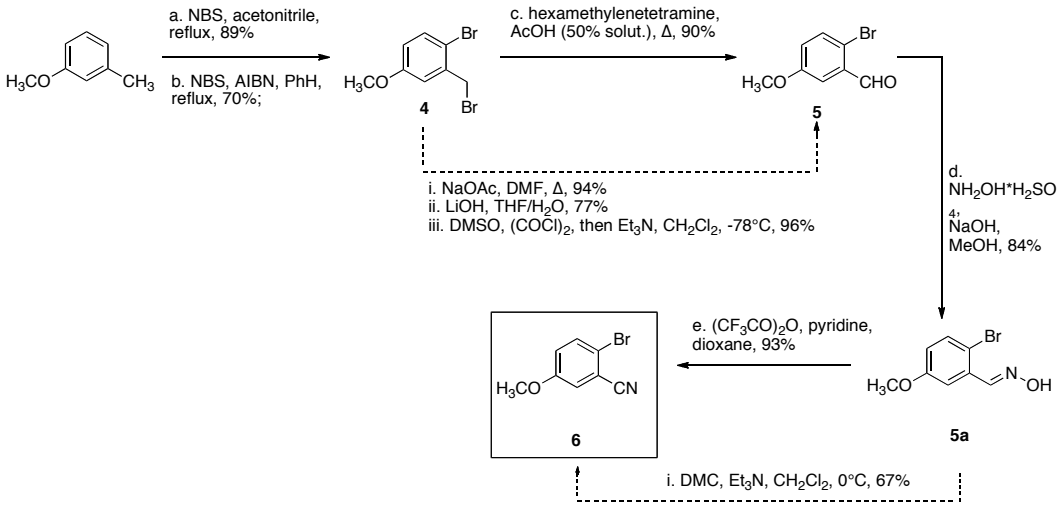

Figure 2.3. Synthesis of the 2-bromo-3-methoxybenzonitrile.

The synthesis of the second key intermediate, **6** (***Figure 2.3***), began with electrophilic bromination of 3-methylanisole followed by radical bromination. Transformation of benzyl bromide **4** to aldehyde **5** via Sommelet reaction [6], followed by conversion to the oxime and dehydration with TFAA [7], provided **6** in an overall yield of 44%.

The aromatic components **3** and **6** were combined via Negishi coupling (***Figure 2.4***). The hydrogenation of the CN groups in **7** proved more reliable than our previous $NiCl_2/NaBH_4$ reduction protocol, and in the presence of Boc anhydride consistently provided reasonable yields of **8**. Removal of the TBS group and subsequent Swern oxidation [8], followed by Wittig-Horner coupling with ethyl phosphonoacetate [9], provided Boc protected diamine **9**, which is a stable and convenient precursor for **1**. This represents an overall net reduction of 3 steps relative to our original route.

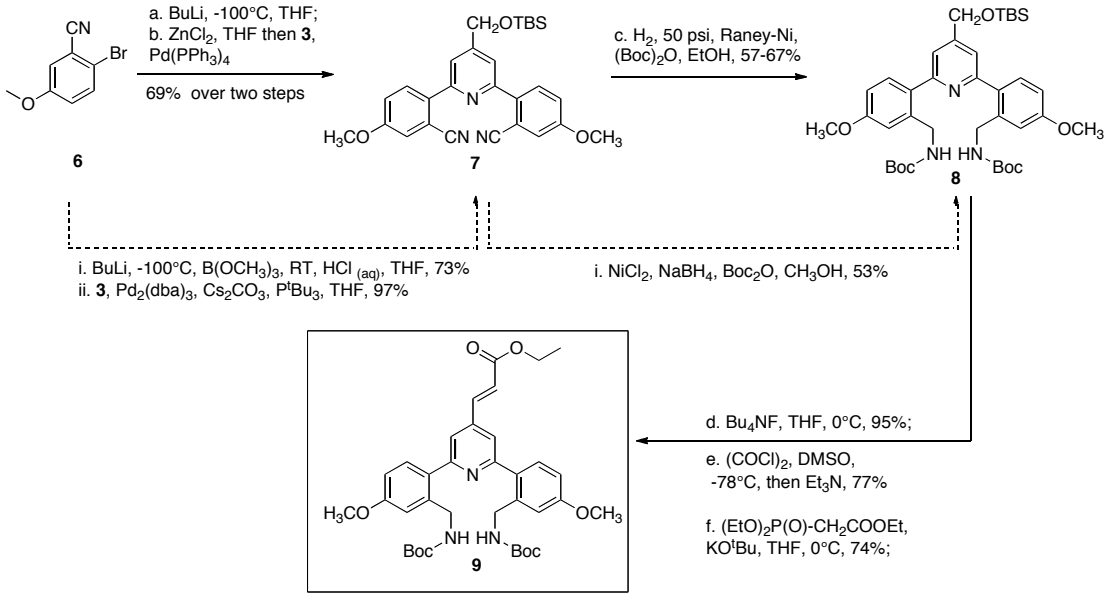

Figure 2.4. Synthesis of the boc-diprotected diamine.

The syntheses of **1a-e** and **i-k** consist of two steps: deprotection of **9** with HCl/dioxane and coupling with the corresponding carboxylic acid.

Several coupling reagents (***Figure 2.5***) were tested until an optimal system was found. EDC in combination with HOAt has emerged as the most suitable reagent and was then used in the synthesis of all library members.

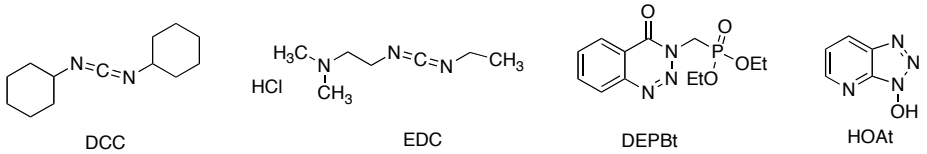

Figure 2.5. Coupling reagents used.

Synthesis of chemosensor **1a** could be achieved through coupling of deprotected **9** with Boc-glycine, subsequent deprotechtion and treatment with phenylisothiocyanite under basic conditions (***Figure 2.6***).

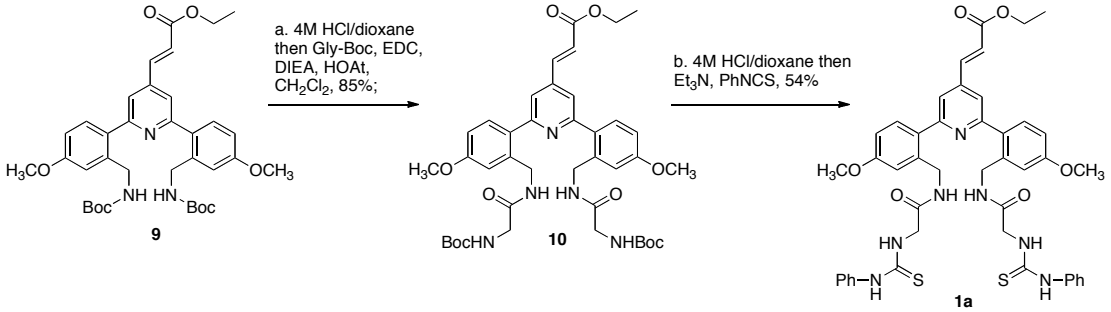

Figure 2.6. Synthesis of the fluorescent chemosensor **1a**.

Reaction with phenylisothiocyanite right after the deprotection of **9** leads to the formation of **1b** (***Figure 2.7***).

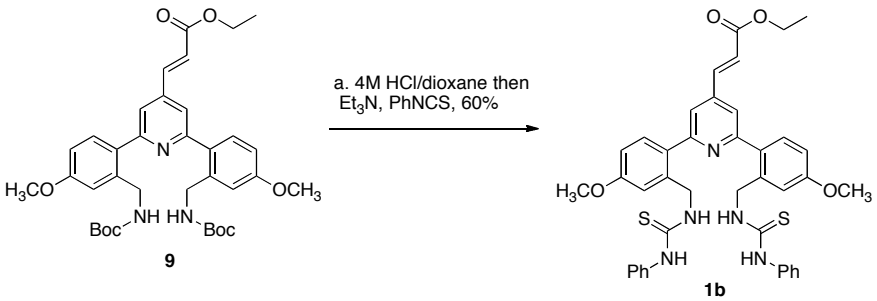

Figure 2.7. Synthesis of the fluorescent chemosensor **1b**.

For **1f-h**, deprotected **9** was coupled with α-bromoacetic acid and then alkylated with morpholine, thiomorpholine or 7-aza-1,4-dithiacyclo-nonane (***Figure 2.8***).

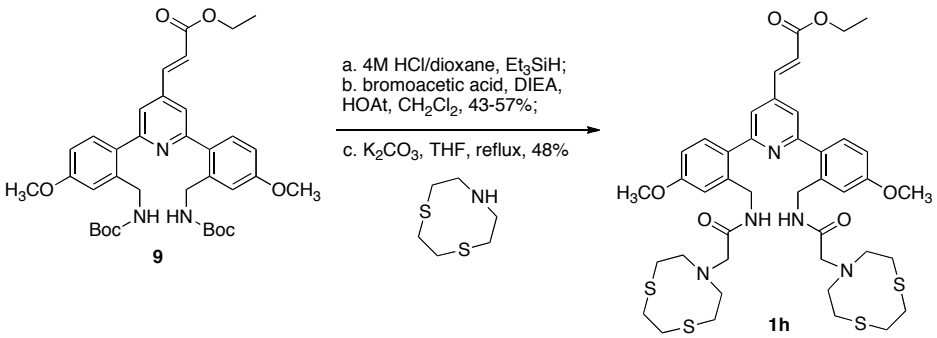

Figure 2.8. Synthesis of the fluorescent chemosensor **1h**.

7-Aza-1,4-dithiacyclo-nonane was prepared from the commercially available bis-(2-chloroethyl) amine hydrochloride (***Figure 2.9***) [10].

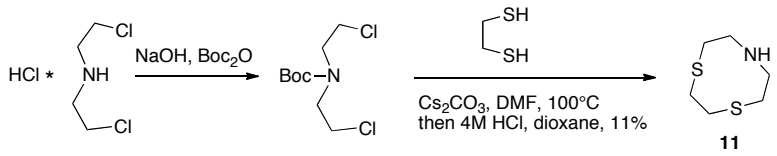

Figure 2.9. Crown-ether synthese.

Preparation of the library member **1i-j** was achieved through the use of diprotected triflylguanidine as a guanidinylation reagent under mild conditions (***Figure 2.10***).

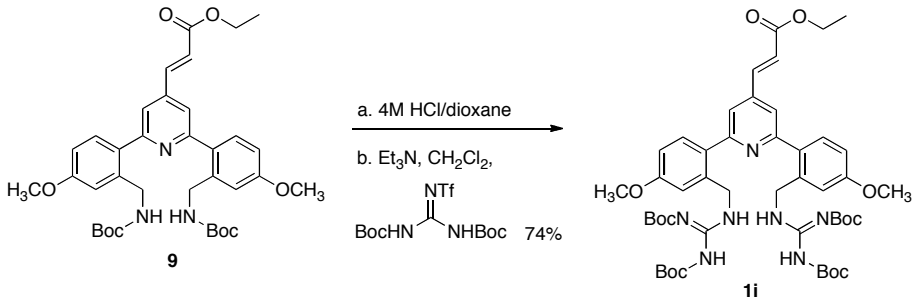

Figure 2.10. Synthesis of the fluorescent chemosensor **1i**.

Diprotected triflylguanidine was obtained in two steps from guanidine hydrocarbonate (***Figure 2.11***) [11].

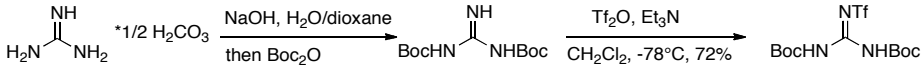

Figure 2.11. Synthesis of guanidine hydrocarbonate.

Synthesis of potential chemosensors **1d-e, k** consists of one (for **1e**, **1k**) or two (for **1d**) subsequent coupling reactions with the corresponding acids.

2.2. Ion Binding Properties.

This collection of potential fluorescent chemosensors was evaluated in the presence of ions chosen on the basis of physiological or environmental relevance. The cations chosen for titration were: Li^+, Na^+, K^+, Cs^+, Ca^{2+}, Ba^{2+}, Sr^{2+}, Cu^{2+}, Zn^{2+}, Cd^{2+}, Pb^{2+}, Ni^{2+}, $Fe^{2+/3+}$, Ag^+ and Hg^{2+}. Anions used were: F^-, Cl^-, Br^-, I^-, SO_4^{2-}, CO_3^{2-}, PO_4^{3-}, ClO_4^-,

acetate, malonate, and oxalate. Li^+, Na^+ and K^+ were added as perchlorate salts, and Ag^+ as its tosylate salt. All other metal ions were added as their chlorides. Anions were added as Li^+ salts except acetate, malonate and oxalate, which were added as their Na^+ salts.

1a-k are only modestly water-soluble, and thus titrations were carried out with 5×10^{-5} M solutions of fluorophore in 1:1 DMSO MOPS (pH 7.4) buffer. Salts were added as 10^{-3} M solutions in the same solvent mixture. Somewhat surprisingly, the majority of titrations led to little or no change in emission intensity. (This will be discussed below.) However, one compound, **1k**, showed some response to the addition of fluoride and iodide ions and three compounds and **1a**, **1b** and **1h** showed strong responses to the addition of Ag(I) and Hg(II) salts (***Table 2.1***).

Compound **1k** exhibited ca. 1.4-fold increase in emission intensity upon addition of F^- and ca. 2.4-fold increase upon addition of I^- (***Figure 2.12***).

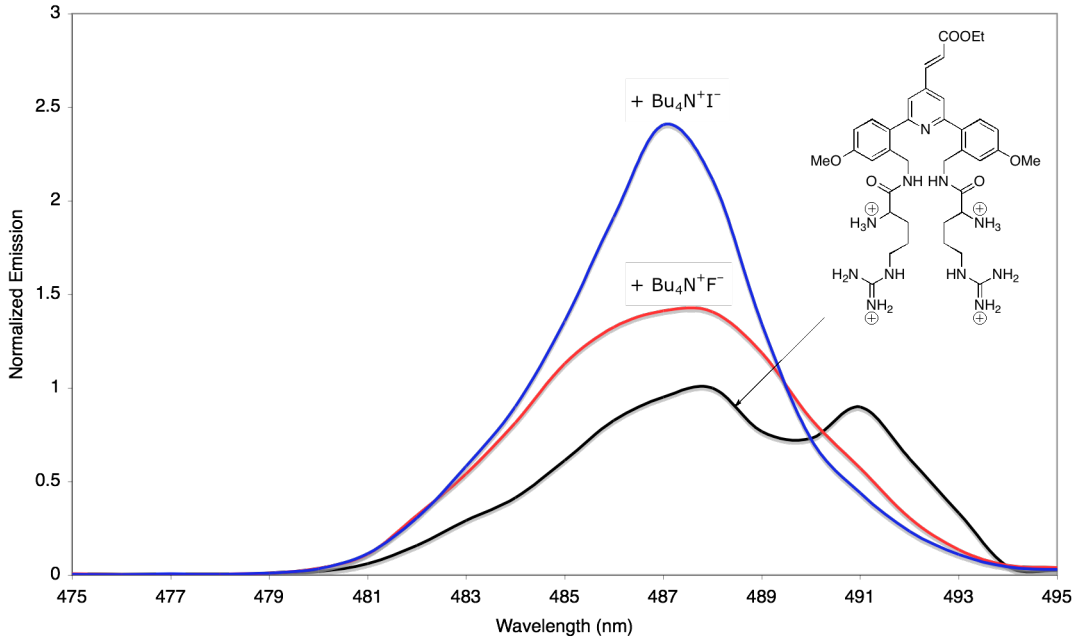

Figure 2.12. Emission of **1k** (10^{-5}M in DMSO/$MOPS_{aq}$) upon addition of crystalline $Bu_4N^+F^-$ and $Bu_4N^+I^-$.

However, the sensitivity of **1k** was so low (response can be seen only if crystalline $Bu_4N^+F^-$ or $Bu_4N^+I^-$ are added) that it can hardly be considered as a fluorescent chemosensor.

The response of **1a** was anticipated, as this is a close analog of the Hg(II)-responsive chemosensors discovered from the previous combinatorial library. Fluorescence emission from **1a** increased ca. 4-fold upon titration with Hg(II) (***Figure 2.13***).

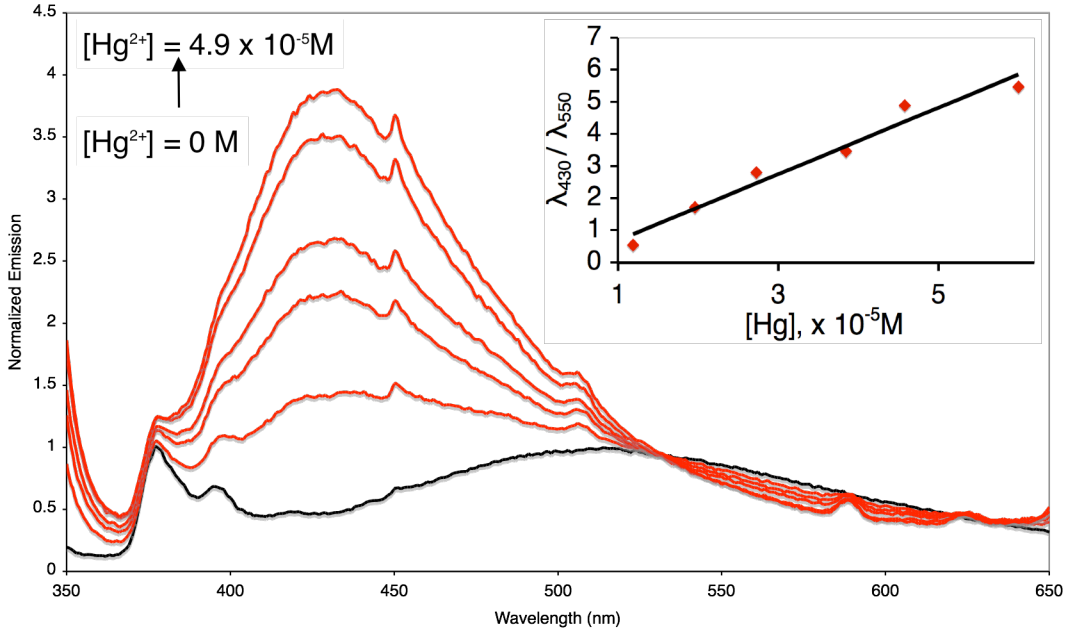

Figure 2.13. Titration of **1a** (5×10^{-5} M) in DMSO/pH 7.4 $MOPS_{aq}$ solution with $HgCl_2$ (***inset:*** Change of I_{430}/I_{550}).

In addition, it exhibited a significant (80 nm) blue-shift in emission – something not observed in the titration of previous biarylpyridine fluorophores. This allows for ratiometric Hg(II) analysis, which can in principle provide more accurate and quantitative measurements of metal ion concentration in biological or other heterogenous media. Using intensity at λ = 550 nm as a measure of [**1a**] and at λ = 430 for [**1a**•Hg(II)], we see an excellent linear correlation up to 1:1 **1a**:Hg(II) (***Figure 2.13, inset***)[1]. Binding to Ag(I) occurs with higher affinity and leads to a larger (ca. 10-fold) enhancement of emission, accompanied by a smaller hypsochromic shift (35 nm), which in turn suggests the possibility of discriminating Hg(II) and Ag(I) with a common chromophore (although we are unable to do this by eye).

[1] Three minor features in the emission spectra warrant comment. Two invariant peaks at ca. 380 and 400 nm arise from impurities in the DMSO/buffer solution that we were not able to remove despite repeated purification. The small spike at ca. 450 nm is a Wood's anomaly characteristic of our fluorimeter.

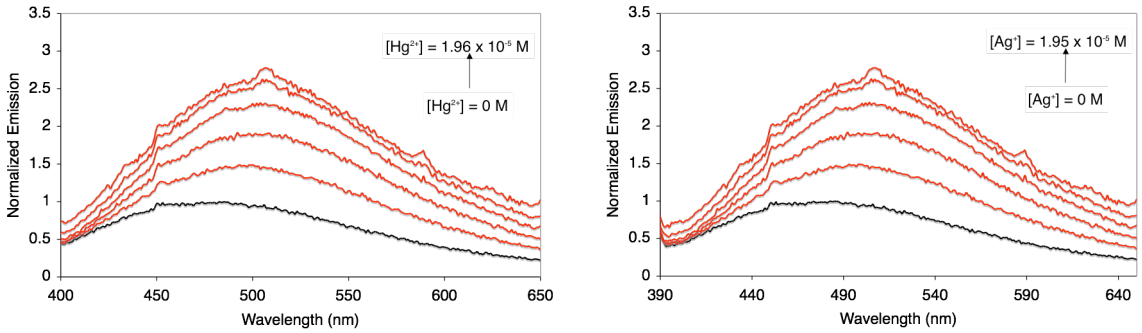

Figure 2.14. Titration of **1b** (5×10^{-5}M) in DMSO/$MOPS_{aq}$ solution with $HgCl_2$(left) and AgOTs (right).

In both cases, we attribute the blue-shift to formation of a more twisted (i.e. less conjugated) yet still conformationally-restricted excited state from the **1a**•metal complexes. Removal of the glycine linker (**1a→1b**) doubles the affinity for mercury and decreases the affinity to silver ions (***Figure 2.14, Table 2.1***). No significant blue shift was observed for either binding event.

Table 2.1. Optical properties and association constants for **1a, b, h.**

1x	ε^a	ϕ^b	K_{eq} 1x•Hg^{2+} $(I/I_0)^c$	K_{eq} 1x•Ag^{+} $(I/I_0)^c$
1a	5.91	0.01	1.97 (4.2)	8.05 (10.1)
1b	5.83	0.01	5.42 (3.0)	1.10 (3.0)
1h	5.79	0.01	17.50 (2.7)	2.45 (2.8)

[a]For longest-wavelength λ_{max}; ε, 10^3 $cm^{-1}M^{-1}$. [b]Relative to pyrene (ϕ=0.32). [c]K_{eq} 10^4 M^{-1}; I/I_0 ratiometric increase of emission at λ_{max} (em); 1:1 DMSO/$MOPS_{aq}$ solution.

While the simple morpholine and thiomorpholine derivatives (**1f**,**g**) did not respond to titration with metal ions, dithioazacrown **1h** exhibits the highest affinity for Hg(II) of any of **1a**/**b**/**h**, as well as responding to Ag(I). Like **1a** and **1b**, **1h** does not respond to the addition of other thiophilic metal ions (***Figure 2.15***).

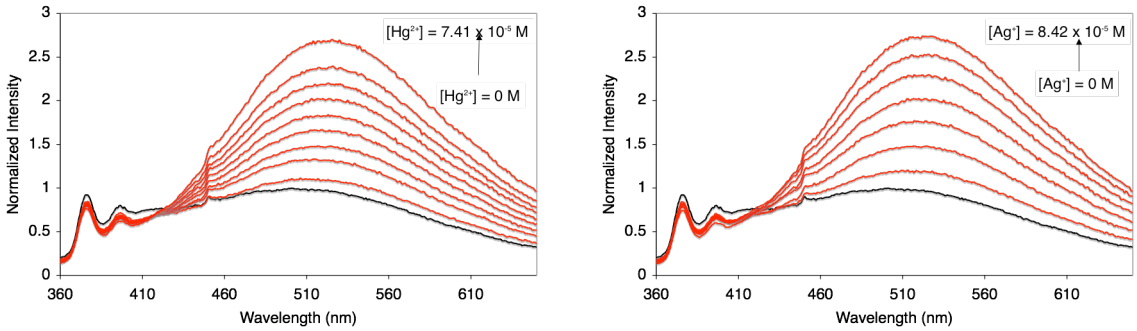

Figure 2.15. Titration of **1h** (5×10^{-5}M) in DMSO/$MOPS_{aq}$ solution with $HgCl_2$(left) and AgOTs (right).

All ligand:Ag(I) complexes were of 1:1 stoichiometry, as determined by the method of continuous variation (***Figure 2.16***). We were not able to accurately evaluate the stoichiometry of Hg(II) complex formation because the increases in emission are almost completely offset by dilution. For purposes of binding constant determination, we have treated them as 1:1 complexes, although we suspect that multiple species are present.

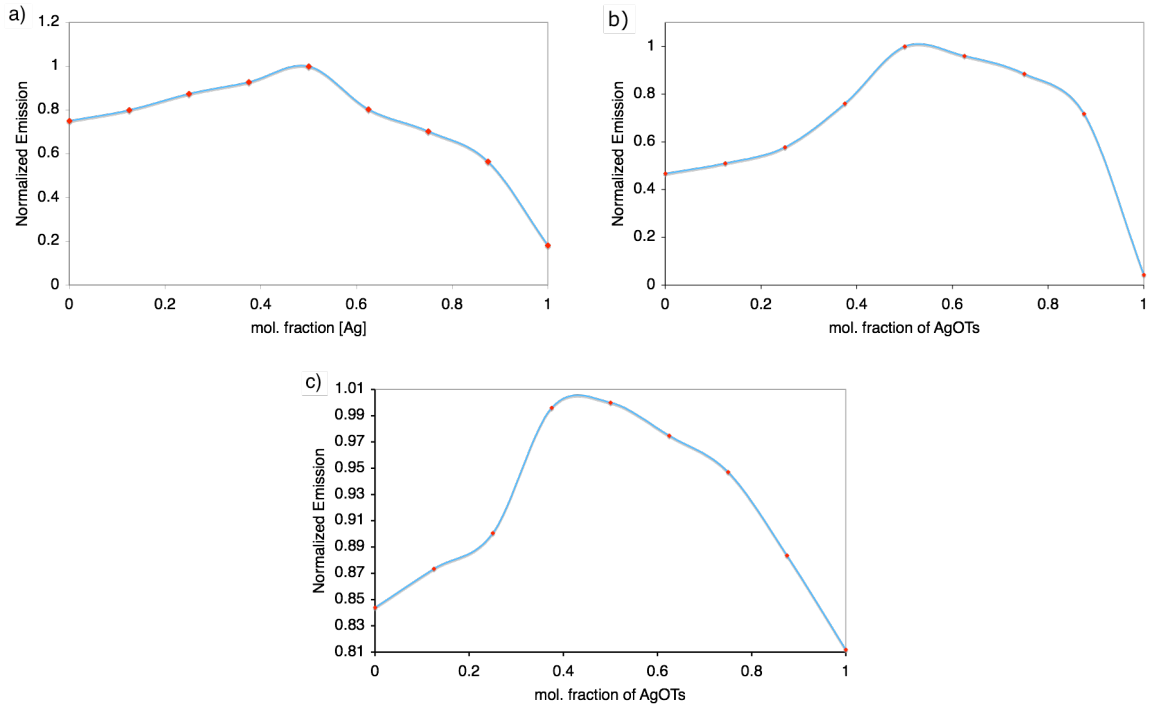

Figure 2.16. Job's plots for the formation of Ag^+ complexes with **1a** (chart "a"), **1b** (chart "b") and **1h** (chart "c"). 3×10^{-5} M solutions of **1a, b, h** respectively and AgOTs in DMSO/$MOPS_{aq}$ were used.

2.3. Computational Study.

There are numerous examples of the formation of $HgCl_2$ complexes with thioureas in polar protic media, including water [12]. To determine the preferred conformation of the Hg(II) complex an X-ray structure is required. Though the Hg•**1a** complex precipitates when solutions of $HgCl_2$ and **1a** in acetonitrile are mixed, it is completely insoluble in common solvents (such as hexane, CH_2Cl_2, Et_2O, ethanol, water, DMSO) and therefore we have not yet been successful in growing diffraction-quality single cristals.

The Hg•**1b** complex readily precipitates from the CH_2Cl_2/ethanol solvent mixture (***Figure 2.17***) and is very good soluble in the most common solvents.[2]

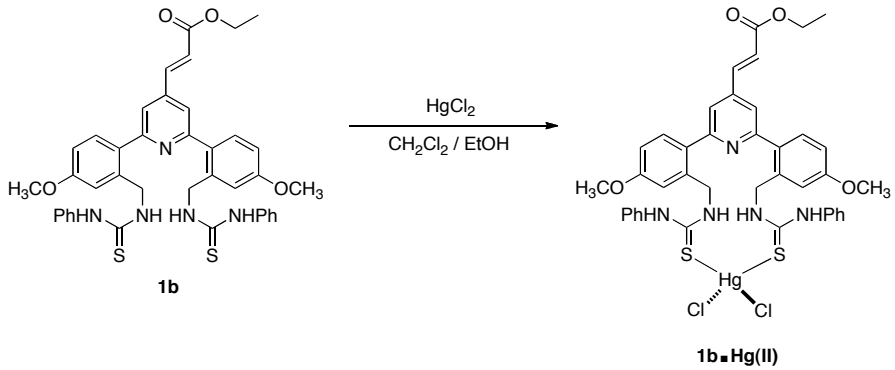

Figure 2.17. Hg(II) complex formation.

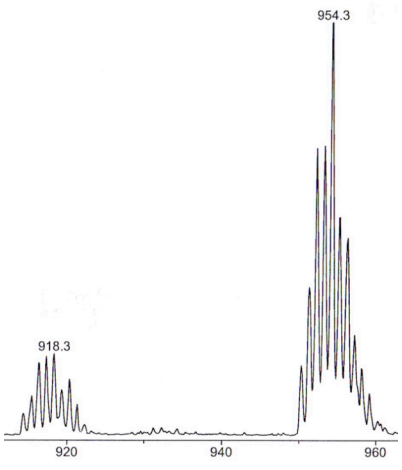

Peak 918.3 corresponds to the [**1b**•Hg^{2+}]

Peak 954.3 corresponds to the [**1b**•HgCl•H^+]

Figure 2.18. ESI-MS of the **1b**•$HgCl_2$ complex.

[2] Powder XRD suggests that the precipitate is largely amorphous.

As an alternative, we have undertaken computational study of simple analogs of the $HgCl_2$ complexes of **1a** and **1b**, in which the OMe, Ph and vinylogous amide have been removed to simplify calculation. The conformational analyses of the molecular systems described in this study, including structural and orbital arrangements as well as property calculations, were carried out using the GAMESS [13] software package. The B98 density functional [14] was used together with the LANL2DZ basis set [15]. Full geometry optimizations were performed and uniquely characterized via second derivatives (Hessian) analysis to determine the number of imaginary frequencies (0=minima; 1=transition state). Molecular orbital contour plots, used as an aid in the analysis of results, were generated and depicted using the programs WEBMO and QMView [16].

We find two low-energy conformations for each complex, inspection of which is highly instructive.

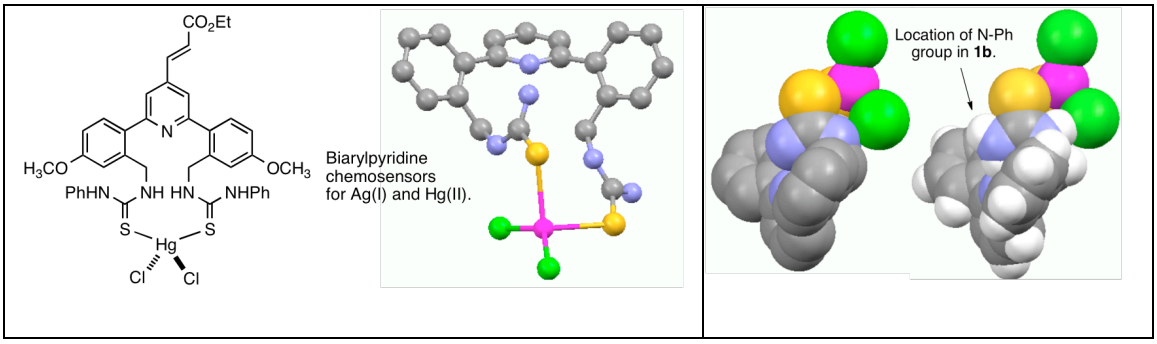

Figure 2.19. The calculated lowest-energy structure for a minimal analog of **1b**•$HgCl_2$, without and with (in white) hydrogen atoms.

The minimum-energy conformations are C_s-symmetry structures, in contrast to what might be intuited by inspection of simple molecular models. The lowest-energy conformation of **1b**•$HgCl_2$ is illustrative (***Figure 2.19***). In addition to S-Hg coordination, there are hydrogen-bonding interactions between the thiourea N-H groups and the chlorine atoms, and the thioureas exist exclusively in the an *s-trans* conformation. In addition, the complexes are highly sterically congested, with the thioureas held very close to the biarylpyridine core. Notably, the presumed location of one of the N-Ph groups would lead to significant steric repulsion between the phenyl group and the fluorophore. Finally, even the inclusion of a glycine spacer (**1a**•$HgCl_2$, not shown) does little to relieve the steric congestion.

These calculations suggest that the majority of **1a-k** are not effective chemosensors because they are too sterically congested to allow cooperative substrate binding, a prerequisite for conformational restriction. As important, the calculations lead to two significant structural predictions. First, it should be possible to increase the affinity of **1a** and **1b** for $HgCl_2$ by removing the N-Ph group of the thiourea or replacing it with a smaller substituent. Second, and more generally, insertion of a longer linkers between the fluorophore and the binding domains should relieve steric congestion and broaden the range of effective binding elements.

2.4. Conclusion.

A library of 10 potential fluorescent chemosensors was prepared. Screening of a large set of cations and anions has revealed three molecules exhibiting response upon addition of aqueous Hg(II) and Ag(I). The generality of these three fluorescent chemosensors is the presence of sulfur atoms in binding domains, though in different oxidation stages. Fluorescent chemosensors **1a, b** contain thiourea as a binding domain, whereas chemosensor **1h** comprises aza-thio crown ether as a binding unit. Though fluorescent chemosensors **1b** and **1h** are selective to mercury (II) and silver (I) among other thiophilic metals they do not allow for discrimination between these two metals. Chemoselsor **1a** exhibited a significant (80 nm) blue shift in emission upon titration with Hg(II) and a smaller (35 nm) shift of the emission maximum. This in turn provides more accurate and quantitative measurement of metal concentration (ratiomentric analysis) and suggests the possibility of discriminating Hg(II) and Ag(I). Thereby we have validated binding-induced conformational restriction as a general signaling mechanism with wide tolerance for structural variation of recognition domains.

We have also made specific, computation-based structural predictions regarding next-generation chemosensors with improved performance: insertion of a longer linkers between the fluorophore and the binding domains should relieve steric congestion and broaden the range of effective binding elements.

2.5. Experimental part.

2.5.1. General notes and procedures

^{1}H NMR spectra were obtained on Bruker AV-300 (300 MHz) or AV2-400 (400 MHz) spectrometers. Chemical shifts are reported in parts per million (ppm) relative to tetramethylsilane (0.00 ppm). Multiplicities are given as: s (singlet), d (doublet), t (triplet), q (quartet), dd (doublet of doublets), m (multiplet).

^{1}H-decoupled ^{13}C NMR spectra were obtained on AV-300 (75 MHz) or AV2-400 (100 MHz) spectrometers. ^{13}C NMR chemical shifts are reported relative to tetramethylsilane (0.00 ppm).

IR frequencies are given in cm^{-1}; spectra were obtained on a Perkin Elmer Spectrum One FT-IR spectrometer in KBr pellets.

Fluorescence measurements were carried out in spectroscopic grade CH_2Cl_2 on an Edinburgh FLS920 spectrophotometer, using 450W Xenon lamp excitation, 1 nm excitation and 5 nm emission slit widths. Emission spectra were obtained by exciting at the longest-wavelength absorption maxima.

Quantum yields were determined by standard methods [17], using pyrene ($\phi = 0.32$) as the standard [18]. The samples were diluted to optical transparency ($A \leq 0.05$), and the integrated emission intensity was compared to an iso-absorptive solution of pyrene in degassed dichloromethane.

UV/Vis measurements were carried out on a Perkin-Elmer Lambda 19 UV/VIS spectrophotometer.

For extinction coefficient determination, four independent solutions of different concentration were prepared, with absorption between 0.04-0.10 AU. The value of ε was calculated by linear least-squares fitting of plots of A vs. concentration. All fits gave R^2 values of ≥ 0.98.

Flash chromatographic purification was performed by with Merck silica gel 60 (particle size 0.040–0.063 mm) packed in glass columns; eluting solvent for each purification was determined by thin layer chromatography (TLC). Analytical thin-layer chromatography was performed with Macherey–Nagel POLYGRAM SIL N-HR/UV254 or ALOX N/UV254. Preparative TLC purification was carried out using PCS-plates silica gel 60 F_{254}, 2 mm.

Synthetic procedures were carried out under an inert atmosphere, in dry solvent, using standard Schlenk techniques, unless otherwise noted.

2.5.2. Synthetic details and tabulated spectroscopic data.

Dichloropyridines **2-3** were prepared as described [5]. The ^{1}H NMR and MS of all compounds were consisted with previously reported data.

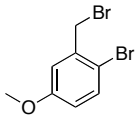

4

The compound was synthesized as described [5]. The ^{1}H NMR of this material was consisted with previously reported data.

^{1}H-NMR (300 MHz, $CDCl_3$): 7.45 (*d*, 1H, *J*=8.8 Hz), 6.99 (*d*, 1H, *J*=3.2 Hz), 6.74 (*dd*, 1H, *J*=8.8, 2.8 Hz), 4.55 (*s*, 2H), 3.80 (*s*, 3H).

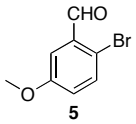

5

The solution of 4-bromo-3-bromomethylanisole **4** (0.70 g, 2.50 mmol, 1.00 eq) and hexamethylenetetramine (0.75 g, 5.40 mmol, 2.20 eq) 50% acetic acid (3.00 mL) was refluxed for 2 h.[5] After cooling to room temperature the mixture was diluted with 10 mL water and extracted with CH_2Cl_2. The organic fraction was washed with H_2O, then $NaHCO_3$ solution, dried over Na_2SO_4 and concentrated. The purification on silica gel (hexane/Et_2O 10/1) provided 0.45 g (90%) of the product.

The ^{1}H NMR of this material was consisted with previously reported data [5].

^{1}H-NMR (300 MHz, $CDCl_3$): 10.32 (*s*, 1H), 7.53 (*d*, 1H, *J*=8.8 Hz), 7.41 (*d*, 1H, *J*=2.8 Hz), 7.03 (*dd*, 1H, *J*=8.8, 2.8 Hz), 3.85 (*s*, 3H).

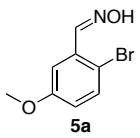

5a

The oxime **5a** was synthesized as described [5]. The ^{1}H NMR of this material was consisted with previously reported data.

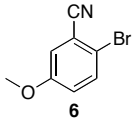

6

The solution of oxime **5a** (1.00 g, 4.00 mmol, 1 eq) and pyridine (1.40 g, 18.00 mmol, 4.40 eq) in dry dioxane (5 mL) was cooled in an ice bath. Trifluoroacetic acid anhydride (0.90 g, 4.40 mmol, 1.10 eq) was added dropwise.[6] The resulting mixture was stirred at 0°C for 1 h and 10 h at r.t. Then 50 mL HCl (~10%) was added. The solution was transferred to a separation funnel and extracted with CH_2Cl_2. The organic phase was washed with water, dried over Na_2SO_4 and concentrated. The residue was passed through a plug of silica gel (hexane/EtOAc 20/1) to remove baseline impurities and the eluent concentrated to yield 0.79 g (93%) of the product.

The ^{1}H NMR of this material was consisted with previously reported data [5].

^{1}H-NMR (300 MHz, $CDCl_3$): 7.54 (*d*, 1H, *J*=8.8 Hz), 7.15 (*d*, 1H, *J*=3.2 Hz), 7.00 (*dd*, 1H, *J*=9.2, 3.2 Hz), 3.83 (*s*, 3H).

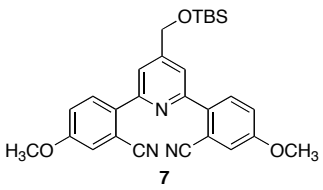

7

Aryl bromide **6** (0.43 g, 2.00 mmol, 2.00 eq) was dissolved in THF (10 mL) and cooled to -100°C, BuLi (1.26 mL, 1.60 M in hexane) was added dropwise and the resulting solution was stirred for 5 min at -100°C. The solution of $ZnCl_2$ (0.27 g, 2.00 mmol, 2.00 eq) in THF (5 mL) was added via syringe and the flask warmed to 23°C. The resulting solution was transferred to the second flask containing dichloropyridine derivative **3** (0.28 g, 1.00 mmol, 1.00 eq), $Pd(PPh)_4$ (0.055 g, 5%) in THF (5 mL) and this was heated for 14 h at 80°C. The solvent was removed with the rotary evaporator and the residue was purified by flash column chromatography (CH_2Cl_2/acetone 50/1) to yield 0.34 g (69%) of the product.

The ^{1}H NMR of this material was consisted with previously reported data [5].

^{1}H-NMR (300 MHz, $CDCl_3$): 8.01 (*d*, 2H, *J*=8.8 Hz), 7.72 (*s*, 2H), 7.25 (*m*, 4H), 4.93 (*s*, 2H), 3.88 (*s*, 6H), 0.99 (*s*, 9H), 0.18 (*s*, 6H).

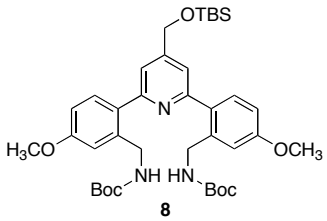

8

The dinitrile **7** (0.60 g, 1.24 mmol, 1.00 eq) was submitted to catalytic hydrogenation (50 psi) over Raney nickel (ca. 5 g) as a catalyst in ethanol (20.00 mL) in the presence of Boc-anhydride (0.75 g, 3.40 mmol, 2.70 eq) in a standard Parr instrument. After 30 h the reaction mixture was filtered through a plug of celite and concentrated. Purification by flash column chromatography (CH_2Cl_2/acetone 50/1) provided 1.50 g (57%) of the product.

The ^{1}H NMR of this material was consisted with previously reported data [5].

^{1}H-NMR (300 MHz, $CDCl_3$): 7.41 (*d*, 2H, *J*=8.4 Hz), 7.33 (*s*, 2H), 7.04 (*d*, 2H, *J*=2.0 Hz), 6.91 (*dd*, 2H, *J*=8.8, 2.4 Hz), 5.73 (*b*, 2H), 4.85 (*s*, 2H), 4.26 (*d*, 4H, *J*=5.6 Hz), 3.86 (*s*, 6H), 1.38 (*s*, 18H), 0.99 (*s*, 9H), 0.17 (*s*, 6H).

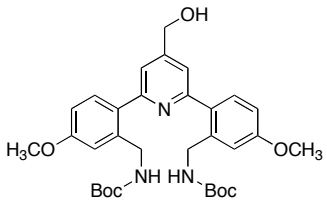

8a

The compound **8a** was synthesized as described [5]. The ^{1}H NMR of this material was consisted with previously reported data.

^{1}H-NMR (300 MHz, $CDCl_3$): 7.47 (*d*, 2H, *J*=8.4), 7.39 (*s*, 2H), 7.00 (*d*, 2H, *J*=2.4), 6.91 (*dd*, 2H, *J*=8.4, 2.4), 5.67 (*b*, 2H), 4.81 (*d*, 2H, *J*=3.6), 4.30 (*d*, 4H, *J*=5.2), 3.86 (*s*, 6H), 2.76 (*b*, 1H), 1.37 (*s*, 18H).

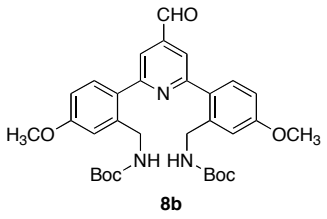

8b

The compound **8b** was synthesized as described [5]. The ^{1}H NMR of this material was consisted with previously reported data.

^{1}H-NMR (300 MHz, $CDCl_3$): 10.15 (*s*, 1H), 7.79 (*s*, 2H), 7.47 (*d*, 2H, *J*=8.4 Hz), 7.06 (*d*, 2H, *J*=2.8), 6.94 (*dd*, 2H, *J*=8.4, 2.8 Hz), 5.61 (*b*, 2H), 4.30 (*s*, 4H), 3.88 (*s*, 6H), 1.38 (*s*, 18H).

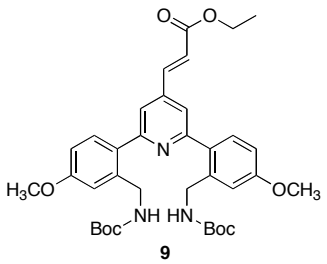

9

The compound **9** was synthesized as described [5]. The ^{1}H NMR of this material was consisted with previously reported data.

^{1}H-NMR (300 MHz, $CDCl_3$): 7.68 (*d*, 1H, *J*=16 Hz), 7.46 (*s*, 2H), 7.42 (*d*, 2H, *J*=8.8), 7.04 (*d*, 2H, *J*=2.4), 6.91 (*dd*, 2H, *J*=8.4, 2.4 Hz), 6.67 (*d*, 1H, *J*=16 Hz), 5.65 (*b*, 2H), 4.28 (*m*, 6H), 3.85 (*s*, 6H), 1.36 (*m*, 21H).

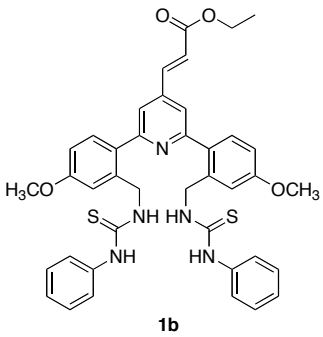

1b

The Boc diamine **9** (30.00 mg, 0.046 mmol, 1.00 eq) was dissolved in 4 M HCl/dioxane ^{i}Pr$_3$SiH (19:1, 5.00 mL) and stirred for 1 h at r.t. The volatile compounds were removed in vacuum and the residue redissolved in 10 mL CH_2Cl_2 and Et_3N (19.00 mg, 0.184 mmol, 4.00 eq). Phenylisothiocyanate (16.00 mg, 0.115 mmol, 2.50 eq) was added and the reaction stirred for 16 h at r.t. Purification by flash chromatography (SiO_2, hexane/acetone 2/1) provided 20.00 mg (60%) of the product **1b**.

^{1}H-NMR (300 MHz, $CDCl_3$): 7.64 (*d*, 1H, *J*=16.1 Hz), 7.38 (*s*, 1H), 7.28-7.22 (*m*, 3H), 7.09-6.98 (*m*, 6H), 6.96-6.83 (*m*, 4H), 6.65 (*d*, 1H, *J*=16.1 Hz), 4.83 (*d*, 4H, *J*=4.98 Hz), 4.28 (*q*, 2H, *J*=7.12 Hz), 3.83 (*s*, 6H), 1.34 (*t*, 3H, *J*=7.14 Hz). **^{13}C-NMR** (100 MHz, $CDCl_3$): 179.98, 165.92, 160.23, 158.92, 143.40, 141.42, 136.84, 131.52, 131.22, 129.54, 126.54, 124.40, 123.64, 120.21, 115.45, 113.79, 61.04, 55.44, 47.82, 14.26. **IR** (KBr), cm^{-1}: 3276 (s), 2957 (m), 2836 (m), 1710 (vs), 1644 (m), 1607 (vs), 1449 (vs), 1310 (vs), 1182 /vs), 1036 (s). **HRMS-ESI:** Calculated for $C_{40}H_{40}N_5O_4S_2$ $[(M+H)]^+$ 718.2522, found 718.2531.

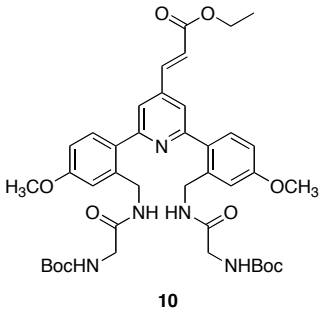

10

The Boc diamine **9** (8.00 mg, 0.0124 mmol, 1.00 eq) was dissolved in 4 M HCl/dioxane : ^{i}Pr$_3$SiH (19/1, 1 mL) and stirred for 1 h at r.t. The volatile compounds were removed in vacuum and the residue redissolved in 5 mL CH_2Cl_2, Boc-Gly (4.30 mg, 0.0248 mmol, 2.00 eq), HOAt (6.60 mg, 0.0496 mmol, 4.00 eq) was added at 0°C, followed by EDC (7.10 mg, 0.0372 mmol, 3 eq) and the resulting solution stirred for 2 h at 0°C and 14 h at r.t. The reaction mixture was filtered, concentrated and purified by preparative TLC (CH_2Cl_2/acetone 10/1, 5/1) provided 6.10 mg (65%) of the product.

^{1}H-NMR (300 MHz, $CDCl_3$): 7.68 (*d*, 1H, *J*=16.0 Hz), 7.45 (*b*, 4H), 7.06-7.01 (*m*, 2H), 6.93 (*dd*, 2H, *J*=2.4, 8.4 Hz), 6.67 (*d*, 1H, *J*=16.0 Hz), 4.42 (*d*, 4H, *J*= 4.6 Hz),

4.30 (*q*, 2H, *J*=7.1 Hz), 3.39 (*s*, 6H), 1.46 (*b*, 18H), 1.38 (*t*, 3H, *J*=7.1 Hz). **^{13}C-NMR** (100 MHz, d_6-acetone): 170.99, 167.67, 162.20, 161.09, 145.21, 143.88, 140.91, 134.10, 133.42, 125.23, 122.09, 114.51, 80.34, 62.29, 56.78, 45.69, 42.96, 29.64, 15.67, 6.96. **IR** (KBr), cm^{-1}: 3426 (s), 2978 (w), 1712 (vs), 1669 (vs), 1608 (s), 1546 (s), 1506 (s), 1286 (s), 1169 (vs), 1038 (m). **HRMS-ESI:** Calculated for $C_{40}H_{51}N_5NaO_{10}$ $[(M+Na)]^+$ 784.3534, found 784.3533.

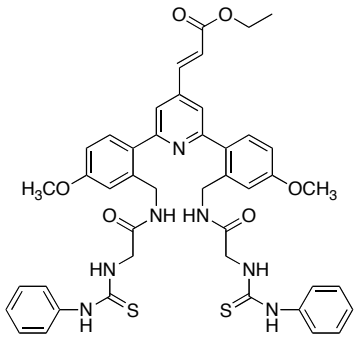

1a

The Boc-Gly compound **10** (37.00 mg, 0.049 mmol, 1.00 eq) was dissolved in 4 M HCl/dioxane ^{i}Pr$_3$SiH (19:1, 5.00 mL) and stirred for 1 h at r.t. The volatile compounds were removed in vac. and the residue redissolved in 10 mL CH_2Cl_2 and Et_3N (50.00 mg, 0.49 mmol, 10.00 eq). Phenylisothiocyanate (80.00 mg, 0.123 mmol, 2.50 eq) was added and the reaction stirred for 16 h at r.t. Purification by flash chromatography (SiO_2, CH_2Cl_2/acetone 10/1) provided 22.00 mg (54%) of the product **1a**. **^{1}H-NMR** (300 MHz, $CDCl_3$): 8.40 (*b*, 2H), 7.68 (*d*, 1H, *J*=16.04), 7.54 (*t*-like, *b*, 2H), 7.47 (*s*, 2H), 7.41 (*d*, 2H, *J*=8.49), 7.36-7.16 (*m*, 11H), 7.12 (*t-like*, 2H), 7.15 (*d*, 2H, *J*=2.64), 6.92 (*dd*, 2H, *J*=8.52, 2.64), 6.69 (*d*, 1H, *J*=16.04), 4.42 (*d*, 4H, *J*=5.84), 4.25 (*q*, 2H, *J*=7.13), 3.79 (*s*, 6H), 1.32 (*t*, 3H, *J*=7.12). **^{13}C-NMR** (100 MHz, $CDCl_3$): 181.22, 168.67, 166.51, 160.92, 159.54, 144.19, 142.04, 138.28, 132.53, 131.96, 127.06, 126.95, 125.18, 123.97, 120.73, 115.87, 113.73, 61.55, 56.06, 48.69, 42.37, 14.61. **IR** (KBr), cm^{-1}: 3337 (s), 1661 (vs), 1608 (vs), 1498 (s), 1311 (m), 1241 (m). **HRMS-ESI:** Calculated for $C_{44}H_{46}N_7O_6S_2$ $[(M+H)^+]$ 832.2951, found 832.2951.

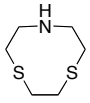

11

7-Aza-1,4-dithiacyclononane was prepared according to the literature [10]. After deprotection, **11** was isolated in 11% overall yield.

^{1}H-NMR (300 MHz, $CDCl_3$): 3.04-2.99 (*m*, 6H), 2.83-2.79 (*m*, 6H).

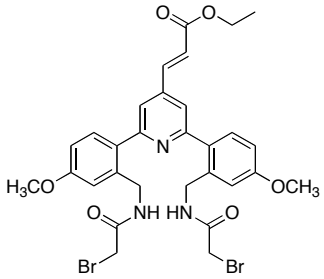

12

Compound **9** (8.00 mg, 0.0124 mmol, 1.00 eq) was dissolved in 4 M HCl/dioxane $^{i}Pr_3SiH$ (19:1, 1.00 mL) and stirred for 1 h at r.t. The volatile compounds were removed in vacuum and the residue redissolved in 3 mL CH_2Cl_2 and DIEA (4.80 mg, 0.0372 mmol, 3.00 eq). α-Bromoacetic acid (3.40 mg, 0.0248 mmol, 2.00 eq), HOAt (6.60 mg, 0.0496 mmol, 4.00 eq), EDC (7.10 mg, 0.0372 mmol, 3.00 eq) was added at 0°C and the resulting solution stirred for 2 h at 0°C and for 4h at r.t. The reaction mixture was filtered, concentrated and purified by preparative TLC (CH_2Cl_2/acetone 10/1) provided 4.50 mg (53%) of **12**. The yield in this reaction varies from 43% to 57%.

^{1}H-NMR (300 MHz, $CDCl_3$): 7.70 (*d*, 1H, *J*=16.1 Hz), 7.56-7.37 (*m*, 6 H), 7.08-7.01 (*m*, 2H), 6.99-6.91 (*m*, 2H), 6.66 (*d*, 1H, *J*=16.06 Hz), 4.30 (*q*, 2H, *J*=7.15 Hz), 3.86 (*s*, 6H), 3.80 (*d*, 4H, *J*=2.19 Hz), 3.62 (*d*, 4H, *J*=1.89), 1.35 (*t*, 3H, *J*=7.15 Hz). **^{13}C-NMR** (100 MHz, $CDCl_3$): 165.34, 160.43, 160.39, 159.61, 141.36, 137.41, 131.14, 131.07, 120.24, 115.79, 115.76, 113.79, 61.08, 55.57, 42.41, 42.27, 14.26. **IR** (KBr), cm^{-1}: 3377 (m), 3265 (m), 3063 (w), 2957 (m), 2837 (w), 1721 (vs), 1667 (vs), 1609 (vs), 1311 (vs), 1039 (vs).**HRMS-ESI:** Calculated for $C_{30}H_{32}Br_2N_3O_6$ $[(M+H)^+]$ 688.0658, found 688.0652.

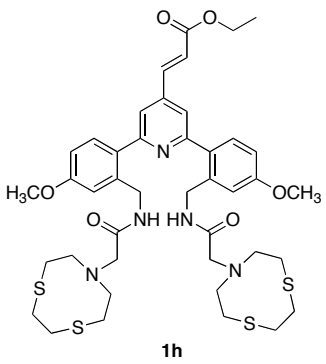

1h

To the solution of **12** (28.00 mg, 0.41 mmol, 1eq) and 7-aza-1,4-dithiacyclononane **16** (20.00 mg, 0.123 mmol, 3 eq) in 5 mL THF K_2CO_3 (170.00 mg, 0.123 mmol, 3 eq) was added. The reaction mixture was stirred and refluxed for 20 h. Then water (20 mL) was added. After extraction with CH_2Cl_2 (x 2) the organic phase was dried over $MgSO_4$ and concentrated. Purification by flash column chromatography yielded 16.00 mg (48%) of the product **1h**. **^{1}H-NMR** (400 MHz, $CDCl_3$): 8.52 (*t-like*, 2H), 7.62 (*d*, 1H, *J*=16.04), 7.42 (*s*, 2H), 7.38 (*d*, 2H, *J*=8.49), 6.85 (*dd*, 2H, *J*=2.64, 8.48), 6.59 (*d*, 1H, *J*=16.01), 4.49 (*d*, 4H, *J*=5.68), 4.22 (*q*, 2H, *J*=7.12), 3.78 (*s*, 6H), 3.06 (*s*, 4H), 2.73-2.65 (*m*, 14H), 2.57-2.52 (*m*, 24H), 1.28 (*t*, 3H, *J*=7.12). **^{13}C-NMR** (100 MHz, $CDCl_3$): 171.09166.52, 160.60, 159.67, 143.28, 142.39, 138.52, 133.03, 131.94, 123.68, 120.68, 115.76, 113.76, 61.44, 60.87, 56.69, 56.00, 41.89, 34.68, 33.26, 14.78. **IR** (KBr), cm^{-1}: 3259 (s), 2908 (s), 2832 (m), 1713 (s), 1666 (vs), 1607

(vs), 1183 (s), 1038 (s). **HRMS-ESI:** Calculated for $C_{42}H_{55}N_5NaO_6S_4$ $[(M+Na+H)^+]$ 876.2933, found 876.2932.

2.5.3. Details of metal titrations.

All metal titrations were carried out using 5×10^{-5} M solutions in 1:1 DMSO/pH 7.4 aqueous MOPS unless otherwise noted. Mercury (II) was added as a 10^{-3} M solution of $HgCl_2$ in 1:1 DMSO/aqueous MOPS via micropipette to 2.500 mL of fluorophore solution in a quartz cuvette. The solutions were equilibrated by stirring prior to acquiring fluorescence spectra.

2.5.4. K_{assoc} Determination

The association constants K_{assoc} for the interaction of **1a, b, h** with Hg^{2+} and Ag^+ ions were estimated by the nonlinear curve-fitting of plots of fluorescence intensity vs. log[M] using *Prism3* (Graphpad, Inc., San Diego, CA). The titrations were carried out in a fluorescence cuvette by adding aliquots of $HgCl_2$ or AgOTs solutions via micropipette to a fluorophore solution of known concentration. DMSO/aqueous MOPS (5μM) solvent mixture was used in all cases. The solutions were equilibrated by stirring prior to acquiring the fluorescence spectra.

2.5.5. Determination of Stoichiometry

To determine binding stoichiometry the method of continuous variation (Job's method) was used, where titrations were performed holding the total concentration of Hg(II) or Ag(I) and ligand constant while varying the mole fraction of both.[8] To correct data for dilution UV spectra of all solutions were taken and the emission maximum (I_{max}) obtained from fluorescent spectra was divided by absorption at the excitation wavelength. The extinction coefficient varies linearly with concentration in all cases [19].

2.5.6. Calculated structures and relative energies

Minimum-energy structures for **1a**•$HgCl_2$.

B98/DZ(2d,p) optimized

Structure	E_{rel} / kcal/mol
1a•$HgCl_2$ O/O	8.3
1a•$HgCl_2$ S/S	3.4
1a•$HgCl_2$ S/O	0.0

Three minimum energy structures found, two similar in energy, one significantly higher in energy.

1a•$HgCl_2$ O/O – $HgCl_2$ coordinated to two carbonyl oxygen atoms.

Relative energy + 8.5 kcal/mol. (***Figures 2.20, 2.21***)

1a•$HgCl_2$ S/S – $HgCl_2$ coordinated to two thiocarbonyl sulfur atoms.

Relative energy + 3.4 kcal/mol. (***Figures 2.22, 2.23***.)

1a•$HgCl_2$ S/O – $HgCl_2$ coordinated to one carbonyl oxygen and one thiocarbonyl sulfur atom. Relative energy 0 kcal/mol. (***Figures 2.24, 2.25***)

Minimum-energy structures for **1b**•$HgCl_2$.

B98/DZ(2d,p) optimized

Structure	E_{rel} / kcal/mol
1b•$HgCl_2$ A	1.5
1b•$HgCl_2$ B	0.0

Two minimum energy structures found, differing only slightly in energy (***Figures 2.26-2.29***).

Figure 2.20. Ball-and-stick view of **1a**•$HgCl_2$ O/O.

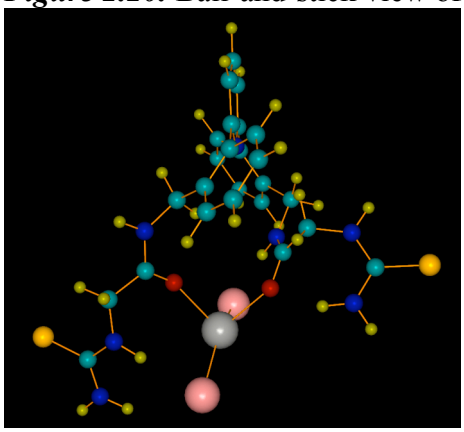

Figure 2.21. Space-filling view of **1a**•$HgCl_2$ O/O, with and without H atoms.

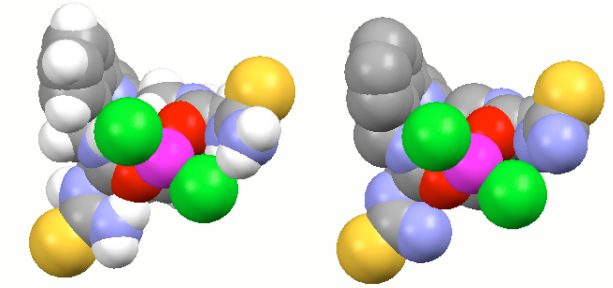

Figure 2.22. Ball-and-stick view of **1a**•$HgCl_2$ S/S.

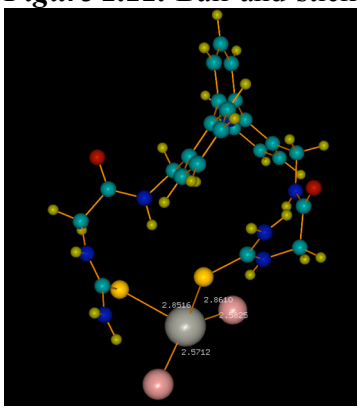

Figure 2.23. Space-filling view of **1a**•$HgCl_2$ S/S, with and without H atoms.

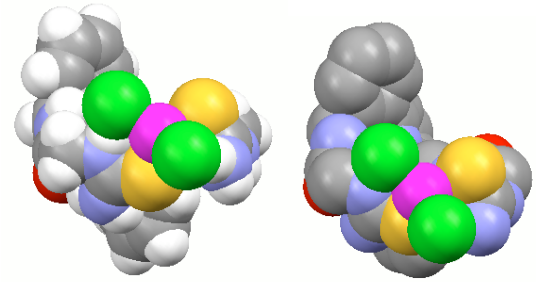

Figure 2.24. Ball-and-stick view of **1a**•$HgCl_2$ S/O.

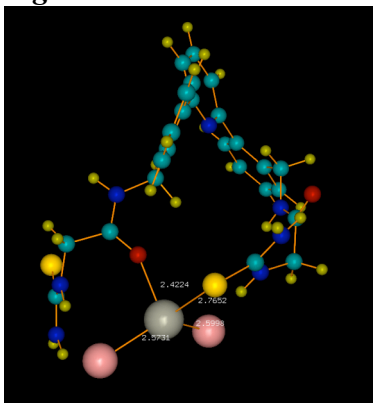

Figure 2.25. Space-filling view of **1a**•$HgCl_2$ S/O, with and without H atoms.

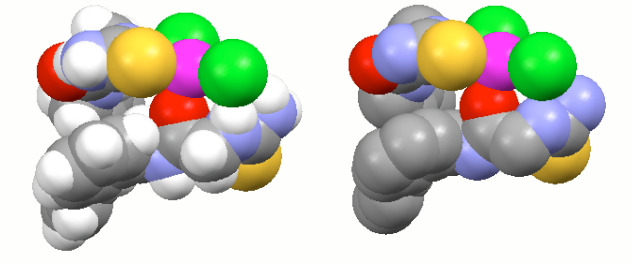

Figure 2.26. Ball-and-stick view of **1b**•$HgCl_2$ A.

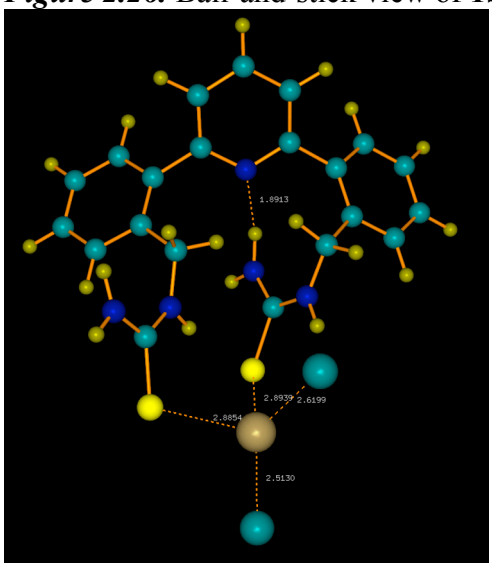

Figure 2.27. Space-filling view of **1b**•$HgCl_2$ A, with and without H atoms.

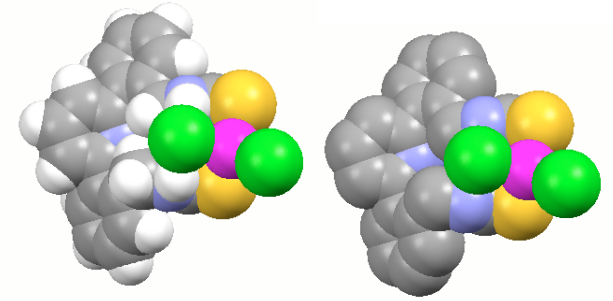

Figure 2.28. Ball-and-stick view of **1b**•$HgCl_2$ B.

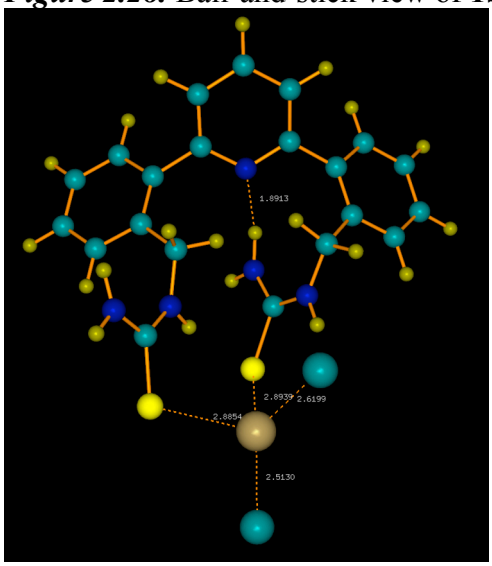

Figure 2.29. Space-filling view of **1b**•$HgCl_2$ B, with and without H atoms.

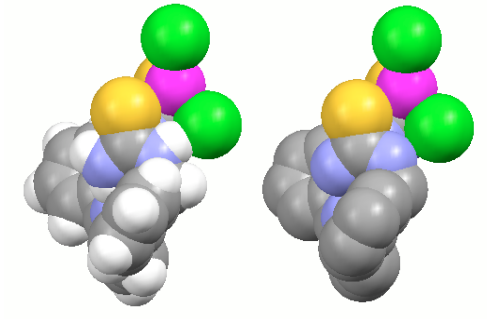

References.

[1] Mello, J.V.; Finney, N. S. *Angew. Chem. Int. Ed.* **2001**, 40, 1536.

[2] Mello, J.V.; Finney, N. S. *Org. Lett.* **2001**, 3, 4263.

[3] Fang, A.G.; Mello, J. V.; Finney, N. S. *Tetrahedron* **2004**, 60, 11075.

[4] Fang, A.G.; Mello, J. V.; Finney, N. S. *Org. Lett.* **2003**, 5, 967.

[5] Mello, J.V.; Finney, N. S. *J. Am. Chem. Soc.* **2005**, 127, 10124.

[6] Angyal, S.J. *Org. React.* **1954**, 8, 197.

[7] Carotti, A.; Campagna, F. *Synthesis* **1979**, 56.

[8] Omura, K.; Swern, D. *Tetrahedron* **1978**, 34, 1651.

[9] Horner, L.; Hoffman, H.; Wippel, H. G.; Klahre, G. *Chem. Ber.* **1959**, 92, 2499.

[10] van de Water, L.G.A.; ten Hoonte, F.; Driessen, W. L.; Reedijk, J.; Sherington, D. C. *Inorg. Chem. Acta.* **2000**, 303, 77.

[11] Feichtinger, K.; Zapf, C.; Sings, H. L.; Goodman, M. *J. Org. Chem.* **1998**, 63, 3804.

[12] Aucken, I. *Inorg. Syn.* **1960**, 6, 27.

[13] Schmidt, M.W.; Baldridge, K. K.; Boatz, J. A.; Elbert, S. T.; Gordon, M. S.; Jensen, J. H.; Koseki, S.; Matsunaga, N.; Nguyen, K. A.; Su, S.; Windus, T. L.; Elbert, S. T. *J. Comp. Chem.* **1993**, 14, 1347.

[14] Schmider, H. L.; Becke, A. D. *J. Chem. Phys.* **1998**, 108, 9624.

[15] Wadt, W.R.; Hay, P. J. *J. Chem. Phys.* **1985**, 82, 284.

[16] Baldridge, K. K.; Greenberg, J. P. *J. Mol. Graphics* **1995**, 13, 63.

[17] a) Lakowicz, J. R. *Principles of Fluorescent Spectroscopy, 2nd ed.*; Kluwer Academic: New York, 1999. b) Demas, J. M.; Grosby, G. A. *J. Phys. Chem.*, **1975**, *75*, 991-1024.

[18] Berlman, I. B. *Handbook of Fluorescent Spectra.* Academic Press: New York, NY, 1965.

[19] Connors, K.A. *Binding Constants: The Measurement of Molecular Complex Stability* **1987**, New York, John Wiley and Sons.

Chapter 3.

Visual Detection of the Explosive TATP.

3.1. Introduction.

Triacetone triperexide (TATP, ***Figure 3.1***) is an organic peroxide known since 19th century [1], and its explosive properties are well characterized. Although it is too unstable for practical use, it has emerged as a weapon in the Middle East. It has been used by suicide bombers in Israel. In Europe it was chosen as a detonator in Dec. 2001 in the Paris-Miami flight by the thwarted "shoe bomber" Richard Reid and also by attacks on public transport in London.

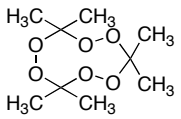

Figure 3.1. Triacetone triperoxide.

TATP is distinguished by:

Extraordinary availability. It can be made in quantity by anyone who has access to 30% hydrogen peroxide, acetone-based nail polish remover and any of a number of common acids such as sulfuric acid. The synthesis of TATP is no more difficult than mixing the ingredients cold, placing them in a refrigerator and isolating the resulting precipitate with a coffee filter.

Difficulty of detection. The majority of high explosives (TNT, RDX, e.g.) contain nitro groups, and the majority of analytical methods for explosive detection are based on detecting nitrogen-containing compounds. TATP is invisible to the common specialized techniques.

In this respect our goal was to design a fluorescent chemosensor capable of rapid visual detecting of TATP in trace concentrations.

3.2. Explosive Detection.

3.2.1. General remarks.

Current methods for the detection of explosives fall into three basic categories [2, 3]:

1) Direct detection by humans and trained dogs.

2) Direct detection by analytical instruments.

3) Indirect detection by analytical methods.

The oldest method for the detection of explosives is physical inspection by humans (as in hand-searching of luggage), in combination with the use of dogs trained to detect explosives. It has proven difficult to train dogs to detect TATP, and in any case trained dogs are in short supply and are not a viable solution to the problem of high-throughput screening of individuals at security checkpoints.

Direct detection of explosive by analytical methods such as mass spectrometry (MS) or microthermal analysis (MTA) can provide reliable and sensitive detection of explosives, and can allow explosives to be differentiated from one another. Progress in instrument miniaturization has permitted field use of certain test instruments and installation of simple instruments in airports.

3.2.2. Explosive detection by fluorescence.

A representative example of the indirect methods from the literature is an enzyme based technique that monitors free hydrogen peroxide with a peroxidase enzyme in conjunction with a dye (***Figure 3.2***) [4].

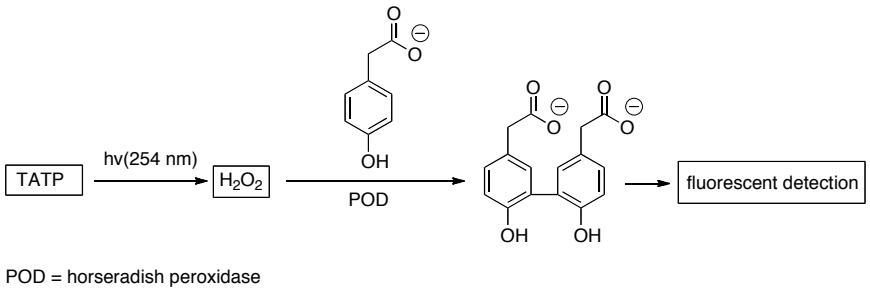

Figure 3.2. Detection of hydrogen peroxide formed after photolysis of TATP [2].

A typical protocol involves pretreating the sample to remove contaminants, then converting any TATP present to free hydrogen peroxide by irradiation with a UV lamp, then treating the hydrogen peroxide solution with a solution of a peroxidase

enzyme and a dye precursor. The enzyme mediates the oxidation of the dye precursor by hydrogen peroxide, leading to a visible change in sample color. This method is selective for TATP and provides good sensitivity (≤ng).

3.2.3. Phosphorus-based fluorescence assay for TATP.

Due to the danger of handling or transporting TATP, a visual 'naked eye' test for rapid first-pass analysis is desirable. No visual fluorescence-based method has been reported, although such a method could benefit from the greater sensitivity associated with fluorescence. The method we describe here falls into the third category (indirect detection by analytical methods). It is based on aromatic sulfoxide reagents designed for visible fluorescence detection of nmol-quantities of TATP. The described sulfoxides also have potential for broader application.

The peroxide character of TATP suggested developing a system in which fluorophore emission was modulated by the oxidation of an adjacent heteroatom. Phosphorus was the first candidate to try. Phosphines (phosphorus (III)) can easily be oxidized to phosphine oxides (phosphorus (V)) with various oxidants including hydroperoxides [5]. Phosphorus(III), like nitrogen, is effective at quenching the fluorescence of appended fluorophores via electron transfer [6]. This property was utilized in fluorescent chemosensor design. Several triarylphosphines having a fluorophore instead of one of the phenyl groups were prepared and diphenyl-1-pyrenylphosphine was chosen as the most suitable reagent for the determination of hydroperoxides due to its reactivity, sensitivity and ease of preparation [6]. The method is based on prevention of photoinduced energy transfer (PET) from phosphorus atom upon oxidation (***Figure 3.3***).

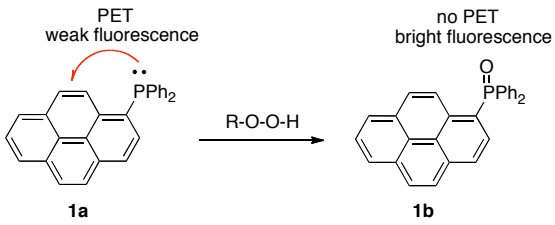

Figure 3.3. Mechanism of hydroperoxide sensing.

Potentially, the appropriate fluorescent chemosensor will allow for visually distinct, real-time detection of TATP due to its peroxide nature.

The use of phosphines for the detection of TATP proved to have two significant limitations. First, even triphenylphosphine does not react directly with TATP [7]. Second, aerial oxidation complicates isolation and handling of phosphines [8].

Attempts to develop air stable phosphorus compound led to the synthesis of a 2-hydroxypyrene based phosphite-phosphate pair (***Figure 3.4***) [8].

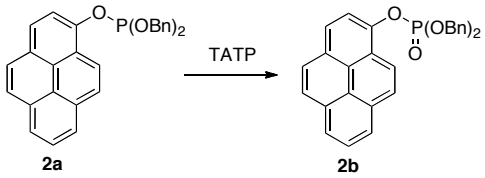

Figure 3.4. A phosphite that provides a fluorescent response to spontaneous reaction with TATP.

This compound shows a 10-fold enhancement in fluorescence and a blue-shift from the phosphite to the phosphate. Phosphite **2a** can be oxidized both by treatment with H_2O_2 and TATP in acetonitrile at room temperature (***Figure 3.5)***. However, the λ_{em} of **2a** is small and the changes in emission upon oxidation are not sufficient for visual detection.

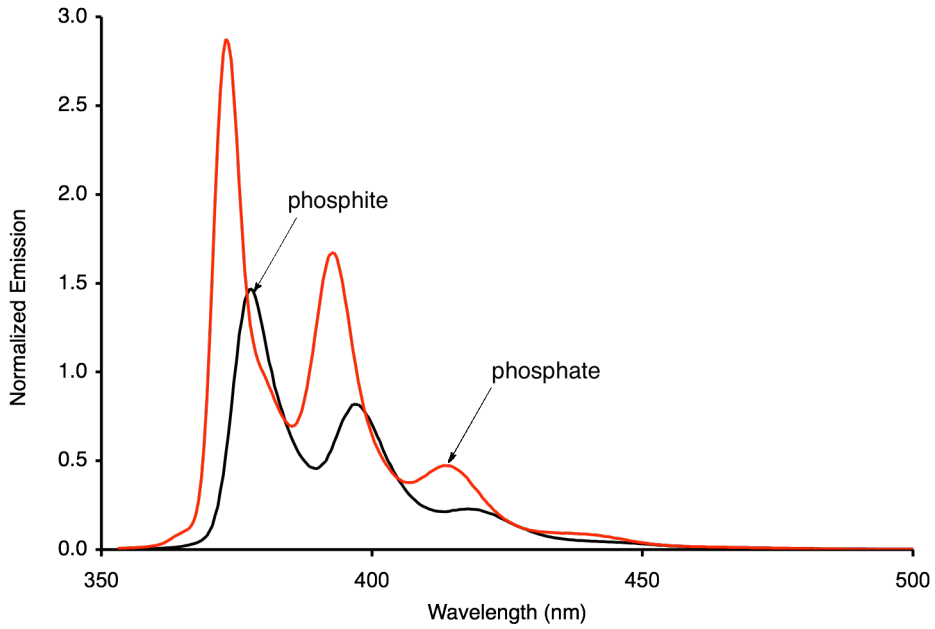

Figure 3.5. Change in emission intensity of phosphite upon oxidation.

While nitrogen atoms quench fluorescence, they are not readily oxidized by peroxides in the absence of acid. Oxygen does not quench fluorescence via electron transfer, and

phosphorus is problematic, as noted above. Conspicuous in its absence from the N/O/P/S tetrad are any reports of sulfur as a reporting element in the development of fluorescent probes.

The necessity to improve fluorescence enhancement observed upon oxidation turned our attention to sulfur-containing substrates.

3.2.4. Sulfur-based visual fluorescence assay for TATP.

While the redox chemistry of sulfur is well-established, to our knowledge there is only a single example in the literature where intramolecular electron transfer involving sulfides is described. Compound **3a** (***Figure 3.6***) has a very low quantum yield (0.04). It is possible to increase the fluorescence intensity by oxidizing the thioether to the corresponding sulfoxide (**3b**) by treatment with hydrogen peroxide in aqueous solution [9]. It suggests that sulfides can participate in electron transfer quenching of fluorescence.

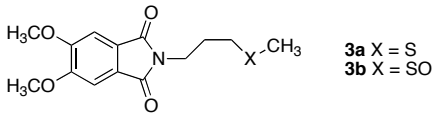

Figure 3.6. A lone example from Griesbeck, et al., of apparent electron transfer quenching involving sulfur.

While the photophysics of sulfur compounds have been studied extensively, little has been reported in terms of correlating fluorescence emission with the oxidation state of a sulfur atom attached to a fluorophore [12].

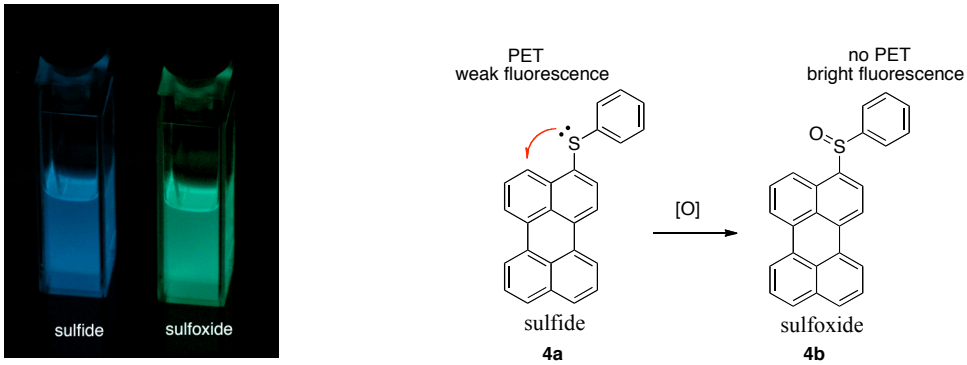

Figure 3.7. Possibility of TATP detection using distinct emitting properties of sulfoxides and sulfones (photograph of emission from 10^{-4} M solutions in $CHCl_3$).

With the aim to test our hypothesis of using sulfides attached to a fluorophore for the detection of TATP we have prepared perylene phenyl sulfide and the corresponding sulfoxide (**4a**, **4b**) and compared their fluorescence properties.

A dramatic difference in emission intensities of the perylenephenyl sulfide and sulfoxide (i.e. before and after oxidation) that can be seen even with the naked eye (***Figure 3.7***) will allow very simple detection of TATP by this method.

At first glance perylene seemed to be an appropriate fluorophore to be used. We were able to obtain perylenephenyl sulfide, sulfoxide and sulfone in spectroscopically pure form. However these compounds are very poor soluble in most of the common solvents used in spectroscopy and tend to adsorb on the glass surface. This forced us to change the fluorophore retaining simplicity of the synthesis. We fixed our choice upon a related polyaromatic compound, pyrene (***Figure 3.8***).

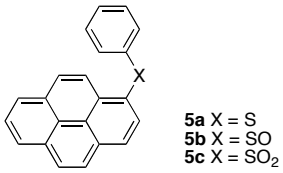

Figure 3.8.

Phenyl 1-pyrenyl sulfide **5a** was prepared from commercially available 1-bromopyrene (***Figure 3.9***).

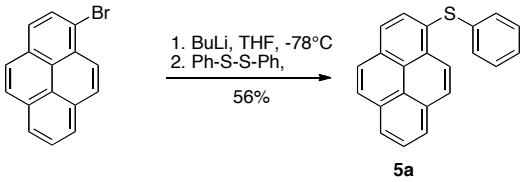

Figure 3.9. Synthesis of the sulfide **5a**.

Oxidation of **5a** with one or two equivalents of *m*CPBA furnished sulfoxide **5b** and sulfone **5c** correspondingly (***Figure 3.10***).

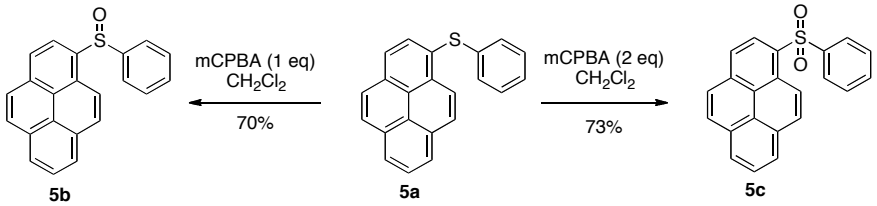

Figure 3.10. Oxidation of sulfide **5a** to the corresponding sulfoxide and sulfone.

Preliminary study of fluorescent properties in the series sulfide-sulfoxide-sulfone derivatives has revealed that the sulfone exhibits the strongest fluorescence and the sulfoxide the weakest (***Figure 3.11***).

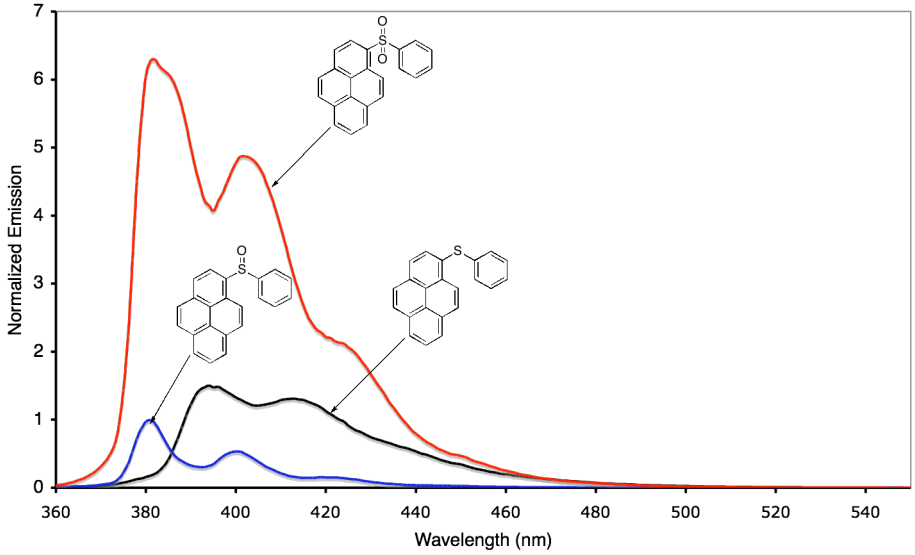

Figure 3.11. Emission of **5a-c** in 5 x 10^{-6}M in $CHCl_3$.

However, small changes in emission upon oxidation of the sulfur atom were not sufficient for visual detection.

In an attempt to overcome the problem of anomalously low emission of the pyrenyl phenyl sulfoxide **5b** two new sulfide-sulfoxide-sulfone series **6a-c, 7a-c** and **8a-c** with varying substituentson the sulfur atom were prepared in which the conjugation between the fluorophore (pyrene) and the sulfur atom is broken (***Figure 3.12***).

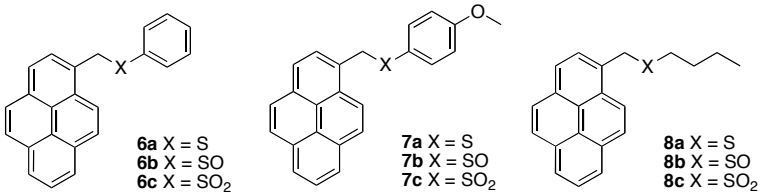

Figure 3.12. First generation sulfides, sulfoxides and sulfones.

To prepare sulfides **6a-8a** pyrene 1-carbaldehyde was reduced with $NaBH_4$ to give 1-hydroxymethylpyrene. Bromination with PBr_3 provides 1-bromomethylpyrene. Nucleophilic displacement with the corresponding thiols (butyl-, phenyl- and *p*-methoxyphenyl-) and DBU as a base furnished sulfides **6a-8a** (***Figure 3.13***).

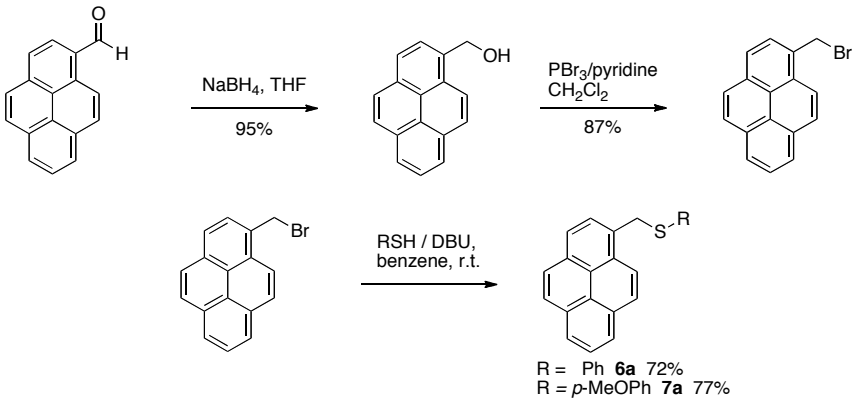

Figure 3.13. Synthesis of the sulfides **6a-8a**.

Oxidation of **5a** with one or two equivalents of *m*CPBA furnished sulfoxide **5b** and sulfone **5c** correspondingly (***Figure 3.14***).

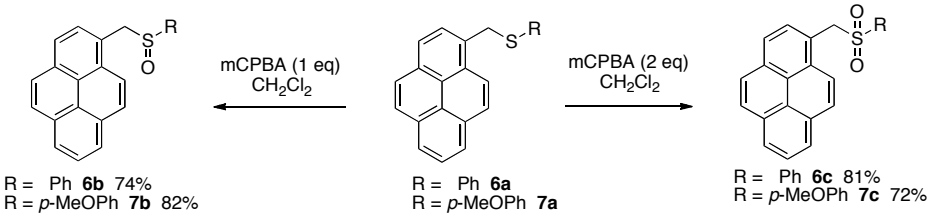

Figure 3.14. Oxydation of sulfides **6a-8a** to the corresponding sulfoxides and sulfones.

Table 3.1. Properties of first generation sulfur-bearing fluorophores.[a]

Compound	E_{ex} (λ)[b]	E_{em} (λ)[b]	Φ_F[c]
6a	82 (349)	76 (377)	0.01
6b	81 (352)	76 (376)	<0.01 (0.009)
6c	82 (350)	76 (377)	0.47
7a	82 (349)	76 (376)	<0.01 (0.006)
7b	81 (352)	76 (377)	<0.01 (0.007)
7c	81 (352)	76 (377)	0.41
8a	82 (348)	76 (377)	0.02
8b	82 (349)	76 (378)	0.09
8c	82 (352)	76 (377)	0.09

[a]Extinction coefficients for longest-wavelength λ_{max} transition are all ca. 3×10^3 $M^{-1}cm^1$. All values are for 10^{-5} M solutions in CH_2Cl_2. [b] Excitation and emission energies in kcal/mol; wavelengths in nm. [c]Relative to pyrene ($\phi = 0.32$). Quantum yield measurement error is estimated at ± 0.002.

For the S-alkyl species (**8a-c**) the sulfide is the least fluorescent and the sulfoxide and sulfone are comparable, consistent in principle with electron transfer quenching of fluorescence (***Table 3.1***).

The emitting properties within series with two aromatic substituents (**6a-c** and **7a-c**) turned out to alter in a similar manner upon changing the sulfur oxidation state whereas sulfoxide-sulfone pair **7b-7c** has slightly larger I/I_0 difference. Therefore **7b-7c** were used for further investigation. The difference in emission intensities between the sulfoxide and sulfone **7b-c** is significantly greater than that of the pair **5b-c** (***Figure 3.15***).

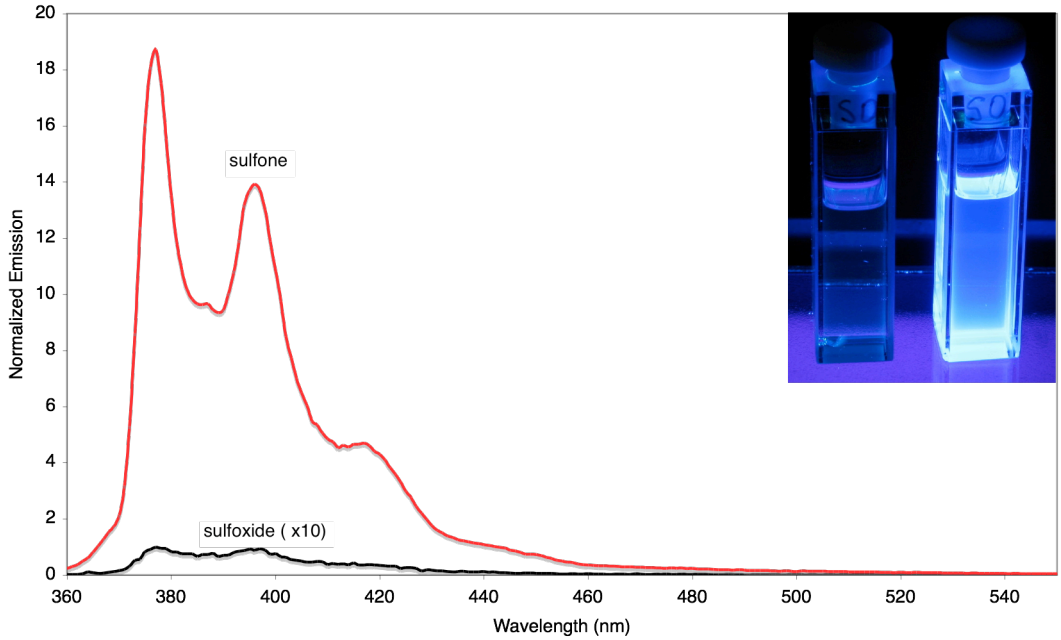

Figure 3.15. Comparative emission of **7a-b** in CH_2Cl_2, normalized to **7a** at 420 nm. (***inset*****:** visible emission from 10^{-4} M of **7a** and **7b** solutions)

Momentarily setting aside the origins of low sulfoxide quantum yield, the fact that sulfone **7b** is much more fluorescent than the corresponding sulfoxide **7c** provides an opportunity for oxidation-based visual TATP detection. An estimate of maximum response is provided by the dramatic increase in visible emission for **7c** relative to **7b**, which can easily be discerned by the naked eye (***Figure 3.15, inset***).

TATP does not react directly with the profluorophore **6b**. However, in the presence of methyltrioxorhenium (MTO) it reacts rapidly with the H_2O_2 generated by UV irradiation of TATP solution on toluene, undergoing oxidation to the corresponding sulfones (***Figure 3.16***).

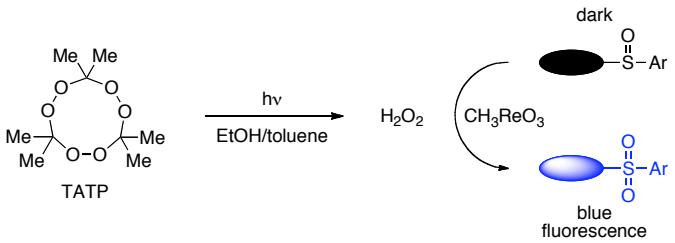

Figure 3.16. Schematic representation of the detection of TATP.

Beginning with photolysis of 500 nmol (ca. 0.1 mg) of TATP, a 5-fold increase in visible fluorescence can be attained within 15 minutes (illustrated with **7b**/**7c**, ***Figure 3.17***). With regard to detection limits, we have found that we can generate a visual response to as little as 100 nmol of TATP. Although a longer reaction time (90 minutes) is required for full development, the fluorescence can still be easily seen with the naked eye (***Figure 3.17*, inset**).

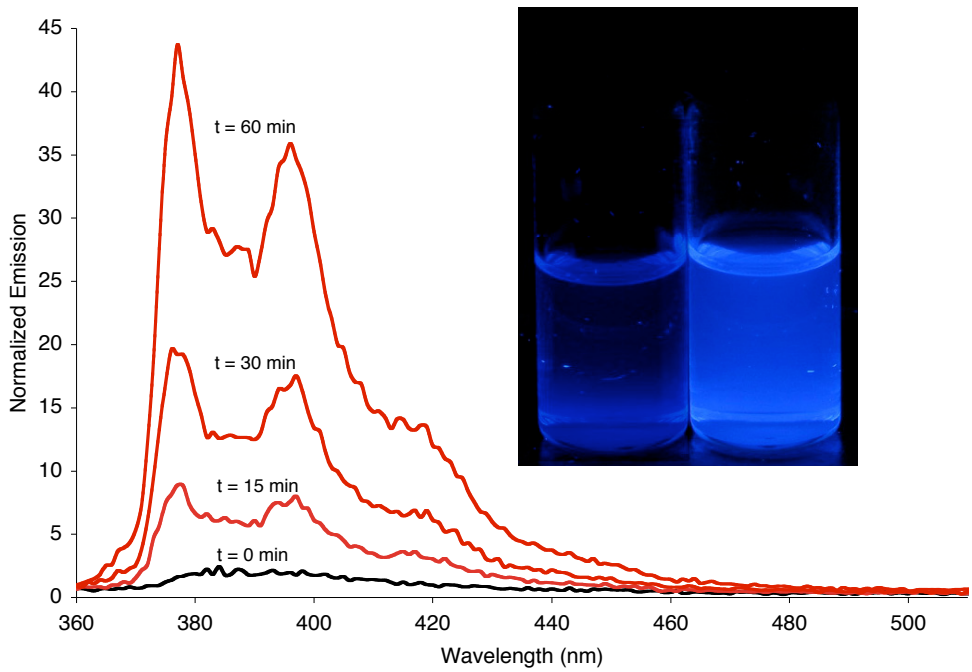

Figure 3.17. Emission during oxidation of **7b** (10^{-4} M in CH_2Cl_2) with 500 nmol photolyzed TATP in the presence of MTO, normalized to t=0 at 420 nm; solutions before and after reaction with 100 nmol photolyzed TATP (**inset**).

A concern for potential practical application is reaction with other oxidants. In this respect, we note that **5b-6b**, with or without MTO, do not react appreciably with oxidants such as ^{t}BuOOH, NaOCl, $LiClO_4$, $K_2Cr_2O_7$ or air. They do react spontaneously, in the absence of MTO, with $KMnO_4$, which is occasionally used in

improvised explosives. A potential limitation of this approach is that benzylic sulfoxides such as **6b** and **7b** are not stable to prolonged UV irradiation (although they are stable to visible light). Given that radical fragmentation/recombination is integral to the signaling mechanism, it is not clear that this limitation can be entirely overcome. However, **5b** degrades more slowly than **7b** while still showing significant fluorescence enhancement upon oxidation to **5c**, indicating that there is potential to suppress degradation through structural modification while retaining useful fluorescence response.

With regard to broader impact, we believe that aryl sulfoxides have application in the detection of species beyond oxidants of interest. As an example, we find that titration of **5b** with metal ions such as Li^{+} and Zn^{2+} leads to fluorescence enhancement (***Figure 3.18***).

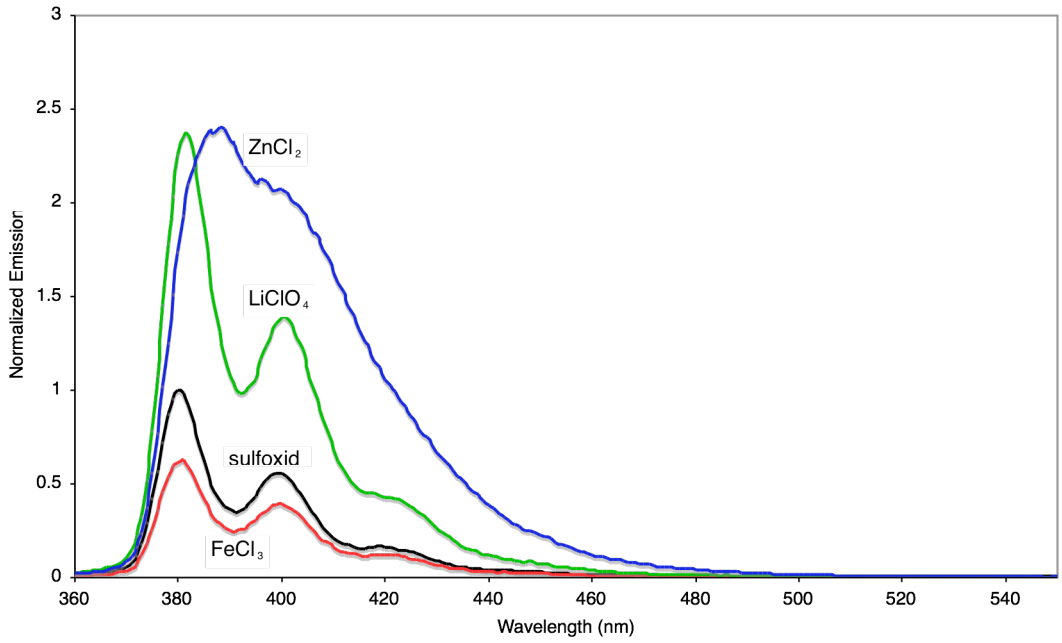

Figure 3.18. Emission spectra for metal titrations of **5b** (5 x 10^{-5}M in CH_2Cl_2).

In the light of these experimental data, understanding of the origin of fluorescent quenching in the aromatic sulfoxides is crucial for deliberate design of sulfur based fluorescent chemosensors. It would clearly be advantageous to develop the second-generation sulfoxide reagents with longer excitation/emission wavelengths and increased stability to simplify visual detection and practical implementation.

Such anomalously low emission of the aromatic sulfoxides **5b-7b** is not consistent with photoinduced electron transfer (PET) quenching. If PET were the case, the

increase in emission intensities upon sulfur oxidation from sulfide to sulfoxide and further to sulfone would be observed.

For this reason another mechanism of excited state deactivation in sulfoxides must be available.

The next section provides an overview of the physical and photochemical properties of sulfoxides and introduces further experimental and computational results aimed to shine light on the nature of fluorescence quenching in aromatic sulfoxides.

3.3. Photochemical properties of aromatic sulfoxides. An overview.

3.3.1. Luminescent properties of Sulfoxides.

In general, aromatic sulfoxides show no luminescence at room temperature. Among simple diaryl and arylmethyl sulfoxides (***Figure 3.19***) described in the literature only three compounds **11, 12, 13** showed weak fluorescence at 77K, which was a relatively minor part of the luminescence, perhaps no more than 10% [11]. Therefore an efficient nonradiative decay from the singlet excited state or intersystem crossing with subsequent phosphorescence or thermal deactivation must occur.

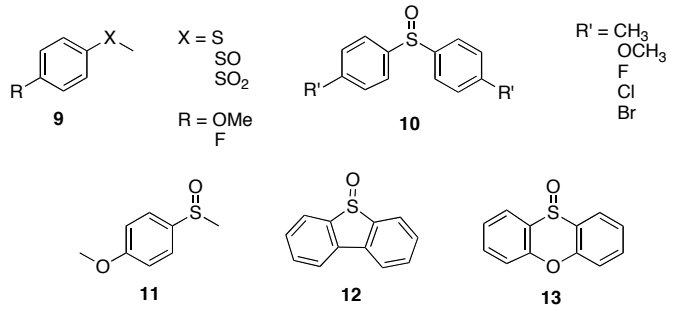

Figure 3.19.

The phosphorescence spectra of most of the sulfoxides are similar in appearance and very weak with quantum yield of under 0.05 and many are <0.01. The lifetimes of emission are under 100 ms.

In general, quantum yield of phosphorescence is given by

$$\Phi_P = \Phi_T (k_P / [\, k_P + \sum k_{nr}])$$

where Φ_T-intersystem crossing yield, k_P-the natural phosphorescence rate constant, $\sum k_{nr}$ the sum of all nonradiative deactivation processes of the triplet. Thus, the source of low phosphorescence yield may be low triplet formation yield (Φ_T), fast

nonradiative decay or both. Because the sum of ($\Phi_T + \Phi_F$)<<1, it is clear that the nonradiative decay is very efficient from either or both of the two. An attempt to distinguish between them made in the course of study of aromatic sulfoxides failed [11].

Replacement of the benzyl ring by a more emissive fluorophores such as naphthalene, antracene, phenanthrene or pyrene was an endeavor to retrace the subsitution-induced changes on the photophysics of the well-characterized parent compounds (***Figure 3.20***) [12].

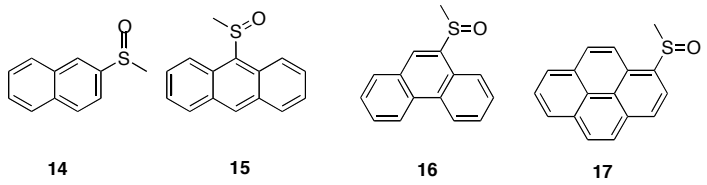

Figure 3.20.

The appearance of the fluorescent spectra is similar to those obtained for the unsubstituted arenes. Differences in spectroscopic singlet energies are within 4 kcal/mole of those of the unsubstituted arenes. The same range of singlet energies is observed for the corresponding sulfides and sulfones, which clearly shows that various effects are not simply based on the sulfur atom heavy atom effect or symmetry breaking.

At room temperature, the sulfoxides have considerably smaller ϕ_F values (0.005-0.009) than the unsubstituted arenes. Fluorescence enhancement and longer life times τ_F are observed on cooling the sulfoxides to 77K because the rigidity (along with the low temperature) of the frozen medium inhibits deactivation of the fluorescent state. In contrast to the fluorescence strong phosphorescence was observed from sulfoxides **14-17** whereas ϕ_P exceed that of the unsubstituted compounds. Phosphorescence lifetimes are close or greater than 1s. Such long lifetimes are typical of aromatic hydrocarbons with $\pi\pi^*$ triplet states and indicates that there is no efficient nonradiative pathway available out of the triplet states at 77K.

In addition, the quantum yields of triplet formation ϕ_T were measured. In all cases ϕ_T of the sulfoxides were lower than those of the parent arenes by a factor of 2 or greater.

Since ($\phi_F+\phi_T$)<<1 there is an important nonradiative decay pathway out of the singlet state available to the sulfoxides.[1]

3.3.2. Sulfoxide Excited States.

In order to investigate deactivation processes of the excited state that is formed on irradiation of aromatic sulfoxides and account for the very low luminescence quantum yields as well as to ascertain the multiplicity of the excited state from which racemization and radical formation occurs several experiments with triplet sensitizer and quenching experiments described in the series of publications of W. Jenks and coworkers were carried out.

Common triplet sensitizer such as benzophenone, acetophenone and acetone were used. It is evident that benzophenone (E_T=69 kcal/mol) does not have enough energy for efficient energy transfer to aromatic sulfoxides (whose triplet energies lie in the range of 77-80 kcal/mol e.g. **9-11**) unless they have extended conjugated system (e.g. **12**). Acetophenone (E_T=74 kcal/mol) or acetone (E_T=82 kcal/mol) are more appropriate sensitizers.

Triplet energies of sulfoxide in comparison to that of the corresponding sulfides and sulfones are ordered as follows: $E_T(R_2SO_2) > E_T(R_2SO) > E_T(R_2S)$. The triplet energies of the aromatic sulfoxides are a few kilocalories per mole higher than those of their ketone analogues and a few kilocalories per mole lower than the corresponding aromatic system without the sulfoxide group.

The triplet states are delocalized on the aromatic ring (they are aromatic $\pi\pi^*$-type states that are strongly perturbed by the presence of the sulfoxide) and involve charge transfer away from the sulfoxidic oxygen. This is shown by examining the energy of emission as a function of solvent polarity. Large (3-10 kcal/mol) blue shift in the phosphorescence is observed by switching from nonpolar to polar solvent implying that the triplet state of the sulfoxides is less polar than the ground state [11].

---

[1] If the quantum yield of inversion ϕ_{inv} (representative of half of the racemization) multiplied by 2 is added to the above sum the latter raises dramatically (e.g. from 0.2 to 0.70 for naphthalene sulfoxide). These facts confirms the hypothesis that the racemization is intimately tied to the nonradiative decay of a singlet state (see ref. 12 and Section 4.3 for the discussion of racemization)

Beside primary radiative or nonradiative deactivation processes of an excited state there are several secondary pathways. The most common secondary photochemical process that is available for an excited molecule of an aromatic sulfoxide is the inversion of the tetrahedral sulfur atom. This in case of a chiral sulfoxide leads to racemization. There exist at least two generally accepted mechanisms for the photoracemization of aromatic sulfuxides: α-cleavage of the sulfur-carbon bond with formation and their subsequent recombination and pyramidal inversion without radical formation. The possibility of one or another mechanism depends on the structure of the corresponding sulfoxide and the stability of the radicals formed. The next section provides a short historical overview on the mechanistic investigation of the racemization of chiral sulfoxides, experimental evidence of the α-cleavage as well as a discussion of the experimental and computational results in support of the nonradical mechanism.

3.4. Racemization of Chiral Sulfoxides.

3.4.1. Historical overview. Hypothesis of the exciplex formation.

An important property of a stereogenic center is its ability to undergo racemization. The fact that the tetrahedral structure of sulfoxides retains its configurational integrity has generated considerable interest in understanding the conditions under which stereomutation can take place. An extensive investigation of the racemization of aromatic sulfoxides was initiated by Mislow in 1964. It was found that the stereomutation[2] of sulfoxides can be induced catalytically (by hydrogen chloride or dinitrogen tetroxide) [13] and by heating at elevated temperatures. The activation barriers for methyl-*p*-tolyl sulfoxide and 1-adamantyl-*p*-tolyl sulfoxides are 37 and 42 kcal/mol, respectively [14]. Inversion barriers are not known for most simple dialkyl sulfoxides because thermal elimination of sulfoxides with β-hydrogen takes place and a sulfenic acid and an olefin are formed with a barrier less that 35 kcal/mol [15, 16].
Photochemical behavior of sulfoxides was studied by K. Mislow and G. Hammond in 1960s in terms of photosensitized pyramidal inversion of chiral sulfoxides.

[2] By *stereomutation* is meant the interconversion of stereoisomers, i.e. of enantiomers (inversion, racemization) or of diastereomers (epimerization, *cis*-*trans*-conversion) [14].

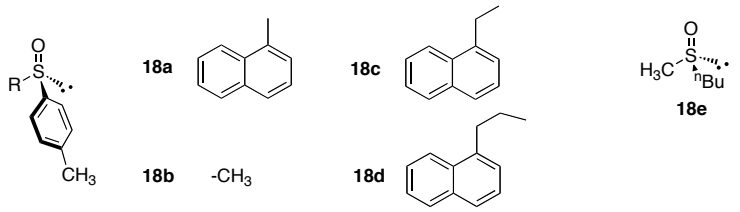

Figure 3.21. Objects of study of light-induced pyramidyl inversion.

It was shown[17], that irradiation of **18a** (***Figure 3.21***) using a Pyrex filter furnished the completely racemized product. Replacement of naphtyl substituent by methyl led to only 5-10% racemization of **18b**. Photosensitization was demonstrated by addition of naphthalene to the solution of **18b**. In this experiment the degree of racemization increased to 24%.

To evaluate intramolecular sensitization compound **18c** and **18d** were prepared. Whereas irradiation of **18c** resulted in extensive decomposition (apparently due to α-cleavage), irradiation of **18d** yielded a completely racemized product. Photolysis of dialkylsulfoxide **18e** did not show racemization both with and without naphthalene. Therefore it was concluded, that aryl-sulfinyl chromophore is required for photoracemization. As reasonable explanation of the sensitized photoracemization energy transfer from a naphthalene unit to *p*-toluensulfinyl unit was suggested [18]. Reinvestigation of these results led to a rather different mechanism than a simple transfer of excitation energy [19].

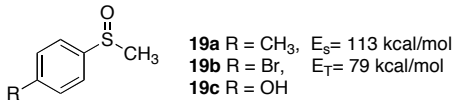

Figure 3.22. Singlet and triplet energies.

Based on determined energies of the singlet and triplet states (***Figure 3.22***) it was inferred that electronic energy transfer from naphthalene (either from its singlet or from its triplet excited state) to the sulfoxide to produce the corresponding excited state would be highly endothermic (by 23 and 18 kcal/mol respectively) and should not occur. Because of correlation of the rate of racemization of sulfoxides with quenching of the naphthalene fluorescence in the sensitized photolysis of chiral sulfoxides, an intermediate exciplex was presumed to be formed, although there was no direct evidence for the species. Further kinetic experiment on **18d** allowed to infer that the photoracemization results from energy transfer from the singlet state of

naphthalene. The complex is formed from excited singlet state of naphthalene and a ground state of the sulfoxide. This excited state undergoes radiationless decay. Vibrational energy affects thermal pyramidal inversion of the aryl sulfoxide with high efficiency (***Figure 3.23)*** [19].

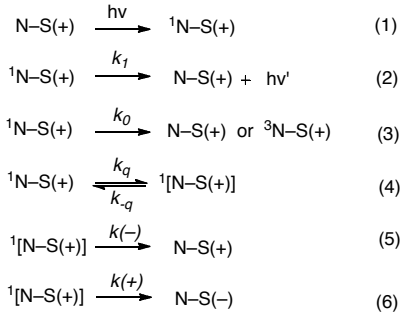

Figure 3.23. Proposed mechanism of the photosensitized racemization.

Use of electron-donating and –withdrawing substituents on the aromatic substituent of the sulfoxide failed to show a clear trend or a large variation in the quenching rate constant which would support the hypothesis that charge transfer interactions are dominant [20].

A further study conducted a few decades later was not able to find a direct evidence of exciplex formation. However, estimation of over 50 rate constants for singlet quenching of various sensitizers by a series of sulfoxides and redox potentials for this series strongly suggest that the mechanism for quenching may involve charge transfer from the sensitizer to the sulfoxide [21].

3.4.2. Radical formation as a possible mechanism of fluorescence quenching.

Irradiation of sulfoxides leads, along with stereomutation, to photochemical degradation. The extend to which the photodecomposition occurs depends on the wavelength of excitation and the irradiation time. Prolonged photolysis results in the complete decomposition of the aryl sulfoxide. The best documented class of photochemical reactions of sulfoxides remains cleavage of S-C bonds (α-cleavage), which yields products derived from the resulting radical pair [22]. Since radical formation on a stereogenic center unambiguously leads to racemization attempts have been made to identify radicals as intermediates in the course of racemization and assign multiplicity of the excited state.

In most cases where an assignment has been made, the photoreactivities of aromatic sulfoxides have been attributed to their triplet state [17, 19, 23-25] although the triplet state of sulfoxides was not characterized in terms of quantum yield or lifetime.

The photolysis of the aromatic sulfoxides is postulated to proceed through formation of sulfinic esters whereas other products are a result of secondary and tertiary photolysis. The general scheme illustrating the photolysis mechanism of aryl benzyl sulfoxides is presented below (***Figure 3.24)*** [26, 27]. The product distribution in such a reaction mixture strongly depends on the reactivity and viscosity of the solvent and the wavelength of excitation. The primary process is always cleavage of S-CH_2 bond of **20** in an excited state. In solvents of a high viscosity (such as 2-methyl-2-propanol) and at modest conversion of the sulfoxide **20** the corresponding sulfinic ester (such as **21**) is formed with almost qualitative yield and inversion of configuration at sulfur in the remained **20** is detected. Independent photolysis of the sulfinic ester **6** proceeds through S-O bond cleavage to yield arenthiyl and alkoxyl radicals. Disproportionation of the radical pair yield **24** and **25** as well as **26** and **27** which are quite competitive.

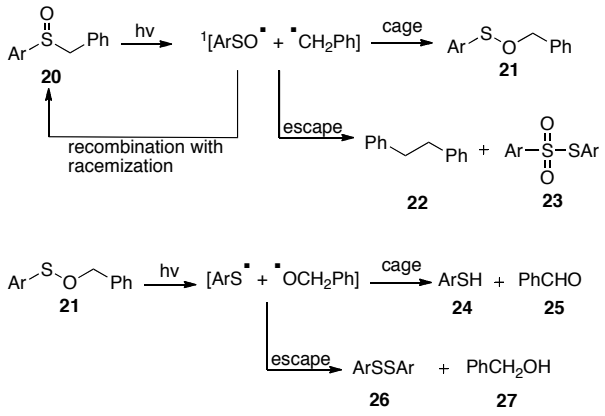

Figure 3.24. Proposed photolysis mechanism of aryl benzyl sulfoxides [27].

Phenylsulfinyl **28** and phenylsulfenyl **29** radicals (***Figure 3.25***) were postulated as intermediates in course of photochemical decomposition of aryl benzyl sulfoxide **20**, and in one case were characterized by extinction coefficient and transient absorbtion spectra (***Table 3.2***) [28].

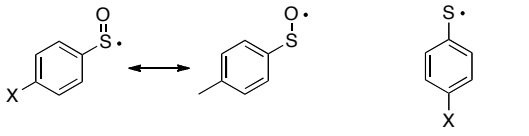

28a **28b** **29**

arylsulfinyl radical arylsulfenyl radical

Figure 3.25. Representation of the Sulfinyl and sulfenyl radicals.

Table 3.2.

Radical	ε, $M^{-1}cm^{-1}$	λ_{max}, nm
Phenylsulfinyl (**28**, X=H)	1.1×10^4	300
	1.3×10^3	450
Phenylsulfenyl (**29**, X=H)	1.0×10^4	295
	2.5×10^3	460

Computational studies of the sulfinyl radical indicate that the singly occupied orbital is largely localized outside the ring on S and O in a π^* configuration constructed almost entirely of S and O *p*-orbitals lying most heavily on O. S-O bond length is estimated to be 1.49 Å (experimental and computed S-O bond lengths of typical sulfoxides are 1.48-1.49 Å) [28].

This data make a very strong case that the photolysis of aryl benzyl sulfoxides proceed through the initial S-C α-cleavage [26].

The question of multiplicity from which racemization occurs has not yet been addressed unambiguously. Though in some cases the triplet sensitization was clearly demonstrated, the product distribution was dramatically different from that obtained in direct photolysis [29]. For the naphthalene sulfoxide **11** sensitized photolysis failed to exhibit any stereomutation. No inhibition of racemization was observed from O_2 in air-saturated solutions. Neither was racemization inhibited by piperylene and isoprene at concentrations up to 25 mM. Therefore it was concluded that the racemization process occurs from the singlet excited state [12].

3.4.3. Nonradical mechanism.

Despite the extreme commonness of the carbon-sulfur bond homolysis it has been asserted that in some cases photoracemization occurs through a direct inversion of the sulfur center [17, 25, 30, 31]. For some sulfoxides low quantum yield for product formation associated with α-cleavage is observed upon irradiation. However, quantum yields for racemization are relatively high [31, 32]. This can serve as a

circumstantial evidence in favor of the existence of a nonhomolytical pathway for racemization.

Other arguments in favor nonradical pathway in the photoracemization of aryl sulfoxides are observed from the simple sulfoxide derivatives of large aromatic chromophores (naphthalene, antracene, pyrene). Introduction of the sulfinyl group dramatically lowers the quantum yield of fluorescence. This is not accompanied by a rise in triplet yield or product formation and is unique to the sulfoxides (see Section 1.4) [12].

To obtain direct chemical evidence for a nonradical racemization process (R_S, S_C)-1-deutero-2,2-dimethylpropyl *p*-tolyl sulfoxide **30** was photolyzed (***Figure 3.26***) [33]. Analysis of the reaction mixture showed that mainly (S_S, S_C)-**30** is formed at low conversion. Thus, only sulfur inversion is observed without inversion of the adjacent CHD stereogenic center (the latter would provide all three new isomers without any preference).

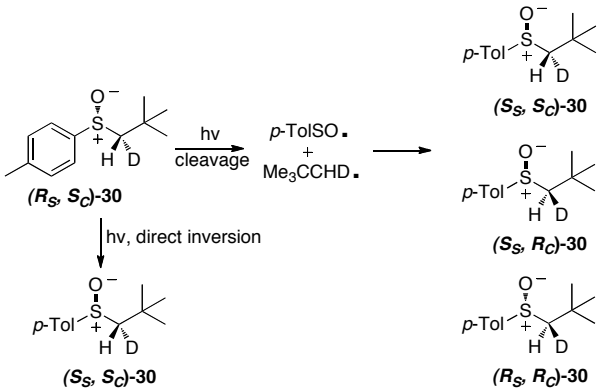

Figure 3.26. Photolysis of a sulfoxide with two adjacent stereogenic centers.

It was hypothesized that the racemization event was the source of the nonradiative decay (see Section 1.4) [12]. Stereomutation is a result of a geometrical relaxation of the electronically excited sulfoxide from its highly pyramidalized ground state (C_s symmetry) to one that is at least approximately trigonal at sulfur, followed by nonradiative decay to the ground state at or near a geometry that is planar at the sulfur center (C_{2v} symmetry, ***Figure 3.27***). To demonstrate that for DMSO stationary points exist on excited-state energy surface that have C_{2v} symmetry and are lower in energy than any geometry with C_s symmetry multireference *ab initio* methods have been

used. A value of 41.5 kcal/mol was calculated for the ground state pyramidal inversion of sulfur for DMSO (no experimental value is available) [34].

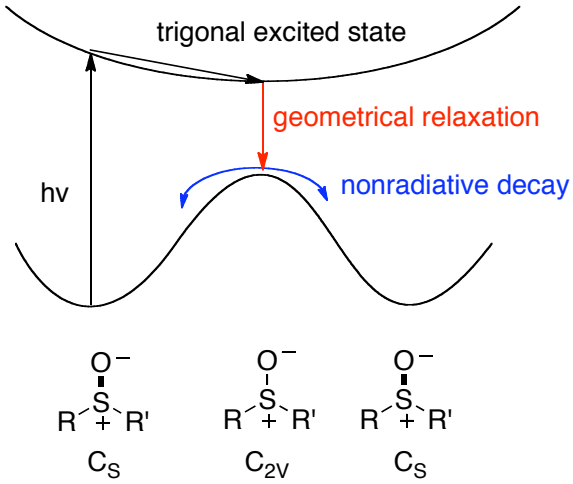

Figure 3.27. Simplified diagram for photoracemization without radical formation.

These experimental and computational data can be considered as the strongest evidence for a noncleavage mechanism for photochemical stereomutation in sulfoxides.

3.5. Conclusion.

While TATP can be detected using standard analytical methods such as mass spectrometry, it is invisible to the common specialized techniques developed to detect nitrogen-containing explosives. Several attempts were made to develop a visual 'naked eye' test for rapid first-pass analysis. Fluorophores with adjacent phosphorus atom (aromatic phosphines) were initially explored. They proved unsuitable due to susceptibility to rapid aerial oxidation, complicating their isolation and handling. Though phosphites are more stable, the change in emission upon oxidation with TATP is not sufficient for visual detection.

We have presented here the first visual fluorescent assay for TATP detection. The underlying idea is dramatic change in emission intensity upon oxidation of the pyrenyl sulfoxide to the corresponding sulfone. The described fluorescenct chemosensor is capable of detecting nmol-quantities of TATP, requiring no sample

preparation beyond brief photolysis with a UV hand-held lamp, and is more sensitive than the reported visual colorimetric detection method [3].

Very low fluorescence quantum yields of aromatic sulfoxides can be ascribed to radical formation-recombination (α-cleavage) as the main deactivation pathway available for the sulfoxide excited state. This mechanism is well documented in the literature. Complete decomposition and product formation upon prolonged irradiation of methylpyrenyl phenyl sulfoxide (our fluorescent chemosensor for TATP) is consistent with the proposed mechanism.

3.6. Experimental part.

Phenyl 1-pyrenyl sulfide **5a**.

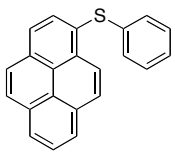

5a

n-BuLi (1.30 mL, 1.6M in hexane, 0.20 mmol, 1.1 eq) was added dropwise to a solution of 1-bromopyrene (0.50 g, 0.18 mmol, 1 eq) in dry THF (40 mL) at –78 °C. After stirring for 10 minutes, a solution of diphenyl disulfide (0.39 g, 0.18 mmol, 1.0 eq) in THF (3 mL) was added via syringe. After 30 minutes, the reaction warmed to RT, diluted with CH_2Cl_2 (50 mL) and washed with H_2O (3×30 mL). The organic phase was dried over $MgSO_4$ and concentrated under vacuum. Purification by chromatography (hexane:benzene 20:1) provided **5a** as a yellow solid (0.31 g, 56 %).

^{1}H-NMR (400 MHz, $CDCl_3$), δ: 8.66 (d, 1H, J=9.2 Hz), 8.21-8.00 (m, 8H) 7.22-7.15 (m, 5H). **^{13}C-NMR** (100 MHz, $CDCl_3$), δ: 137.84, 132.49, 132.43, 131.69, 131.23, 130.98, 129.08, 128.61, 128.55, 128.17, 128.04, 127.23, 126.30, 125.98, 125.65, 125.61, 125.42, 125.20, 124.89, 124.44. **IR** (KBr), cm^{-1}: 3041 (m), 1924 (w), 1871 (w), 1581 (s), 1478 (s), 1437 (m), 1079 (m), 846 (s). **HRMS-ESI**(+): Calculated for $C_{22}H_{14}S$ [$(M+H)^+$] 310.0816; found 310.0815.

5a has been reported previously [34], and these data are consistent with this previous report.

[3] The previously reported colorimetric assay (Itzhaky, H.; Keinan, E. Method and kit for the detection of explosives. U. S. Pat. 6,767,717, Jul 7, 2004; *Chem. Abstr.* **1999**, *131*, 172322) is applicable to mg-quantities of TATP. The method described here is thus more sensitive, and comparable in terms of ease-of-use, although slightly slower. The reported instrument-based fluorescence method (ref. 4) for TATP detection is ca. 100-fold more sensitive than the method described here.

Phenyl 1-pyrenyl sulfoxide **5b**.

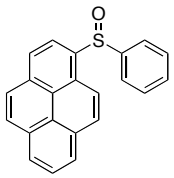

5b

To a solution of phenyl 1-pyrenyl sulfide (**5a**, 0.077g, 0.250 mmol, 1 eq) in CH_2Cl_2 (3 mL) at 0 °C was added *m*-chloroperbenzoic acid (70 %, 0.056 g, 0.225 mmol, 0.90 eq). After 30 min at 0°C, the reaction mixture was concentrated and was purified by preparative TLC (50:1 CH_2Cl_2:acetone), providing 0.057 g (70 %) of sulfoxide **5b**.

^{1}H-NMR (400 MHz, $CDCl_3$), δ: 8.64-8.58 (m, 2H), 8.32-8.06 (m, 8H) 7.72-7.70 (m, 1H), 7.41-7.35 (m, 1H). **^{13}C-NMR** (100 MHz, $CDCl_3$), δ: 145.89, 137.52, 133.37, 131.14, 130.72, 130.43, 129.40, 129.32, 129.27, 128.57, 127.55, 126.64, 126.52, 126.36, 125.56, 124.88, 124.68, 124.32, 122.42, 121.35. **IR**(KBr), cm^{-1}: 3030 (m), 1639 (w), 1591 (m), 1442 (w), 1189 (w), 1049 (vs), 840 (s). **HRMS-ESI**(+): Calculated for $C_{22}H_{14}ONaS$ $[(M+Na)^+]$ 349.0663; found 349.0660.

Phenyl 1-pyrenyl sulfone **5c**.

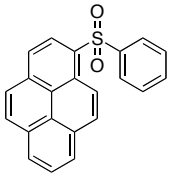

5c

m-Chloroperbenzoic acid (70 %, 0.053 g, 0.210 mmol, 2.2 eq) was added to a solution of phenyl 1-pyrenyl sulfide (**5a**, 0.030 g, 0.097 mmol mmol, 1 eq) in CH_2Cl_2 (3 mL) at 0 °C. After 30 minutes, the reaction mixture was concentrated and purified by preparative TLC (hexane:CH_2Cl_2 1:1), providing 0.024 g (73 %) of sulfone **5c**.

^{1}H-NMR (400 MHz, $CDCl_3$), δ: 8.98 (d, J=8 Hz), 8.93 (d, J=8 Hz), 8.28-8.18 m, 8.09-8.00 m, 7.51-7.43 m. **^{13}C-NMR** (100 MHz, $CDCl_3$), δ: 142.61, 135.47, 132.87, 131.96, 130.84, 130.61, 130.22, 129.99, 129.10, 128.77, 127.32, 127.27, 127.11, 127.02, 127.00, 126.83, 125.13, 124.19, 123.89, 122.84. **IR**(KBr), cm^{-1}: 3064 (w), 3043 (w), 1883 (w), 1813 (w), 1591 (m), 1302 (s), 1147 (s), 1078 (m). **HRMS-ESI(+):** Calculated for $C_{22}H_{14}NaO_2S$ $[(M+Na)^+]$ 365.0612; found 365.0615.

5c has been reported previously,[4] and these data are consistent with this previous report.

Pyrene-1-carbaldehyde.

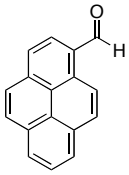

A solution of $TiCl_4$ (1.5 mL, 13.6 mmol, 1.8 eq) in CH_2Cl_2 (3 mL) was added to a solution of pyrene (1.5 g, 7.4 mmol, 1 eq) and dichloromethyl methyl ether (1.0 g, 9.3 mmol, 1.3 eq) in CH_2Cl_2 (60 mL) at 0°C, and the mixture was stirred for 1 h at 0°C and 1.5 h at RT. The reaction was poured into ice-water and extracted with CH_2Cl_2 (2×70 mL). The organic layer was washed with water (2×100 mL), dried over $MgSO_4$ and concentrated. Purification by chromatography (hexane:CH_2Cl_2 1:1) to afford **6** as a yellow solid (1.3 g, 76 %; m.p. 126 °C, lit. 126-127 °C) [35].

^{1}H-NMR (300 MHz, $CDCl_3$), δ: 10.80 (s, 1H), 9.45 (d, 1H, J=7.96 Hz), 8.48-8.08 m.

1-Hydroxymethylpyrene [36]

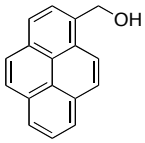

A solution of $NaBH_4$ (0.2 g, 5.4 mmol, 3.0 eq) in 15 ml 90 % ethanol containing a few drops of 1M NaOH (aq.) was added to a solution of pyrene-1-carbaldehyde (0.5 g, 1.8 mmol, 1 eq) in THF (30 mL) at 0°C. The reaction mixture was stirred for 3h then quenched with dilute HCl (aq., 1:10). The resulting solution was diluted with water (50 mL) and extracted with CH_2Cl_2 (3×30 mL). The organic phase was washed with saturated $NaHCO_3$ (30 mL) followed by water (30 mL), dried over $MgSO_4$ and concentrated under reduced pressure providing 0.4 g (95 %) of 1-hydrohymethylpyrene, which was used without further purification.

1-Bromomethylpyrene.

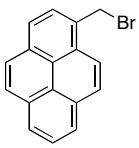

A solution of phosphorus tribromide (0.062 g, 0.230 mmol, 1.0 eq) in CH_2Cl_2 (0.5 mL) was added dropwise to a solution of 1-hydroxymethylpyrene (0.106 g, 0.460 mmol, 2 eq) and pyridine (0.018 g, 0.23 mmol, 1.0 eq) in CH_2Cl_2 (10 mL) at 0°C. After 3 hours, cracked ice and CH_2Cl_2 (30 mL) were added. The organic layer was washed with water, saturated $NaHCO_3$, and water, and then dried over $MgSO_4$. Evaporation of the solvent under reduced pressure afforded dark yellow powder. The crude product was recrystallized from

benzene to give 1-bromomethylpyrene (0.150 g, 87 %; m.p. 131.5°C, lit. 131-133°C) [37].

^{1}H-NMR (300 MHz, $CDCl_3$), δ: 8.41-7.99 (m, 9H), 5.25 (s, 2H).

1-Methylpyrenyl phenyl sulfide **6a**.

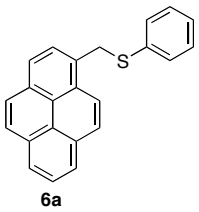

6a

The solution of 1-bromomethylpyrene (0.200 g, 0.680 mmol, 1 eq), thiophenol (0.076 g, 0.680 mmol, 1.0 eq) and DBU (0.104 g, 0.680 mmol, 1.0 eq) in benzene (15 mL) was stirred for 12 hours at RT, then filtered and concentrated. Purification preparative TLC (hexane:CH_2Cl_2 3:1) provided 0.160 g (72 %) of sulfide **6a**.

^{1}H-NMR (400 MHz, $CDCl_3$), δ: 8.37-7.85 (m, 8H), 7.38-7.20 (m, 6H), 4.84 (s, 2H).

^{13}C-NMR (100 MHz, $CDCl_3$), δ: 136.57, 131.30, 130.94, 130.84, 130.55, 130.41, 129.03, 128.92, 127.93, 127.76, 127.41, 127.33, 126.64, 126.01, 125.27, 125.23, 125.11, 124.80, 124.64, 123.23, 37.61. **IR**(KBr), cm^{-1}: 3038 (m), 2933 (w), 1585 (m), 1480 (s), 848 (s). **HRMS-ESI(+):** Calculated for $C_{23}H_{16}NaS$ $[(M+H+Na)^{2+}]$ 347.0870; found 347.0873.

1-Methylpyrenyl phenyl sulfoxide **6b**.

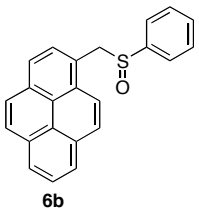

6b

Procedure as for **5b**. Purification by preparative TLC (silica, CH_2Cl_2) provided sulfoxide **6b** in 74 % yield.

^{1}H-NMR (300 MHz, $CDCl_3$), δ: 8.24-7.95 (m, 8H), 7.47 (d, J=7.92 Hz, 1H), 7.44-7.28 (m, 5H), 5.01 (d, J=12.6 Hz, 1H), 4.65 (d, J=12.6 Hz, 1H). **^{13}C-NMR** (100 MHz, $CDCl_3$), δ: 143.04, 131.51, 131.29, 131.24, 130.65, 130.03, 129.35, 128.85, 128.21, 127.92, 127.33, 126.21, 125.62, 125.46, 124.54, 124.44, 122.93, 122.70, 62.41. **IR**(KBr), cm^{-1}: 3033 (w), 2952 (w), 2922 (w), 1444 (m), 1034 (vs), 845 (vs). **HRMS-ESI(+):** Calculated for $C_{23}H_{16}NaOS$ $[(M+H+Na)^{2+}]$ 363.082; found 363.0819.

1-Methylpyrenyl phenyl sulfone **6c**.

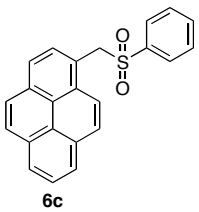
6c

Procedure as for **5c**. Separation by TLC (silica, CH_2Cl_2) provided sulfone **3c** in 81 % yield.

^{1}H-NMR (400 MHz, $CDCl_3$), δ: 8.24-8.11 (m, 8H), 7.70 (d, J=7.92 Hz, 1H), 7.59-7.47 (m, 3H), 7.34-7.28 (m, 2H), 5.10 (s, 2H). **^{13}C-NMR** (100 MHz, $CDCl_3$), δ: 137.98, 133.71, 131.84, 131.17, 130.52, 130.35, 129.88, 128.92, 128.71, 128.27, 127.26, 126.22, 125.71, 125.54, 124.85, 124.56, 124.44, 122.67, 121.61, 60.42. **IR**(KBr), cm^{-1}: 3037 (w), 2975 (w), 2927 (w), 1447 (s), 1306 (vs), 1154 (s), 1085 (s), 846 (s). **HRMS-ESI(+):** Calculated for $C_{23}H_{16}NaO_2S$ $[(M+H+Na)^{2+}]$ 379.0769; found 379.0769.

Methylpyrenyl-*p*-methoxyphenyl sulfide **7a**.

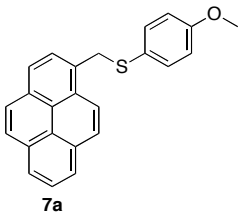
7a

A solution of 1-bromomethylpyrene (0.050 g, 0.170 mmol, 1 eq), *p*-methoxythiophenol (0.024 g, 0.17 mmol, 1.0 eq) and DBU (0.026 g, 0.17 mmol, 1.0 eq) in benzene (10 mL) was stirred for 12 hours at RT, then filtered and concentrated. Purification by preparative TLC (silica, hexane:Et_2O 10:1), followed by recrystallization from benzene-hexanes provided 0.046 g (77 %) of sulfide **7a**. **^{1}H-NMR** (400 MHz, $CDCl_3$), δ: 8.29 (d, 1H, J=9.25 Hz), 8.19-7.95 (m, 7H), 7.67 (d, 1H, J=7.84 Hz), 7.25-7.22 (m, 2H), 6.75-6.72 (m, 2H), 4.67 (s, 2H), 3.73 (s, 3H). **^{13}C-NMR** (100 MHz, $CDCl_3$), δ: 159.38, 134.54, 131.24, 130.81, 130.73, 128.82, 127.87, 127.52, 127.39, 127.15, 126.16, 125.91, 125.12, 125.10, 125.05, 124.78, 124.45, 123.31, 114.43, 55.26, 39.51. **IR**(KBr), cm^{-1}: 3037 (m), 3005 (m), 2951 (m), 2906 (m), 2834 (m), 1595 (m), 1492 (s), 1240 (s), 1182 (s), 1032 (s). **HRMS-ESI(+):** Calculated for $C_{24}H_{18}NaOS$ $[(M+H+Na)^{+}]$ 377.0976; found 377.0979.

Methylpyrenyl-*p*-methoxyphenyl sulfoxide **7b**.

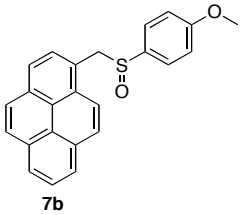
7b

Procedure as for **5b**. Purification by preparative TLC (CH_2Cl_2/acetone 40:1) provided sulfoxide **7b** in 82 % yield.

^{1}H-NMR (400 MHz, $CDCl_3$), δ: 8.22-7.99 (m, 8H), 7.47 (d, 1H, J=7.8), 7.22-7.18 (m, 2H), 6.81-6.77 (m, 2H), 5.03 (d, 1H, J=13.1), 4.61 (d, 1H, J=12.6), 3.35 (s, 3H). **^{13}C-NMR** (100 MHz, $CDCl_3$), δ: 162.20, 133.85, 131.43, 131.23, 130.65, 129.38, 128.13, 127.86, 127.34, 126.29, 126.19, 125.58, 125.41, 124.80, 124.55, 123.09, 122.77, 114.36, 62.51, 55.45. **IR**(KBr), cm^{-1}: 3053 (w), 3006(w), 2921 (w), 2837 (w), 1899 (w), 1590 (vs), 1575 (s), 1495 (vs), 1252 (vs), 1035 (vs). **HRMS-ESI(+):** Calculated for $C_{24}H_{18}NaO_2S$ $[(M+H+Na)^{2+}]$ 393.0925; found 393.0925.

Methylpyrenyl-*p*-methoxyphenyl sulfone **7c**.

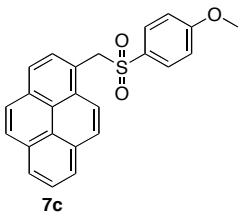

7c

Procedure as for **5c**. Purification by preparative TLC (hexane/CH_2Cl_2 1:1) provided sulfone **7c** in 72 % yield.

^{1}H-NMR (400 MHz, $CDCl_3$), δ: 8.23-8.00 (m, 8H), 7.70 (d, J=7.88, 1H), 7.46-7.41 (m, 2H), 6.75-6.71 (m, 2H), 5.07 (s, 2H), 3.73 (s, 3H). **^{13}C-NMR** (100 MHz, $CDCl_3$), δ: 163.80, 131.73, 131.14, 130.84, 130.51, 130.33, 129.89, 129.44, 128.33, 128.16, 127.27, 126.18, 125.64, 125.45, 124.81, 124.53, 124.44, 122.79, 122.05, 114.07, 60.60, 55.57. **IR**(KBr), cm^{-1}: 3040 (w), 2992 (w), 2948 (w), 2833 (w), 1594 (vs), 1580 (s), 1497 (s), 1292 (vs), 1259 (vs), 1137 (vs), 1087 (s), 847 (s). **HRMS-ESI(+):** Calculated for $C_{24}H_{18}NaO_3S$ $[(M+H+Na)^{2+}]$ 409.0874, found 409.0877.

Butyl-(1-methylpyrenyl) sulfide **8a**

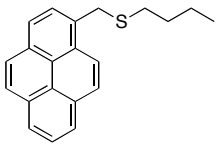

8a

The solution of 1-bromomethylpyrene (0.050 g, 0.170 mmol, 1eq), 1-butanethiol (0.015 g, 0.170 mmol, 1eq) and DBU (0.026 g, 0.170 mmol, 1 eq) in benzene (5 mL) was stirred for 12 hours at r.t. The resulting solution was filtered. Purification by TLC chromatography (silica, hexane/CH_2Cl_2 3:1) provided 0.042 g (81%) of the sulfide **8a**. **^{1}H-NMR** (400 MHz, $CDCl_3$), δ: 8.38 (d, 1H, J=9.24 Hz), 8.21-8.09 (m, 4H), 8.04-7.91 (m, 4H), 4.43 (s, 2H), 2.54-2.49 (m, 2H), 1.65-1.57 (m, 2H), 1.43-1.33 (m, 2H), 0.88 (t, 3H, J=7.33 Hz). **^{13}C-NMR** (100 MHz, $CDCl_3$), δ: 132.06, 131.32, 130.90, 130.74, 128.93, 127.71, 127.58, 127.41, 127.18, 125.98, 125.26, 125.16, 125.14, 124.87, 124.50, 123.39, 34.35, 31.88, 31.87, 31.57, 31.56, 31.55, 30.92, 22.08, 13.69.

IR(KBr), cm^{-1}: 3040 (w), 2952 (m), 2928 (m), 2869 (w), 2858 (w), 1601 (w), 1463 (w), 847 (s). **HRMS-ESI(+):** Calculated for $C_{21}H_{20}S$ $[M^+]$ 304.1286; found 304.1289.

Butyl-(1-methylpyryl) sulfoxide **8b**

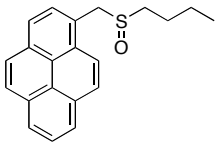

8b

Procedure as for **5b**. Separation by TLC (silica, CH_2Cl_2/acetone 50:1) provides the sulfoxide **8b** with 68% yield. **^{1}H-NMR** (400 MHz, $CDCl_3$), δ: 8.31 (d, 1H, J=9.32), 8.24-7.99 (m, 7H), 7.91 (d, 1H, J=7.2), 4. 88 (d, 1H, J=12.99), 4.62 (d, 1H, J=12.99), 2.75-2.64 (m, 1H), 2.61-2.50 (m, 1H), 1.88-1.61(m, 1H), 1.47-1.24 (m, 1H), 0.86 (t, 3H, J=7.32). **^{13}C-NMR** (100 MHz, $CDCl_3$), δ: 131.60, 131,29, 130.73, 129.80, 128.77, 128.46, 127.99, 127.29, 126.32, 125.73, 125.55, 125.11, 124.96, 124.58, 123.64, 122.84, 57.16, 51.22, 24.51, 22.01, 13.63. **IR**(KBr), cm^{-1}: 3040 (m), 2951 (m), 2926 (m), 2867 (m), 1696 (s), 1303 (s), 1019 (s), 845 (s). **HRMS-ESI(+):** Calculated for $C_{22}H_{15}ONaS$ $[(M+H+Na)^+]$ 343.1133; found 343.1134.

Butyl-(1-methylpyryl) sulfone **8c**

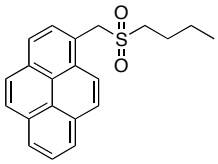

8c

Procedure as for **5c**. Separation byTLC (silica, CH_2Cl_2) provides the sulfone **8c** with 70% yield. **^{1}H-NMR** (400 MHz, $CDCl_3$), δ: 8.33 (d, 1H, J=6.02 Hz), 8.25-8.18 (m, 4H), 8.14-8.03 (m, 4H), 5.00 (s, 2H), 2.90-2.86 (m, 2H), 1.85-1.77 (m, 2H), 1.40-1.31 (m, 2H), 0.86 (t, 3H, J=7.33). **^{13}C-NMR** (100 MHz, $CDCl_3$), δ: 132.05, 131.24, 130.64, 130.28, 129.53, 128.84, 128.41, 127.27, 126.38, 125.93, 125.70, 125.19, 124.98, 124.54, 122.81, 121.39, 57.29, 51.37, 23.57, 21.71, 13.50. **IR**(KBr), cm^{-1}: 3038 (w), 2963 (w), 2943 (w), 2876 (w), 1265 (s), 1120 (vs), 844 (s). **HRMS-ESI(+):** Calculated for $C_{21}H_{20}NaO_2S$ $[(M+H+Na)^+]$ 359.1082; found 359.1082.

References.

[1] Wolffenstein, R., *Chem. Ber.* **1895**, 28, 2265.

[2] Schulte-Labeck, R.V.; Vogel, M.; Karst, U. *Anal. Bioanal. Chem.* **2006**, 386, 559.

[3] Hage, D.S.; Burks, R. M. *Anal. Bioanal. Chem.* **2009**, 395, 301.

[4] Schulte-Labeck, R.K.; Kolla, P.; Karst, U. *Analyst* **2002**, 127, 1152.

[5] Kosolapoff, G.M. *Organic Phosphorus Compounds*. Willey & Sons: New York, 1972.

[6] Akasaka, K.; Ohrui, H. *J. Chromatogr. A* **2000**, 881, 159.

[7] Bellamy, A.J. *J. Forensic Sci.* **1999**, 44, 603.

[8] Fang, A.G. Development of novel fluorescent chemosensors. PhD Thesis, University of California, San Diego, La Jolla, CA, 2003.

[9] Griesbeck, A.G.; Schieffer, S. *Photochem. Photobiol. Sci.* **2003**, 2, 113.

[10] Guo, Y.; Jenks, W. J. *J. Org. Chem.* **1997**, 66, 857.

[11] Jenks, W.S.; Lee, W.; Shutters, D. *J. Phys. Chem.* **1994**, 98, 2282.

[12] Lee, W.; Jenks, W. S. *J. Org. Chem.* **2001**, 66, 474.

[13] Mislow, K.; Simmons, T.; Melillo, J. T.; Ternay, A. L. *J. Am. Chem. Soc.* **1964**, 86, 1452.

[14] Rayner, D.R.; Gordon, A. J.; Mislow, K. *J. Am. Chem. Soc.* **1968**, 90, 4854.

[15] Kingsbury, C.A.; Cram, D. J. *J. Am. Chem. Soc.* **1960**, 82, 1819.

[16] Emerson, D.W.; Craig, A. P.; Potts, I. *J. Org. Chem.* **1967**, 32, 102.

[17] Mislow, K.; Axelrod, M.; Rayner, D. R.; Gotthardt, H.; Coyne, L. M.; Hammond, G. S. *J. Am. Chem. Soc.* **1965**, 87, 4958.

[18] Hammond, G.S.; Gotthardt, H.; Coyne, L. M.; Axelrod, M.; Rayner, D. R.; Mislow, K. *J. Am. Chem. Soc.* **1965**, 87, 4959.

[19] Cooke, R.S.; Hammond, G. S. *J. Am. Chem. Soc.* **1968**, 90, 2958.

[20] Cooke, R.S.; Hammond, G. S. *J. Am. Chem. Soc.* **1970**, 92, 2739.

[21] Charlesworth, P.; Lee, W.; Jenks, W. S. *J. Phys. Chem.* **1996**, 100, 15152.

[22] Chantgilialoglu, C. In *The Chemistry of Sulfoxides and sulfones*; Patai, S.; Rappaport, Z.; Stirling, C. J. M., Eds.; John Willey & Sons, Ltd.; New York, 1988; pp 1081.

[23] Schultz, A.G.; DeBoer, C. D.; Schlessinger, R. H. *J. Am. Chem. Soc.* **1968**, 90, 5314.

[24] Schultz, A.G.; Schlessinger, R. H. *J. Chem. Soc. Chem. Commun.* **1969**, 1483.

[25] Schultz, A.G.; Schlessinger, R. H. *J. Chem. Soc. Chem. Commun.* **1970**, 1294.

[26] Guo, Y.; Jenks, W. S. *J. Org. Chem.* **1995**, 60, 5480.

[27] Guo, Y.; Jenks, W. S. *J. Org. Chem.* **1997**, 62, 857.

[28] Darmanyan, A.P.; Gregory, D. G.; Guo, Y.; Jenks, W.S. *J. Phys. Chem. A* **1997**, 101, 6855.

[29] Guo, Y.; Darmanyan, A. P.; Jenks, W. S. *Tetrahedron Lett.* **1997**, 38, 8619.

[30] Tsurutani, Y.; Machida, S.; Horie, K.; Kawashima, Y.; Nakano, H.; Hirao, K. *J. Photochem. Photobiol. A* **1999**, 122, 161.

[31] Tsurutani, Y.; Yamashita, T.; Horie, K. *Polym. J.* **1998**, 30, 11.

[32] Vos, B.W.; Jenks, W. S. *J. Am. Chem. Soc.* **2002**, 124, 2544.

[33] Cubbage, J.W.; Jenks, W. S. *J. Phys. Chem. A* **2001**, 105, 10588.

[34] Baliah, V.; Pillay, M. K. Indian J. Chem. **1971**, *9*, 503-504.

[35] Yamato, T.; Miyazawa, A.; Tashiro, M. *J. Chem. Soc. Perkin Trans. 1*, **1993**, 3127-3137.

[36] Bair, K. W.; Tuttle, R. L.; Knick, V. C.; Cory, M.; McKee, D. *J. Med. Chem*., **1990**, *33*, 2385-2393

[37] Akiyama, S.; Nakasuji, K.; Nakagawa, M. *Bull. Chem. Soc. Japan*, **1971**, *44*, 2231.

Appendix.

Absorption and emission spectra of compounds 5(a-c)-8(a-c).

All absorption spectra were measured using 1×10^{-5} M solutions in CH_2Cl_2 unless otherwise noted. Emission spectra were measured using 5×10^{-6} M solutions in CH_2Cl_2. At concentrations above 5×10^{-5} M, the emission from sulfones **5c-8c** begins to decrease, presumably as the result of the formation of non-emissive excimers. We observe no detectible degradation of sulfoxides under these measurement conditions.

Figure A3.1. Absorbtion spectra of **5a-5c** (left) and **6a-6c** (right).

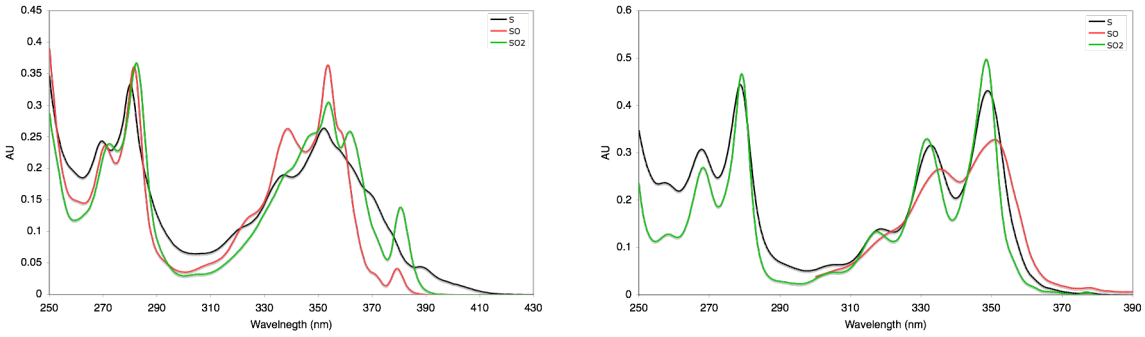

Figure A3.2. Absorbtion spectra of **7a-7c** (left) and **8a-8c** (right).

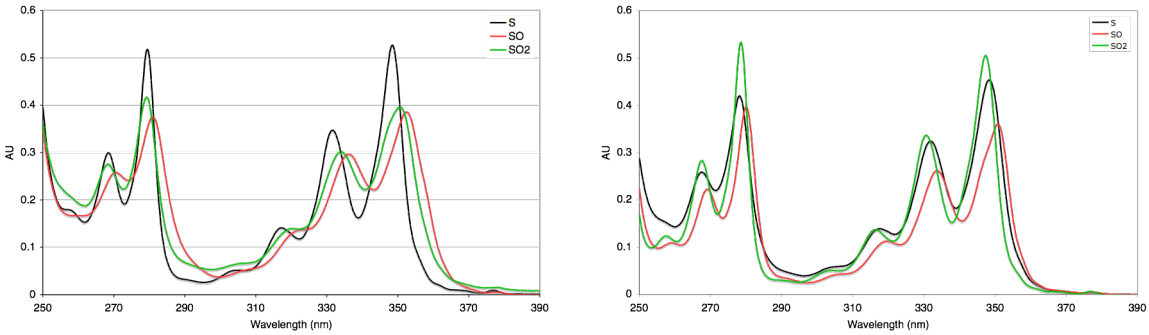

Figure A3.3. Emission spectra of **6a-6c** (left) and **8a-8c** (right).

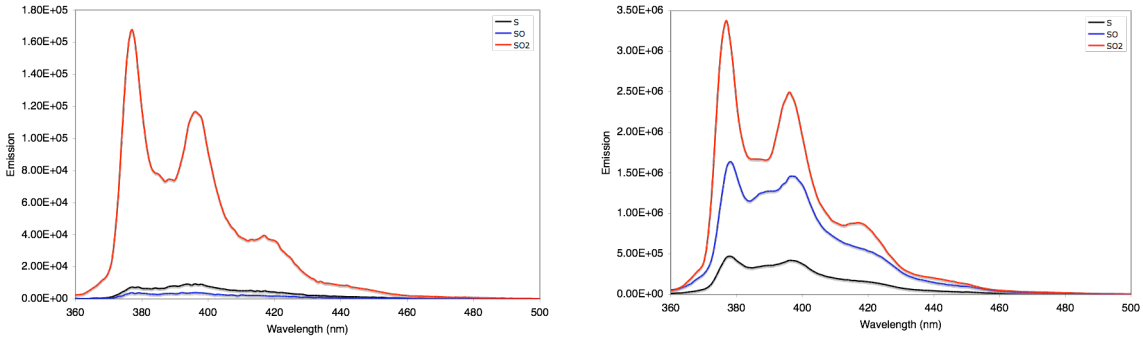

Chapter 4.

The origins of sulfoxide "non-emission"

4.1. Experimental and computational study.

We have taken a combined experimental and theoretical approach to understanding the behavior of these and related sulfoxides and sulfones. Beginning with structural variation first, in addition to the above described benzylic sulfide/sulfoxide/sulfone series **1a-c**, **2a-c**, **3a-c** (***Figure 4.1***, see Chapter 3) we prepared four new sulfide/sulfoxide/sulfone series **4(a-c)-7(a-c)** (***Figure 4.2-4.4***) in which the sulfur atom bears a butyl or phenyl group and the chain connecting the sulfur atom to the pyrene fluorophore contains either 2 or 4 carbon atoms.

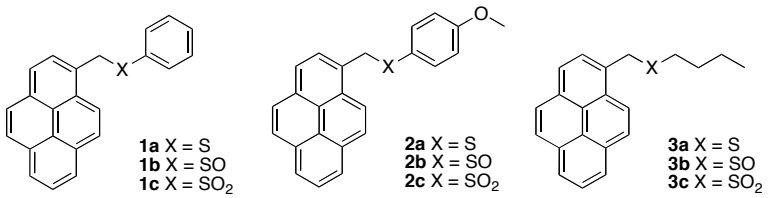

Figure 4.1. First generation sulfides, sulfoxides and sulfones.

Table 4.1. Properties of first generation sulfur-bearing fluorophores.[a]

Compound	E_{ex} (λ)[b]	E_{em} (λ)[b]	Φ_F[c]
1a	82 (349)	76 (377)	0.01
1b	81 (352)	76 (376)	<0.01 (0.009)
1c	82 (350)	76 (377)	0.47
2a	82 (349)	76 (376)	<0.01 (0.006)
2b	81 (352)	76 (377)	<0.01 (0.007)
2c	81 (352)	76 (377)	0.41
3a	82 (348)	76 (377)	0.02
3b	82 (349)	76 (378)	0.09
3c	82 (352)	76 (377)	0.09

[a]Extinction coefficients for longest-wavelength λ_{max} transition are all ca. 3×10^3 $M^{-1}cm^1$. All values are for 10^{-5} M solutions in CH_2Cl_2. [b] Excitation and emission energies in kcal/mol; wavelengths in nm. [c]Relative to pyrene (ϕ = 0.32). Quantum yield measurement error is estimated at ± 0.002.

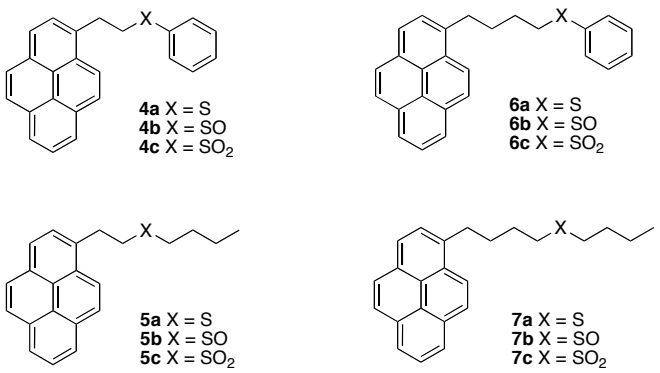

Figure 4.2. New sulfur containing pyrene derivatives.

To prepare sulfides **4a-5a** 1-pyreneacetic acid was reduced with $LiAlH_4$ followed by bromination and subsequent nucleophilic substitution with the corresponding thiol (***Figure 4.3***). Oxydation of sulfides **4a-5a** with one or two equivalents of *m*CPBA furnished sulfoxides **4b-5b** and sulfones **4c-5c.**

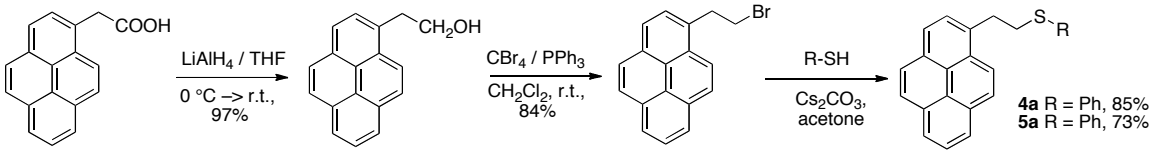

Figure 4.3. Synthesis of sulfides **4a** and **5a**.

Bromination of 1-pyrenebutanol and subsequent nucleophilic substitution with thiophenole or butylthiol provides sulfides **6a-7a** (***Figure 4.4***).

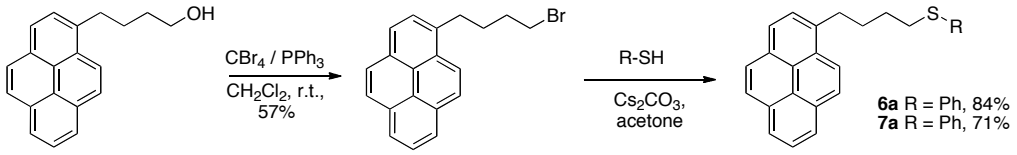

Figure 4.4. Synthesis of sulfides **4a** and **5a**.

Oxydation of sulfides **6a-7a** with one or two equivalents of *m*CPBA furnished sulfoxides **6b-7b** and sulfones **6c-7c.**

With minor variations in extinction coefficient and quantum yield, all 12 of the new compounds are very similar to pyrene, the changes in sulfur oxidation state having no significant impact on the efficiency of fluorescence emission (***Table 4.2***). While this failed to clarify the origin of low sulfoxide fluorescence, it argues strongly against a quenching mechanism involving photoinduced electron transfer: electron transfer should have an exponential distance dependence [1] and the sulfides and sulfoxides with a 2 carbon spacer should still exhibit some reduction in fluorescence relative to the sulfone if electron transfer were operating.

Table 4.2. Quantum yields of additional sulfur containing pyrene derivatives.[a]

Compound	Φ_F[b]	Compound	Φ_F[b]
4a	0.43	**6a**	0.49
4b	0.41	**6b**	0.59
4c	0.44	**6c**	0.51
5a	0.42	**7a**	0.50
5b	0.52	**7b**	0.58
5c	0.45	**7c**	0.46

[a]All absorption and emission maxima are essentially identical to those of pyrene; extinction coefficients for the longest wavelength λ_{max} are all ~ 4×10^3 $M^{-1}cm^{-1}$. [b]Relative to pyrene ($\phi = 0.32$).

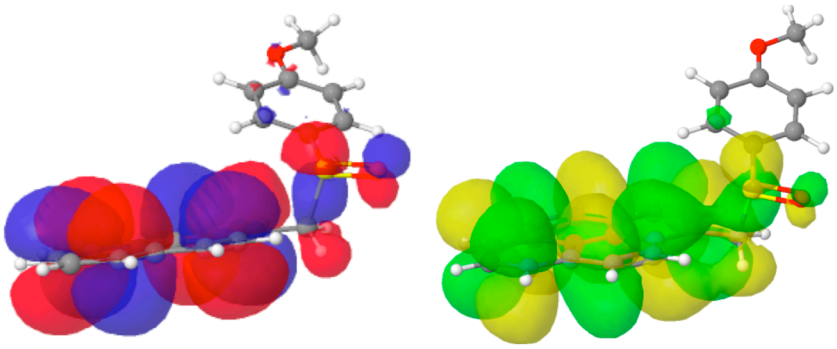

Figure 4.5. HOMO (left) and LUMO (right) for **2b**. Molecular orbital surface shows the 0.01 isocontour value; grid uses 64000 points.

Inspection of calculated HOMOs and LUMOs [2] for all compounds of the **1-3** series show that, in retrospect, our anticipation of electron transfer quenching of fluorescence was naive. We had expected the quenching to arise via transfer of an electron from a non-bonding lone pair of a sulfide (or even possibly a sulfoxide) to the excited state of the attached pyrene. The HOMOs and LUMOs reveal that, in all cases, the "lone pairs" are in fact not "lone" at all, but are fully delocalized over the pyrene-CH_2 fragment. The HOMO and LUMO of **2b** are representative (***Figure 4.5***).

In parallel with computational efforts, experimental work has established that the excited state of the S-aryl sulfoxides (**1b**, **2b**) is deactivated by reversible α-cleavage of the benzylic C-S bond (***Figure 4.6***). There is (fortunately) significant literature precedent for this reaction pathway [3], the defining empirical manifestation of which is the formation of pyrenecarboxaldehyde upon prolonged photolysis. While the initial fragmentation is followed by reformation of the starting sulfoxide most of the time, it occasionally leads to formation of the isomeric sulfenate ester **5**. This undergoes secondary photolysis and H-atom transfer to form the carboxaldehyde. (The aldehyde can be isolated in ≥ 70% yield.) It should be noted that no significant photocleavage is observed for the **3b**, or for the sulfides **1a** and **2a** or sulfones **1c** and **2c**.

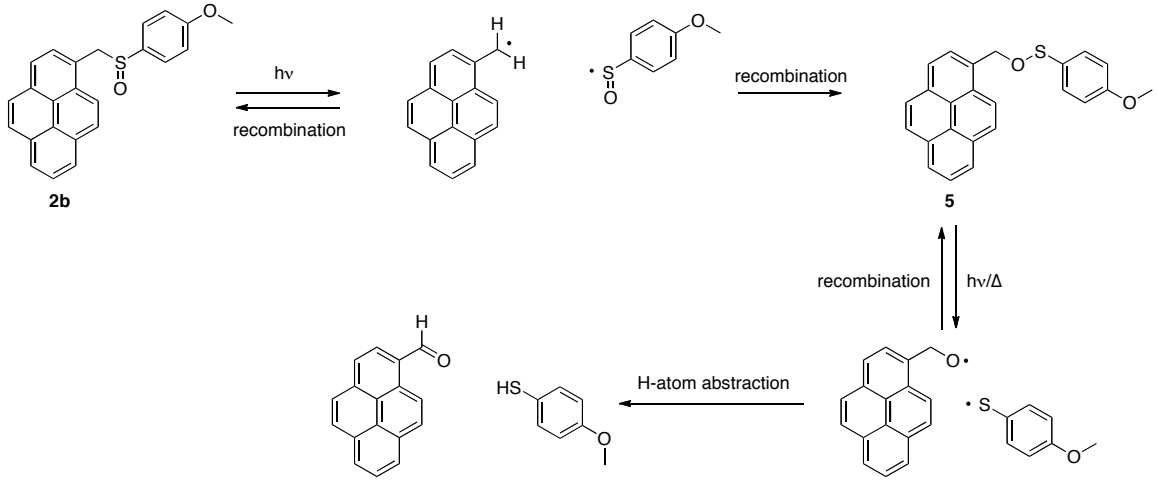

Figure 4.6. Deactivation of the excited state of **2b** by reversible α-cleavage.

While, as mentioned, there is ample precedent for this α-cleavage pathway, our systems are distinct in that all previous reports of α-cleavage have involved direct excitation of the aryl sulfoxide fragment (or possibly simultaneous excitation of the aryl sulfoxide and the benzylic fragment), whereas ours involve the selective excitation of the appended benzylic chromophore. This is particularly significant in that the pyrenylmethyl fragment has a much lower excited state energy (ca. 77 kcal/mol based on the longest wavelength λ_{em}) than the sulfoxide fragment ($PhS(O)CH_3$ has a singlet energy of 99 kcal/mol.

A simple explanation for these observations could be that **1b** and **2b** have anomalously low bond dissociation energies (BDEs) for the benzylic C-S bond. There are very few C-S BDEs available in the literature, although the values for $(CH_3)_2S$, $(CH_3)_2SO$ and $(CH_3)_2SO_2$ are established as 77, 55 and 68 kcal/mol [4], respectively. It was not clear that these values – in either absolute or relative terms – would be relevant to our system, and thus we undertook computational determination of the BDEs for all molecules in the **1-3** series (***Table 4.3***). An important caveat is that we are interested in an excited state process, while the calculated BDEs are all for the ground state of the molecules. However, it is not yet computationally feasible to calculated excited state BDE values (the data in ***Table 4.3*** represent several months of CPU time on a fast cluster).

Table 4.3. Calculated benzylic BDEs and excited-state bond lengths for **1-3** series sulfur species.

Compound	C-S BDE (kcal/mol)	Ground state (S_0) C-S bond length (Å)	Excited state (S_1) C-S bond length (Å)
1a	55	1.87	
1b	39	1.90	1.87
1c	58	1.86	
2a	53	1.88	
2b	39	1.90	1.86
2c	57	1.86	
3a	59	1.87	
3b	39	1.89	1.85
3c	56	1.86	

In lieu of excited state BDEs, we have calculated optimized ground (S_0) structures for all molecules in the **1-3** series and excited state structures for the sulfoxides (S_1) (***Table 4.3***),

assuming that variation in BDE between the ground and excited states would be reflected in the length of the benzylic C-S bond.

There are several significant aspects of the calculated BDEs and bond lengths. First, the sulfoxides exhibit the weakest BDEs, the values lying 15-20 kcal/mol below those of the corresponding sulfides and sulfones. This is consistent with previous work indicating that the sulfinyl radical (in analogy to the nitroxyl radical) benefits from significant resonance stabilization that distributes the unpaired electron over both the sulfur and oxygen atoms [4]. Second, the BDEs for the sulfides and sulfones are similar in energy, which fails to explain why the S-Bu and S-Ar series are different, and why the sulfides are non-emissive relative to the sulfones.

Third, and perhaps most surprising, the C-S bond lengths for the sulfoxides are *shorter* in the excited state by an average of 0.04 Å (data not shown). This indicates that the ground state BDE values represent an lower limit on the excited state (S_1) BDEs, which must be higher, as reflected by the shortened bond length. (This point will be addressed again shortly.) Finally, all of the BDEs lie below the estimated singlet energy of pyrene (ca. 77 kcal/mol), and understanding the photophysics of these compounds is thus more complicated than simply identifying cases in which the excitation energy exceeds the benzylic C-S bond strength.

Two lines of analysis clarify these issues. First, regarding the low emission intensity from all of the sulfides in the **1-3** series, it is important to note that low emission is observed for the S-Bu and S-Ar compounds, and that there is no evidence for photochemical C-S bond cleavage, based on the compounds' photochemical stability. The simplest explanation for the low sulfide quantum yields is thus heavy atom effect induced intersystem crossing (ISC). This is foreshadowed by previous studies on aryl sulfides such as thioanisole [5], and is supported by our observation of weak phosphorescence emission from the **1-3** series sulfides at 77K (***Figure 4.7***). While the phosphorescence is weak, it clearly indicates that the triplet excited state is populated from the initial singlet under the measurement conditions.

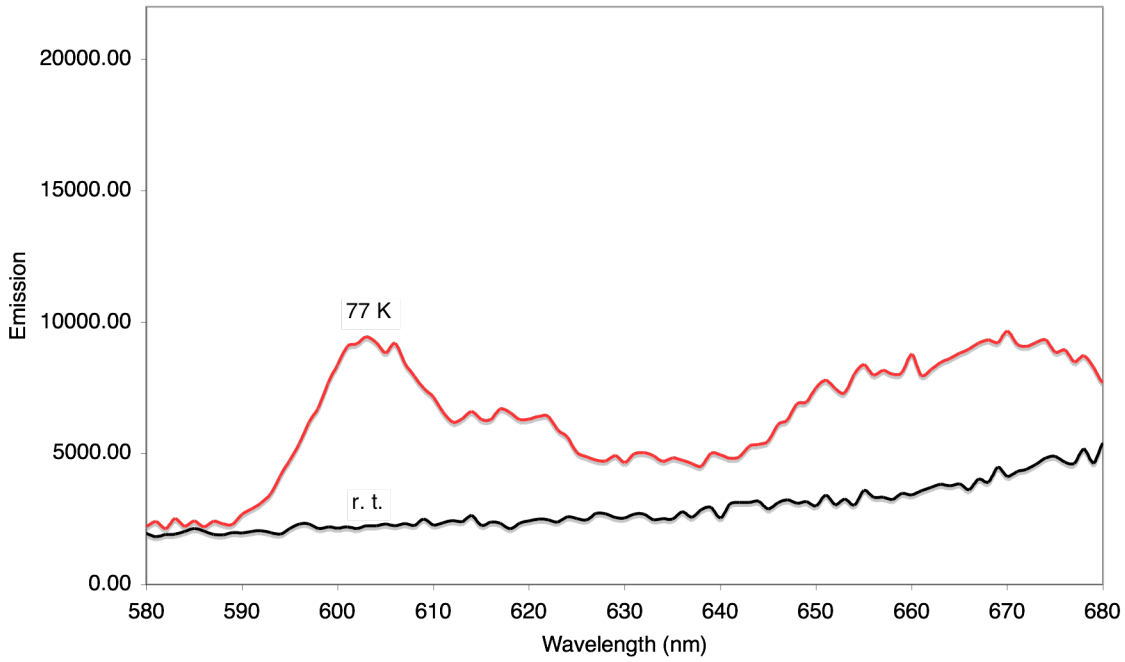

Figure 4.7. Emission from **2a** (10^{-5}M in 2-methyltethahydrofurane) at 77 K.

This leaves only the disparity between S-Bu and S-Ar sulfoxide emission to explain. The requirement for an S-Ar group to "provide" low efficiency sulfoxide emission indicates that the aryl fragment must be electronically coupled in some way to the pyrene chromophore being excited. (This is also consistent with the absence of photochemical degradation in **3b**.) That is, there must be some mechanism by which the excited state of the pyrene fragment transfers excited state energy to the S-Ar fragment, leading ultimately to C-S bond cleavage [6]. Inspection of the S_1 excited state structures in the **1-3** series does not provide a basis for making these distinctions: like the HOMOs and LUMOs for the series, essentially all of the electron density is predicted to reside on the pyreneCH_2X fragment, without significant involvement of the other subsituent on S, be it alkyl or aryl.

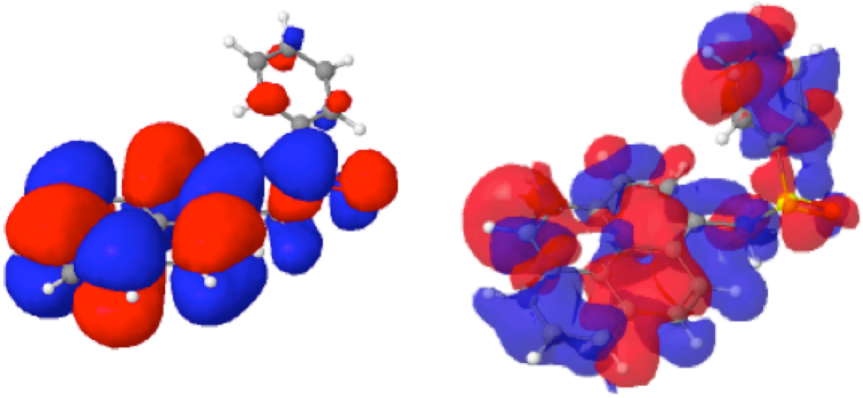

Figure 4.8. Calculated singly-occupied HOMOs for S_1 and S_2 of **1b**. Molecular orbital surface shows the 0.01 isocontour value; grid uses 64000 points.

This issue has been resolved by a computational search for additional singlet excited states. Focusing on **1b** as a representative case (as the calculations are very time consuming) we find an additional low lying singlet (which we denote as S_2; ***Figure 4.8***). This S_2 state lies only 6 kcal/mol in energy above S_1, and would be associated with significant electron density on the S-Ar fragment of the molecule. This then explains the difference between the S-Bu and S-Ar sulfoxides: the S-Ar sulfoxides possess an additional low lying singlet state with sufficient electron density on the S-Ar fragment to rationalize selective cleavage of the C-S bond in these species. Significantly, we calculate the C-S bond length of S_2 to be 1.93 Å – a significant lengthening relative to the ground state, which, in contrast to the observations for S_1, is consistent with weakening of the C-S bond. Qualitatively, this can be regarded as a through-bond uphill energy transfer from an initially generated pyrene-localized excited state donor (S_1) to the aryl sulfoxide acceptor. C-S bond cleavage takes place on the potential energy surface of the S_2 excited state whereas fluorescence emission occurs from the S_1 excited state. At low temperature (77 K) thermal population of the low-lying S_2 becomes less efficient and increase in fluorescence intensity is observed (***Figure 4.9***). We have considered the possibility of contact mediated/through-space energy transfer, but reject it based on molecular geometry and the absence of fluorescence quenching in experiments where pyrene is titrated with a large excess of $PhS(O)CH_3$ (***Figure 4.10***).

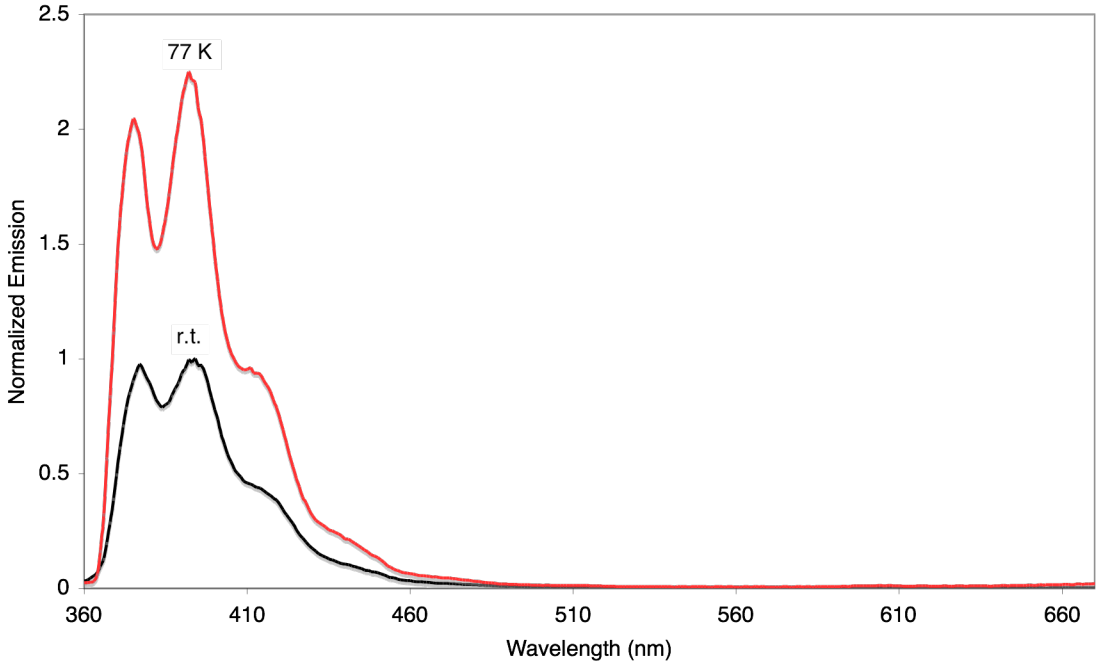

Figure 4.7. Emission from **2b** (10^{-5}M in 2-methyltethahydrofurane) at r.t. and at 77 K .

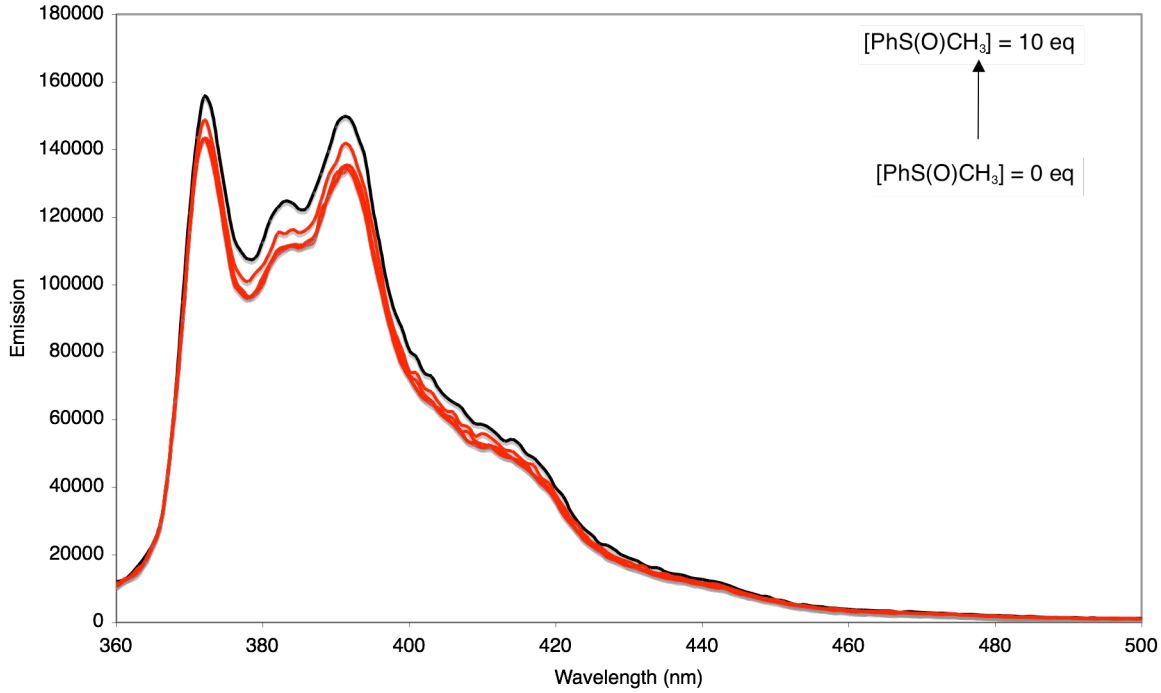

Figure 4.10. Emission from pyrene (10^{-5} M in CH_2Cl_2) in the presence of 0–10 equivalents of $PhS(O)CH_3$.

4.2. Next generation oxidation-responsive probes.

Beyond their intrinsic scientific merit, these studies provide two key insights regarding the design of next-generation sulfur based oxidation probes. First, if the calculated C-S BDEs are taken as the ultimate limitation on the singlet energy of fluorophores that can be employed, virtually any visibly emissive fluorophore should be suitable. (A BDE of 40 kcal/mol correlates with an emissive singlet state energy of ~700 nm.) At long visible wavelength emission, deactivation by internal conversion (rather than α-cleavage) is likely to be the most problematic issue, rather than specific choice of reporting fluorophore based on emission wavelength. Second, and in retrospect more surprising, it is now clear that the structure of the aryl substituent on the aryl sulfoxide "acceptor" must be considered. If our hypothesis that a requirement for C-S bond cleavage is the formation of an excited state that is delocalized over not just the initially excited fluorophore but also the S-Ar fragment, altering the structure of the fluorophore likely also requires adjusting the structure of the accepting S-Ar unit. (That is, relying on S(O)Ph as an acceptor is not certain to be successful.)

4.3. Possible targets for future work.

A set of nine new sulfoxides probes will be synthesized (***Figure 4.11***). While it would be desirable to attempt to predict the excited state properties of these molecules computationally the calculations for the **1-3** series are already pushing the limits of our computational resources. As such, we have not yet been able to identify 'preferred' sulfoxides and we are currently planning to prepare all nine. These nine targets are based on the combination of three known haloalkyl chromophore derivatives with three known thioaryls [8]. The reporting chromophores have been selected for their well established visible emission, one coumarin framework, one fluorescein scaffold and one dipyrromethane (coumarin emission ca. 450 nm; fluorescein and borodipyrromethane emission 500-600 nm). The sulfides have been chosen based on accessibility and variation in the degree of conjugation, with the aryl substituent ranging from phenyl to anthracenyl to pyrenyl. It should be noted that "known" by no means equates to "easily prepared" – much of the reported synthetic chemistry is low yielding, for both the

haloalkyl species and the thioaryls, and the purification of these molecules is certain to be challenging at best.

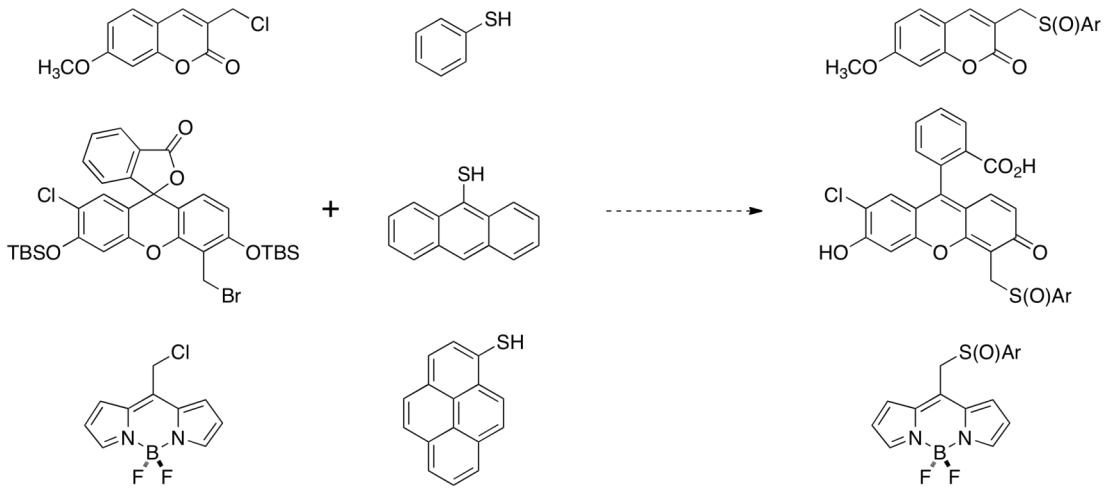

Figure 4.11. Nine second generation sulfoxide targets.

Once prepared, the optical properties of the thiol/fluorophore conjugates will be evaluated at the sulfide, sulfoxide and sulfone oxidation states. We will subsequently explore the response of the sulfoxide probes to H_2O_2 generated from TATP, using the protocol described in the introductory section. While the new probes have been selected in part for solubility in organic solvents (as TATP is not water soluble), one can imagine the synthesis of water soluble probes. These would have potential application for the detection, or even cellular imaging, of other reactive oxygen and reactive nitrogen species such as superoxide or NO. (Superoxide is known to oxidize sulfoxides to sulfones; NO is known to oxidize sulfides to sulfoxides, although there are no reports of reaction with sulfoxides to sulfones [9].)

4.4. A final caveat.

A distinct risk associated with moving the emission of our sulfoxide probes into the visible region is that the absobance will also, eventually, move into the visible region of the spectrum as well. While this is not likely to be an issue for coumarin chromophores, it

will be for longer wavelength chromophores such as those related to fluorescein. This in turn raises the issue of photochemical instability under ambient lighting conditions. Should this prove an impediment to the development of new probes, and alternative strategy would be to retain the chromophore structures selected but remove the benzylic carbon entirely. We have previously found that pyreneS(O)Ph and pyreneSO_2Ph have quantum yields of 0.02 and 0.76, respectively. Thus, it should be possible to exploit this sulfoxide/sulfone and related sulfoxide/sulfone redox pairs, although the origin of low emission from the sulfoxides is mechanistically distinct from the work presented here.

4.5. Conclusion.

At this stage of our research we have conducted a combined experimental and theoretical study to understand the nature of anomalously low emission of aromatic sulfuxides used as visual fluorescent assay for TATP (see Chapter 3). An initial series of pyrenylmethyl sulfide/sulfoxide/sulfone with varying substituents (aryl or butyl) on the sulfur atom was prepared. For the S-butyl species the sulfide is the least fluorescent whereas in the S-aryl species the sulfide and sulfoxide are both essentially non-emissive, while the sulfone is strongly emissive.

Fluorescence measurements on the new set of aromatic sulfides/sulfoxides/sulfones allowed us to reject our initial assumption that photoinduced electron transfer from the lone electron pair of sulfur atom is the cause of fluorescence quenching in aromatic sulfoxides (as well as sulfides). Photochemical experiments have established that the excited state of the benzylic aryl sulfoxides is deactivated by reversible α-cleavage of the C-S bond.

Bond dissociation energies (BDE) and ground state bond lengths for all benzylic sulfur species were calculated. Sulfoxides exhibit the weakest BDEs in comparison to sulfides and sulfones within each series. BDEs for the sulfides and sulfones are similar in energy.

Weak phosphorescence from sulfides at 77K suggests that intersystem crossing induced by heavy atom effect is the source of low quantum yield of aromatic sulfides.

Further computational study showed that aryl fragment in S-aryl sulfoxides is electronically coupled to the pyrene being excited and the excited state of the pyrene fragment transfers excitation energy to the S-Ar fragment leading to C-S bond cleavage. This process takes place on the low lying S_2 state surface. This explains higher emission and photochemical stability of the S-Bu sulfoxides compared to S-Ar.

4.6. Experimental part.

4.6.1. General procedure for oxidation of Sulfides to Sulfoxides.

The solution of a sulfide (1 eq) and *m*-Chloroperbenzoic acid (70%, 0.9 eq) in 3 mL CH_2Cl_2 was stirred for 30 min at 0°C. Purification of reaction mixture by flash column chromatography (silica, CH_2Cl_2/acetone 50:1) without preliminary working up provides the corresponding sulfoxides.

4.6.2. General procedure for oxidation of Sulfides to Sulfones

The solution of a sulfide (1 eq) and *m*-Chloroperbenzoic acid (70%, 2.2 eq) in 3 mL CH_2Cl_2 was stirred for 30 min at 0°C. Purification of reaction mixture by flash column chromatography (silica, hexane/CH_2Cl_2 1:1) without preliminary working up provides the corresponding sulfoxides.

4.6.3. Synthetic details and tabulated spectroscopic data

2-Pyrenylethyl-phenyl sulfide **4a**

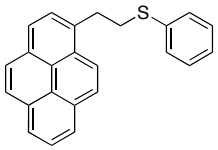

4a

To the solution of 2-pyrenyl-1-bromoethane[3] (0.2g, 0.65 mmol, 1eq) and thiophenole (0.072g, 0.65 mmol, 1eq) in 7 ml dry acetone Cs_2CO_3 (0.64 g, 1.95 mmol, 3 eq) was added. The resulting mixture was stirred at r.t. for 14 h. Water (10ml) was then added to the reaction mixture. The organic phase was separated, washed with water, dried over $MgSO_4$ and

concentrated. Purification by flash column chromatography (silica, hexane/CH_2Cl_2 5:1) yielded sulfide **4a** (73%). **^{1}H-NMR** (400 MHz, $CDCl_3$), δ: 8.19-7.80 (*m*, 9H), 7.49-7.18 (*m*, 5H), 3.69-3.58 (*m*, 2H), 3.40-3.30 (*m*, 2H). **^{13}C-NMR** (100 MHz, $CDCl_3$), δ: 136.16, 134.23, 131.31, 130.74, 130.21, 129.67, 128.60, 127.54, 127.36, 127.25, 126.84, 126.17, 125.81, 124.99, 124.78, 122.77, 35.34, 33.40. **IR**(KBr), cm^{-1}: 3037 (m), 2958 (w), 2936 (w), 1587 (m), 1480 (s), 1435 (m), 1281 (m), 1185 (m), 1091 (s), 840 (s). **HRMS-EI**(+): Calculated for $C_{24}H_{18}S$ [M^+] 338.1129; found 338.1123.

2-Pyrenylethyl-phenyl sulfoxide **4b**

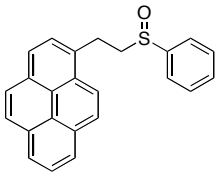

4b

Oxidation according to the general procedure provides sulfoxide **4b** with 72% yield. **^{1}H-NMR** (400 MHz, $CDCl_3$), δ: 8.18-7.3 (*m*, 14H), 3.86-3.70 (*m*, 1H), 3.61-3.49 (*m*, 1H), 3.38-3.10 (*m*, 2H). **^{13}C-NMR** (100 MHz, $CDCl_3$), δ: 142.99, 134.42, 133.06, 132.36, 131.87, 131.23, 131.06, 130.63, 130.38, 130.07, 129.57, 129.25, 128.50, 128.06, 127.87, 127.29, 127.00, 125.91, 125.13, 125.01, 124.96, 124.87, 124.72, 124.09, 122.33, 57.47, 25.37. **IR**(KBr), cm^{-1}: 3039 (m), 2998 (w), 2661 (w), 1669 (vs), 1447 (w), 1305 (m), 1041 (s), 842 (s). **HRMS-ESI**(+): Calculated for $C_{24}H_{18}NaOS$ [M+Na]$^+$ 377.0976; found 377.0971.

2-Pyrenylethyl-phenyl sulfone **4c**

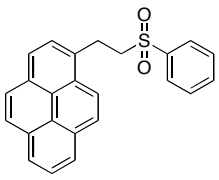

4c

Oxidation according to the general procedure provides sulfone **4c** with 77% yield. **^{1}H-NMR** (400 MHz, $CDCl_3$), δ: 8.21-7.97 (*m*, 9H), 7.80-7.52 (*m*, 5H), 3.82-3.72 (*m*, 2H), 3.60-3.50 (*m*, 2H). **^{13}C-NMR** (100 MHz, $CDCl_3$), δ: 131.09, 130.71, 130.68, 129.41, 128.54, 128.29, 128.15, 127.34, 127.30, 127.08, 126.13, 125.41, 125.23, 125.12, 124.99, 124.79, 122.08, 57.34, 26.56. **IR**(KBr), cm^{-1}: 3040 (m), 2942 (w), 1603 (w), 1449 (m), 1319 (s), 1306 (vs), 1142 (vs), 1081 (vs). **HRMS-ESI**(+): Calculated for $C_{24}H_{18}NaO_2S$ [M+Na]$^+$ 393.0925; found 393.0920.

2-Pyrenylethyl-butyl sulfide **5a**

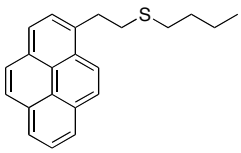

5a

To the solution of 2-pyrenyl-1-bromoethane[3] (0.2g, 0.65 mmol, 1eq) and butanethiol (0.059g, 0.65 mmol, 1eq) in 7 ml dry acetone Cs_2CO_3 (0.64 g, 1.95 mmol, 3 eq) was added. The resulting mixture was stirred at r.t. for 20 h. Water (10ml) was then added to the reaction mixture. The organic phase was separated, washed with water, dried over $MgSO_4$ and concentrated. Purification by flash column chromatography (silica, hexane/CH_2Cl_2 7:1) yielded sulfide **5a** (84%). **^{1}H-NMR** (400 MHz, $CDCl_3$), δ: 8.22 (*d*, 1H, J=9.27 Hz), 8.16-7.93 (*m*, 7H), 7.85 (*d*, 1H, J=7.77 Hz), 3.59 (*t*-like, dH), 2.97 (*t*-like, 2H), 2.59 (*t*, 2H, J=7.23), 1.64-1.55 (*m*, 2H), 1.47-1.34 (*m,*2H), 0.90 (*t*, 3H, J=7.32 Hz). **^{13}C-NMR** (100 MHz, $CDCl_3$), δ: 134.70, 131.32, 130.78, 130.11, 128.54, 127.46, 127.39, 127.23, 126.75, 125.78, 125.01, 124.94, 124.76, 122.89, 34.12, 33.69, 32.12, 31.74, 21.95, 13.60. **IR**(KBr), cm^{-1}: 3038 (m), 2952 (m), 2866 (w), 1603 (m), 1456 (m), 1431 (m), 1208 (w), 842 (vs). **HRMS-EI**(+): Calculated for $C_{22}H_{22}S$ [M^+] 318.1442; found 318.1438.

2-Pyrenylethyl-butyl sulfoxide **5b**

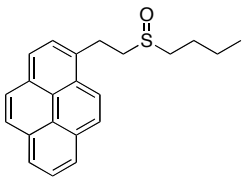

5b

Oxidation according to the general procedure provides sulfoxide **5b** with 68% yield. **^{1}H-NMR** (400 MHz, $CDCl_3$), δ: 8.28 (*d*, 1H, J=9.24 Hz), 8.20-7.90 (*m*, 8H), 3.95-3.70 (*m*, 2H), 3.21-3.01 (*m*, 2H), 2.85-2.73 (*m*, 1H), 2.69-2.58 (*m*, 1H), 1.80-1.65 (*m*, 2H), 1.55-1.34 (*m*, 2H), 0.92 (*t*, 3H, J=7.31Hz). **^{13}C-NMR** (100 MHz, $CDCl_3$), δ: 132.73, 131.27, 130.70, 130.44, 128.52, 127.94, 127.33, 127.05, 125.94, 125.16, 125.00, 124.89, 124.78, 122.54, 53.53, 52.22, 26.40, 24.59, 21.94, 13.52. **IR**(KBr), cm^{-1}: 3047 (w), 2953 (m), 2931 (w), 2866 (m), 1602 (m), 1465 (m), 1435 (m), 1027 (vs), 985 (s), 848 (vs).

2-Pyrenylethyl-butyl sulfone **5c**

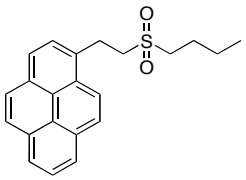

5c

Oxidation according to the general procedure provides sulfone **5c** with 72% yield. **^{1}H-NMR** (400 MHz, $CDCl_3$), δ: 8.28-8.00 (*m*, 8H), 7.92 (*d*, J=7.68 Hz), 3.95-3.85 (*m*, 2H), 3.47-3.38 (*m*, 2H), 2.95-2.87 (*m*, 2H), 1.83-1.72 (*m*, 2H), 1.46-1.30 (*m*, 2H), 0.86 (*t*, 3H, J=7.30 Hz). **^{13}C-NMR** (100 MHz, $CDCl_3$), δ: 131.62, 130.47, 129.72, 129.24, 128.44, 127.55, 127.21, 127.02, 126.84, 125.77, 125.12, 124.92, 124.64, 122.54, 56.72, 54.32, 28.52, 25.66, 21.97, 13.55. **IR**(KBr), cm^{-1}: 3041 (w), 2959 (w), 2871 (w), 1451 (w), 1323 (s), 1125 (vs), 840 (vs). **HRMS-EI**(+): Calculated for $C_{22}H_{22}O_2S$ [M^+] 350.1341; found 350.1338

4-Pyrenylbutyl-phenyl sulfide **6a**

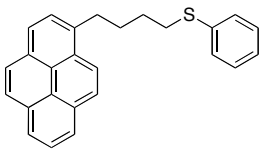

6a

To the solution of 2-pyrenyl-1-bromobutane[3] (0.15g, 0.45 mmol, 1eq) and butanethiol (0.049g, 0.45 mmol, 1eq) in 7 ml dry acetone Cs_2CO_3 (0.44 g, 1.35 mmol, 3 eq) was added. The resulting mixture was stirred at r.t. for 16 h. Water (10ml) was then added to the reaction mixture. The organic phase was separated, washed with water, dried over $MgSO_4$ and concentrated. Purification by flash column chromatography (silica, hexane/CH_2Cl_2 7:1) yielded sulfide **6a** (71%). **^{1}H-NMR** (400 MHz, $CDCl_3$), δ: 8.22 (*d*, 1H, J=9.27), 8.15-7.94 (*m*, 7 H), 7.81 (*d*, 1H, J=7.84), 7.31-7.12 (*m*, 5H), 3.33 (*t*, 2H, J=7.57), 2.96 (*t*, 2H, J=7.21), 2.04-1.94 (*m*, 2H), 1.86-1.76 (*m*, 2H). **^{13}C-NMR** (100 MHz, $CDCl_3$), δ: 136.60, 136.31, 131.37, 130.84, 129.77, 129.20, 128.72, 128.53, 127.41, 127.15, 127.09, 126.50, 125.75, 124.97, 124.77, 124.69, 124.60, 123.23, 33.62, 32.91, 30.64, 28.99. **IR**(KBr), cm^{-1}: 3040 (w), 2949 (w), 2927 (w), 1600 (m), 1479 (s), 1435 (m). **HRMS-EI**(+): Calculated for $C_{26}H_{22}S$ [M^+] 366.1442; found 366.1444.

4-Pyrenylbutyl-phenyl sulfoxide **6b**

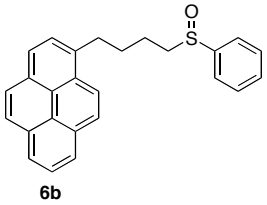

6b

Oxidation according to the general procedure provides sulfoxide **6b** with 70% yield.

^{1}H-NMR (400 MHz, $CDCl_3$), δ: 8.20-7.94 (*m*, 8H), 7.77 (*d*, 1H, J=7.8), 7.54-7.50 (*m*, 2H), 7.43-7-38 (*m*, 3H), 3.42-3-25 (*m*, 2H), 2.86-2.72 (*m*, 2H), 2.05-1.70 (*m*, 4H). **^{13}C-NMR** (100 MHz, $CDCl_3$), δ: 143.33, 135.70, 131.34, 130.75, 129.86, 129.02, 128.47, 127.37, 127.27, 127.09, 126.60, 125.75, 124.85, 124.67, 123.85, 123.04, 57.07, 32.99, 30.64, 22.15. **IR**(KBr), cm^{-1}: 3045 (m), 2950 (w), 2933 (m), 1601 (s), 1440 (s), 1031 (vs), 839 (s). **HRMS-ESI**(+): Calculated for $C_{26}H_{22}S$ $[M+H]^+$ 383.1470; found 383.1470.

4-Pyrenylbutyl-phenyl sulfoxide **6c**

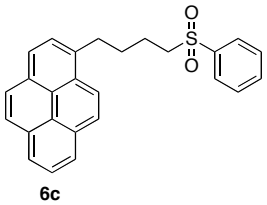

6c

Oxidation according to the general procedure provides sulfone **6c** with 78% yield. **^{1}H-NMR** (400 MHz, $CDCl_3$), δ: 8.18-7.96 (*m*, 8H), 7.84-7.74 (*m*, 3H), 7.57-7.41 (*m*, 3H), 3.34-3.29 (*m*, 2H), 3.14-3.09 (*m*, 2H), 2.16-1.84 (*m*, 4H). **^{13}C-NMR** (100 MHz, $CDCl_3$), δ: 135.29, 133.41, 130.75, 129.05, 127.87, 127.33, 127.02, 126.65, 125.78, 124.89, 124.69, 122.91, 56.04, 32.74, 30.12, 22.63. **IR**(KBr), cm^{-1}: 3058 (m), 3037 (m), 2936 (s), 1602 (s), 1584 (s), 1446 (s), 1305 (vs), 1146 (vs). **HRMS-ESI**(+): Calculated for $C_{26}H_{23}O_2S$ $[M+H]^+$ 399.1419; found 399.1413.

4-Pyrenylbutyl-butyl sulfide **7a**

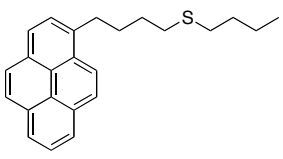

7a

To the solution of 2-pyrenyl-1-bromobutane[3] (0.30g, 0.89 mmol, 1eq) and butanethiol (0.080g, 0.89 mmol, 1eq) in 10 ml dry acetone Cs_2CO_3 (0.87 g, 2.67 mmol, 3 eq) was added. The resulting mixture was stirred at r.t. for 16 h. Water (10ml) was then added to the reaction mixture. The organic phase was separated, washed with water, dried over $MgSO_4$ and concentrated. Purification by flash column chromatography (silica, hexane/CH_2Cl_2 7:1) yielded sulfide **7a** (71%). **^{1}H-NMR** (400 MHz, $CDCl_3$), δ:

8.25 (*d*, 1H), 8.06-7.22 (*m*, 8H), 3.33 (*t*, 2H, J=7.6), 2.56 (*t*, 2H, J=7.24), 2.47 (*t*, 2H, 7.23), 2.00-1.90 (*m*, 2H), 1.80-1.70 (*m*, 2H), 1.58-1.50 (*m*, 2H), 1.43-1.30 (*m*, 2H). **^{13}C-NMR** (100 MHz, $CDCl_3$), δ: 136.52, 131.37, 130.84, 129.73, 128.54, 127.42, 127.12, 126.47, 125.69, 125.02, 124.97, 124.74, 124.69, 124.58, 123.30, 33.03, 31.97, 31.83, 31.75, 30.86, 29.61, 13.58. **IR**(KBr), cm^{-1}: 3036 (m), 2957 (m), 2930 (m), 2858 (w), 1458 (w), 1413 (w), 1180 (w), 838 (vs). **HRMS-ESI**(+): Calculated for $C_{24}H_{26}NaS$ $[M+Na]^+$ 369.1653; found 369.1647.

4-Pyrenylbutyl-butyl sulfoxide **7b**

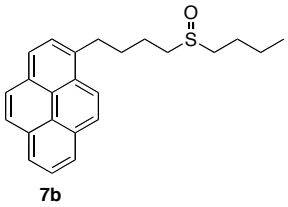

7b

Oxidation according to the general procedure provides sulfoxide **7b** with 69% yield. **^{1}H-NMR** (400 MHz, $CDCl_3$), δ: 8.23-7.94 (*m*, 8H), 7.82 (*d*, 1H, J=7.77 Hz), 3.39-3.34 (*m*, 2H), 2.72-2.46 (*m*, 4H), 2.04-1.84 (*m*, 4H), 1.73-1.62 (*m*, 2H), 1.48-1.34 (*m*, 2H), 0.91 (*t*, 3H, J=7.29 Hz). **^{13}C-NMR** (100 MHz, $CDCl_3$), δ: 136.90, 132.45, 131.90, 130.99, 129.60, 128.53, 128.44, 128.29, 127.76, 126.92, 126.14, 126.02, 125.88, 125.83, 124.21, 53.32, 53.26, 34.22, 32.02, 25.62, 23.77, 23.09, 14.71. **IR**(KBr), cm^{-1}: 3038 (m), 2951 (m), 2924 (m), 2865 (m), 1461 (m), 1409 (w), 1009 (vs), 839 (vs). **HRMS-ESI**(+): Calculated for $C_{24}H_{27}OS$ $[M+H]^+$ 363.1783; found 363.1777.

4-Pyrenylbutyl-butyl sulfone **7c**

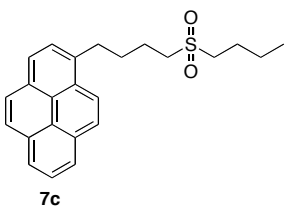

7c

Oxidation according to the general procedure provides sulfone **7c** with 74% yield. **^{1}H-NMR** (400 MHz, $CDCl_3$), δ: 8.21-7.94 (*m*, 6H), 7.80 (*d*, 1H, J=7.8), 7.57-7.54 (*m*, 1H), 7.38 (*t*, 1H, J=7.9), 3.38-3.33 (*t-like,* 2H), 2.97-2.84 (*m*, 4H), 2.04-1.96 (*m*, 4H), 1.79-1.69 (*m*, 2H), 1.45-1.32 (*m*, 2H), 0.89 (*t*, 3H, J=7.28). **^{13}C-NMR** (100 MHz, $CDCl_3$), δ: 170.62, 135.29, 134.60, 133.74, 131.32, 130.91, 130.75, 130.13, 129.94, 129.71, 128.47, 128.19, 127.37, 127.09, 126.68, 125.80, 125.03, 124.92, 124.73, 122.92, 52.48, 32.85, 30.38, 23.77, 21.86, 21.60, 13.37. **IR**(KBr), cm^{-1}: 3039 (m),

2954 (m), 2939 (m), 2870 (m), 1603 (w), 1467 (s), 1315 (s), 1260 (vs), 1124 (vs), 1097 (s), 839 (vs). **HRMS-ESI**(+): Calculated for $C_{24}H_{26}NaO_2S$ $[M+Na]^+$ 401.1551; found 401.1557.

4.6.4. Preliminary results from photolysis of 1b and 2b.

Preliminary photolyses were carried out in quartz cuvettes at ca. 10^{-5} M in THF containing 5 – 10 equivalents of Et_3SiH. Samples were exposed to unfiltered UV light from the short-wavelength (254 nm) bulb of a hand-held UV lamp (with glass filter removed) for varying periods of time.

Sulfoxides **1b** and **2b** completely degraded within 30 minutes under these conditions, although photolysis of **1b** for 60 minutes did not fully consume the starting sulfoxide. Irradiation of sulfide **1a** for a period of one hour led to partial decomposition (products uncharacterized) although the majority of the material was unreacted. Photolysis of sulfone **1c** for up to 2 hours did not produce any detectable reaction.

Complete photolysis of **1b** or **2b** produces complex reaction mixtures. This is in part due to the formation of sulfenate ester recombination products, which undergo secondary photolysis and thermolysis to form a range of products.

One of the most easily identified products of the photolysis of **1b** or **1b** is pyrene carboxaldehyde.

References.

[1] Ji, H.F.; Dabestani, R.; Brown, G. M.; Hettich, R. L. *Photochem. Photobiol. Sci.* **1999**, 69, 513.

[2] All calculations have been carried out using the GAMESS[a] and GAUSSIAN[b] software packages. The BMK density functional theory method was used together with several basis sets for comparative purposes. Dunning basis sets were employed including, DZ(2d,p),[c] DZ+(2d,p),[d] and cc-pVDZ.[e] The Hessian (matrix of second derivative) was calculated for each optimized geometry to determine local minima (positive definite) or nth-order saddle point (n negative eigenvalues), and zero-point energy corrections. Ionization potentials were determined by both Koopmans'[f] and DSCF (E_{neu}-E_{cat}) methods. Excited state structure and properties were carried out using both TD-DFT[g] and CIS[h] methods. G3MP2 theory was employed for heat of formation computations.[i] Visualization and analysis of structural (e.g., HOMO/LUMO molecular orbitals) and property results were obtained using QMView[j] and MacMolPlt.[k] a) M. Schmidt, K. K. Baldridge, J. A. Boatz, S. Elbert, M. Gordon, J. H. Jenson, S. Koeski, N. Matsunaga, K. A. Nguyen, S. J. Su, T. L. Windus, M. Dupuis, and J. A. Montgomery, *J. Comp. Chem.*, 1993, **14**, 1347. b) M. J. Frisch, G. W. Trucks, H. B. Schlegel, G. E. Scuseria, M. A. Robb, J. R. Cheeseman, J. A. Montgomergy, Jr., T. Vreven, K. N. Kudin, J. C. Burant, J. M. Millam, S. S. Iyengar, J. Tomasi, V. Barone, B. Mennucci, M. Cossi, G. Scalmani, N. Rega, G. A. Petersson, H. Nakatsuji, M. Hada, M. Ehara, K. Toyota, R. Fukuda, J. Hasegawa, M. Ishido, T. Nakajima, Y. Honda, O. Kitao, H. Nakai, M. Klene, X. Li, J. E. Knox, H. P. Hratchian, J. B. Cross, V. Bakken, C. Adamo, J. Jaramillo, R. Gomperts, R. E. Stratmann, O. Yazyev, J. Austin, R. Cammi, C. Pomelli, J. W. Ochterski, P. Y. Ayala, K. Morokuma, G. A. Voth, P. Salvador, J. J. Doannernberg, V. G. Zakrzewski, S. Dapprich, A. D. Daniels, M. C. Strain, O. KFarkas, D. K. Malick, A. D. Rabuck, K. Raghavachari, J. B. Foresman, J. V. Ortiz, Q. Cui, A. G. Baboul, S. Clifford, J. Cioslowski, B. B. Stefanov, G. Liu, A. Liashenko, P. Piskorz, I. Komaromi, R. L. Martin, D. G. Fox, T. Keith, M. A. Al-Laham, C. Y.

Peng, A. Nanayakkara, M. Challocombe, P. M. W. Gill., B. G. Johnson, W. chen, M. W. Wong, C. Gonzalez, and J. A. Pople, in 'Gaussian03', Wallingford, 2004. c) T. Dunning and P. Hay, in 'Gaussian basis sets for molecular calculations', ed. H. F. Schaefer, New York, London, 1977. d) T. H. Dunning, *J. Chem. Phys.*, 1971, **55**, 716. e) T. H. Dunning, *J. Chem. Phys.*, 1989, **90**, 1007. f) T. Koopmans, *Physica*, 1934, **1**, 104. g) Stratmann, R.E.; Scuseria, G.E.; Frisch, M.J. *J. Chem. Phys.* **1998**, *109*, 8218. h) el Bene, J.; Ditchfield, R.; Pople, J.A. *J. Chem. Phys.* **1971**, *55*, 2236. i) L. A. Curtiss, P. C. Redfern, K. Raghavachari, V. A. Rassolov, and J. A. Pople, *J. Chem. Phys.*, 1999, **110**, 4703. j) K. K. Baldridge and J. P. Greenberg, *J. Mol. Graphics*, 1995, **13**, 63. k) B. M. Bode and M. S. Gordon, *Mol. Graph. Mod.*, 1999, **16**, 133.

[3] Of particular importance to the present work are fundamental studies on the photochemistry of aryl sulfoxides: a) Vos, B. W.; Jencks, W. S. *J. Am. Chem. Soc.* **2002**, *124*, 2544. b) Cubbage, J. W.; Jencks, W. S. *J. Phys. Chem. A* **2001**, *105*, 10588. c) Lee, W.; Jencks, W. S. *J. Org. Chem.* **2001**, *66*, 474. d) Guo, Y.; Jencks, W. J. *J. Org. Chem.* **1997**, *62*, 857, and references therein.

[4] Benson, S. W. *Chem. Rev.* **1978**, *78*, 23.

[5] Becker, R. S.; Jordan, A. D.; Kolc, J. *J. Chem. Phys.* **1973**, *59*, 4024.

[6] For two cases in which “uphill” sensitization (inter- or intramolecular) has been shown to be responsible for photochemically-induced pyramidal inversion of aryl alkyl sulfoxides, see: a) Hammond, G. S.; Gotthard, H.; Coyne, L. M.; Axelrod, M.; Rayner, D. R.; Mislow, K. *J. Am. Chem. Soc.* **1965**, *87*, 4959. b) Cooke, R. S.; Hammond, G. S. *J. Am. Chem. Soc.* **1970**, *92*, 2739.

[7] Chloromethyl coumarin: a) Piloto, A. M.; Fonseca, A. S. C.; Costa, S. P. G.; Goncalves, M. S. T. *Tetrahedron* **2006**, *62*, 9258. Bromomethyl chlorofluorescein: b) Nolan, E. M.; Lippard, S. J. *J. Am. Chem. Soc.* **2003**, *125*, 14270. c) Nolan, E. M.; Lippard, S. J. *Inorg. Chem*. **2004**, *43*, 8310. Chloromethyl difluoroborodypyrromethane: d) Zeng, L.; Miller, E. W.; Pralle, A.; Isacoff, E. Y. and Chang, C. J. *J. Am. Chem. Soc*. **2006**, *128*, 10.

[8] Chloromethyl coumarin: a) Piloto, A. M.; Fonseca, A. S. C.; Costa, S. P. G.; Goncalves, M. S. T. *Tetrahedron* **2006**, *62*, 9258-9267. Bromomethyl chlorofluorescein: b) Nolan, E. M.; Lippard, S. J. *J. Am. Chem. Soc.* **2003**, *125*, 14270-14271. c) Nolan, E. M.; Lippard, S. J. *Inorg. Chem*. **2004**, *43*, 8310-8317.Chloromethyl difluoroborodypyrromethane: d) Zeng, L.; Miller, E. W.; Pralle, A.; Isacoff, E. Y. and Chang, C. J. *J. Am. Chem. Soc*. **2006**, *128*, 10-11.

[9] For a review of fluorescence methods for NO detection, see: Gomes, A.; Fernandes, E.; Lima, J. L. F. C. *J. Fluoresc.* **2006***, 16,* 119-140.

Appendix.

Absorbance and emission spectra of compounds 4(a-c)-7(a-c).

All absorption spectra were measured using 1×10^{-5} M solutions in CH_2Cl_2 unless otherwise noted. Emission spectra were measured using 10^{-6} M solutions in CH_2Cl_2.

Figure A4.1. Absorbtion spectra of compounds **4a-4c** (left) and **5a-5c** (right)**.**

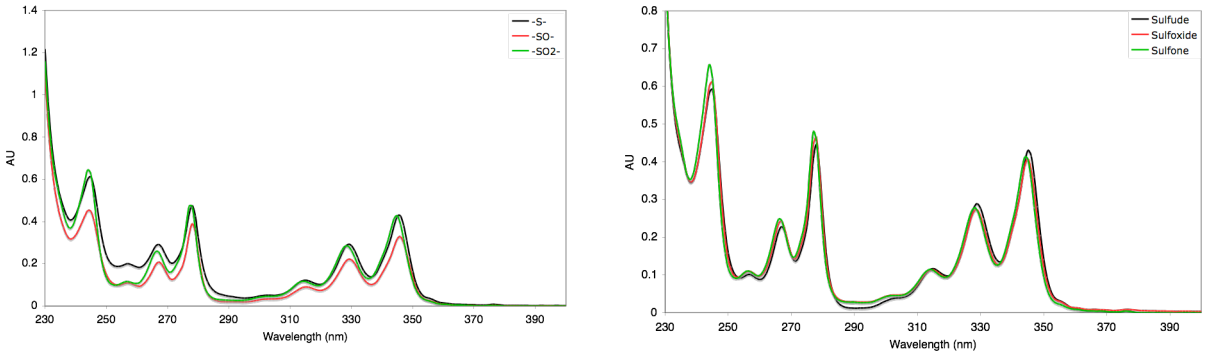

Figure A4.2. Absorbtion spectra of compounds **6a-6c** (left) and **7a-7c** (right)**.**

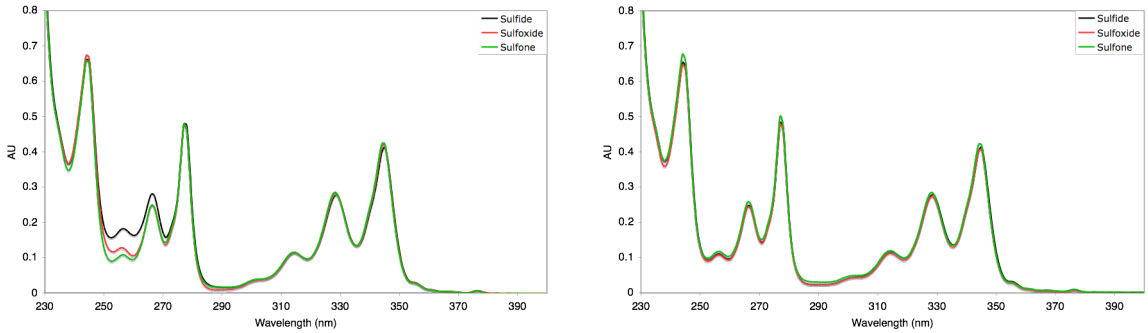

Figure A4.3. Emission spectra of compounds **4a-4c** (left) and **5a-5c** (right)**.**

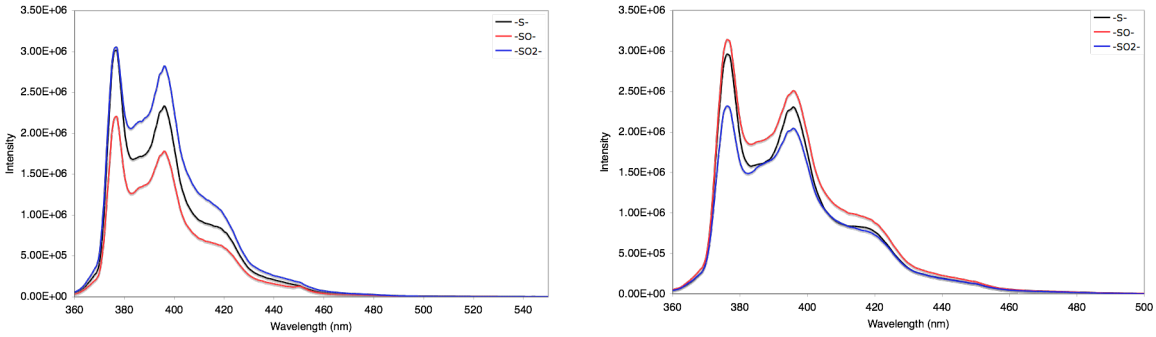

Figure A4.4. Emission spectra of compounds **6a-6c** (left) and **7a-7c** (right)**.**